

Supplemental Information for

Human T-bet governs innate and innate-like adaptive
IFN- γ immunity against mycobacteria

Correspondence to ryang@rockefeller.edu and casanova@rockefeller.edu

This PDF file includes:

Experimental model and subject details (including Case report)

Method details

Figs. S1 to S21

Figure legends for supplemental figures (Figs. S1 to S21)

Table S1 to S4, S8 and S9 (Table S5 – 7 were included separately as excel files)

Figure legends for supplementary tables (Tables. S1 to S9)

Reference for supplementary materials

Materials and Methods

Human subjects

The patient and the relatives studied here were living in and followed up in Morocco. The study was approved by and performed in accordance with the requirements of the institutional ethics committee of Necker Hospital for Sick Children, Paris, France, and the Rockefeller University, New York, USA. Informed consent was obtained for the patient, his relatives, and healthy control volunteers enrolled in the study. This study was also approved by the Sydney Local Health District RPAH Zone Human Research Ethics Committee and Research Governance Office, Royal Prince Alfred Hospital, Camperdown, New South Wales, Australia (protocol X16-0210/LNR/16/RPAH/257). Written informed consent was obtained from participants or their guardians. Informed consent from participants in Switzerland was approved by the local ethical committee (CE3428 authorized by Comitato Etico Cantonale, www.ti.ch/CE). Experiments using samples from human subjects were conducted in the United States, France, Australia and Switzerland, in accordance with local regulations and with the approval of the IRBs of corresponding institutions. Plasma samples from unrelated healthy subjects used as controls for antibody profiling by phage immunoprecipitation-sequencing (PhIP-Seq) were collected at Sidra Medicine in accordance with a study protocol approved by the Clinical Research Ethics Board of Sidra Medicine.

Cell lines

HEK293T and Phoenix A retroviral packaging cells were cultured in IMDM (Gibco) supplemented with 10% fetal bovine serum (FBS). B cells from the patient or controls were

immortalized in-house with Epstein Barr virus (EBV-B cells) and cultured in RPMI 1640 (Gibco) supplemented with 10% FBS. NK-92 cells were cultured in RPMI 1640 (Gibco) supplemented with 10% FBS, 1 mM sodium pyruvate, 200 U/mL recombinant proleukin IL-2 (Prometheus). *Herpesvirus saimiri*-transformed T (HVS-T) cells were generated with either *H. saimiri* strain C488 for transformation or the TERT transformation system (Wang et al., 2016). HVS-T cells were cultured in Panserin/RPMI 1640 (ratio 1:1) supplemented with 20% FBS, L-glutamine, gentamycin and 20 U/mL human rIL-2 (Roche). Isolated CD4⁺ T cells were cultured in X-vivo 15/gentamycin/L-glutamine (Lonza) supplemented with human AB Serum (GemCell). Peripheral blood mononuclear cells (PBMCs) were cultured in RPMI 1640 supplemented with 10% FBS for stimulation experiments. All cell lines used tested negative for mycoplasma. HEK293T, Phoenix A and NK-92 cells were purchased from the ATCC.

Method details

Case report

The patient (P) was born in 2015 to Moroccan first-cousin parents. He was vaccinated with BCG at the age of three months. After vaccination, he developed fever and left axillary lymphadenopathy accompanied by a cutaneous eruption. He received amoxicillin for 10 days, resulting in clinical improvement. At the age of six months, he was hospitalized for persistent fever, weight loss, cutaneous erythema, ear drainage and persistent oral thrush. Axillary adenopathy was present, with fistulation associated with hepatosplenomegaly and multiple abdominal adenopathies. The patient was treated with four antimycobacterial drugs; he displayed a good clinical response to 18 months of treatment and has been off antibiotics for 15 months. He was also found to have mild cytomegalovirus (CMV) viremia at the time (CMV PCR 3.74 log/mL, threshold < 2.4 log/mL), and was treated with ganciclovir. Serological PCR tests for CMV were negative at the age of two years, but weakly positive at the age of three years (IgM anti-CMV weakly positive, CMV PCR 3.62 log/mL, threshold < 2.4 log/mL). However, the patient showed no characteristic features of CMV infection. At the age of 11 months, he was hospitalized for four days due to airway hyperresponsiveness requiring treatment with inhaled steroids and albuterol. The patient had a high blood eosinophil count, documented since the age of six months (1,460/mm³). By the age of 17 months, he had persistent upper respiratory tract inflammation, with manifestations of persistent rhinorrhea, difficult respiration, wheezing and coughing that improved on treatment with oral steroid and salbutamol. The patient has since been treated with inhaled steroids for persistent upper respiratory tract inflammation. The clinical manifestations affecting the upper respiratory tract persisted at the age of three years. No trigger was identified for these symptoms and signs,

which were not triggered by exercise, activity, feeding or parasitic infections. A serum IgE allergen screen was negative for more than 250 allergens tested. The patient requires inhaled steroid therapy (fluticasone spray) every morning and evening. He also frequently visits the emergency room, and is hospitalized about once per month for exacerbations requiring oral steroid (beta-methasone) and inhaled salbutamol. The patient has been vaccinated for *Tetanus*, *Diphtheria*, and *Haemophilus B*, for all of which positive serum IgG result have been obtained. He also tested positive for anti-HSV-1 IgG, anti-EBV IgG, anti-CMV IgG, anti-mumps IgG and anti-parainfluenza IgG in clinical serology examinations. No anatomical abnormalities of the airways were noted. The patient has a brother who is healthy, with no history of severe infectious disease or airway hyperresponsiveness. The genetic cause of the patient's airway hyperresponsiveness will be studied separately.

Phage immunoprecipitation-sequencing (PhIP-Seq)

Patient serum and control samples were analyzed in duplicate by phage immunoprecipitation-sequencing (Hernandez et al., 2018; Xu et al., 2015). We used 10% liquid IVIg from pooled human plasma (Privigen® CSL Behring AG), human IgG-depleted serum (Supplier No HPLASERGFA5ML, Molecular Innovations, Inc.), and plasma samples from two unrelated healthy adult subjects and one unrelated healthy three-year-old boy for comparison. PhIP-Seq was carried out as previously described (Xu et al., 2015), but with the following modifications. We determined levels of total IgG in the serum or plasma samples with the Human IgG total ELISA Ready-SET-Go kit (Thermo Fisher Scientific) and incubated diluted samples containing approximately 4 µg of total IgG at 4°C overnight with 2×10^{10} plaque-forming units (PFUs) of a modified version of the original VirScan phage library (Xu et al., 2015). Specifically, the T7 phage library used here for peptide display contained the same viral peptides as the original

VirScan phage library plus additional peptides derived from protein sequences of various microbial B-cell antigens available from the IEDB (www.iedb.org). For the computational analysis and background correction, we also sequenced the phage library before (input library sample) and after immunoprecipitation with beads alone (mock IP). We performed a number ($n = 46$) pf technical repeats. Single-end sequencing was performed with the NextSeq500 system (Illumina), to generate approximately two million reads per sample and ~20 million reads for the input library samples. As previously described (Xu et al., 2015), reads were mapped onto the original library sequences with Bowtie 2 and read counts were adjusted according to library size. A zero-inflated generalized Poisson model was used to estimate the p -values, to reflect enrichment for each of the peptides. We considered peptides to be significantly enriched only if the $-\log_{10} p$ -value was at least 2.3 in all replicates. Species-specific score values were computed for each serum or plasma sample, by counting the significantly enriched peptides for a given species with less than a continuous seven-residue subsequence, the estimated size of a linear epitope, in common. We corrected for unspecific binding of peptides to the capture matrix, by also calculating species-specific background score values by counting the peptides displaying enrichment to the 90th percentile of the mock IP samples. These peptides were used for background subtraction.

Whole-exome sequencing (WES), genotyping and genome-wide linkage (GWL) analysis

All four members of the family tested were subjected to genomic DNA extraction followed by WES. Exome capture was performed with the SureSelect Human All Exon 50 Mb kit (Agilent Technologies). Paired-end sequencing was performed on a HiSeq 2000 (Illumina), generating 100-base reads. Sequences were aligned with the GRCh39 reference build of the human genome, with the BWA (Li and Durbin, 2009). Reads were then processed and variants were called with Genome

Analysis Toolkit, SAMtools, and Picard (Li et al., 2009; McKenna et al., 2010). The GATK Unified Genotyper was used to detect substitution and InDel calls (Depristo et al., 2011; McKenna et al., 2010). We used an annotation software system developed in-house to annotate all variants. All four members of the family were genotyped with Genome-Wide Human SNP Array 6.0 data. Genotype calling was achieved with the Affymetrix Power Tools Software Package (<https://www.affymetrix.com/support/developer/powertools/changelog/index.html>). Parametric multipoint linkage analysis was performed with MERLIN 1.1.2 software (Abecasis et al., 2002), assuming autosomal recessive inheritance with complete penetrance and a damaging allele frequency of 1×10^{-4} . Allele frequencies were estimated for 562,685 SNP markers, with family founders and HapMap CEU trios. Markers were clustered using an r^2 threshold (--rsq parameter) of 0.4. The genetic variant of interest was confirmed by PCR amplification of the region (forward primer: 5'-gtgaggactacgctacc-3', and reverse primer: 5'-cagaagcattgtcgagccag-3') followed by Sanger sequencing.

cDNA sequencing

We used cDNA sequencing to characterize the consequences of the patients' variant. In brief, total RNA was extracted from EBV-B cells or PBMCs from the patient and healthy donors (Qiagen). We synthesized cDNA from mRNA, using Superscript III (Thermo Fisher Scientific). A region spanning the mutation site was amplified by PCR with the forward (5'-tagaagccaggcgtcagagc-3') and reverse R4 (5'-ctcggcattctgtaggcag-3'), R5 (5'-gcaatgaactgggtttcttgg-3'), or R6 (5'-gactcaaagttctccggaatcc-3') primers. PCR amplicons were sequenced with the BigDye Terminator Cycle Sequencing Kit (Thermo Fisher Scientific). Alternatively, cDNA generated from patient or control PBMCs was amplified by PCR with the

forward primer 5' - tctacactctttccctacacgacgctcttccgatctgtgaggactacgcgctacc-3' and reverse primer 5' - gtgactggagttcagacgtgtgctcttccgatctgcaatgaactgggttcttg-3', to amplify a region spanning the mutation in a first round of PCR. A second round of PCR was then performed on the PCR products from the first PCR as a template. We used the forward primer 5' - aatgatacggcgaccaccgagatctacactctttccctacacgac -3' and the reverse primers 5' - caagcagaagacggcatacagagatcgtattcgggtgactggagttcagacgtgtg -3', 5' - caagcagaagacggcatacagagatctcctagagtgactggagttcagacgtgtg -3', and 5' - caagcagaagacggcatacagagattagttgcggtgactggagttcagacgtgtg -3', to barcode two healthy control cDNAs and the patient's cDNA. Adaptor and barcoded PCR amplicons were mixed and purified, and used for next-generation sequencing by Nano Format 350 paired-end MiSeq sequencing (illumina). We aligned MiSeq data to the reference genome with RNA-STAR aligner (Dobin et al., 2013). The aligned sequencing data were then viewed with Integrative Genome Browser (Robinson et al., 2011).

Reverse transcription-quantitative PCR (RT-qPCR)

Total RNA was extracted from cells with the RNeasy Kit (Qiagen) or the Quick-RNA kit (Zymo Research). Reverse transcription was performed with the SuperScript III enzyme (Thermo Fisher Scientific). Messenger RNAs were quantified with the cDNA as a template and the *TBX21* (Probe 1: Hs00894393 and Probe 2: Hs00894391), *IFNG* (Hs99999041), *TNF* (Hs01113624), *IL5* (Hs01548712) (Thermo Fisher), *GUSB* (Thermo Fisher) probes.

T-bet/*TBX21* overexpression

A wild-type (WT) *TBX21* plasmid with a pCMV6 backbone was purchased from Origene (RC207902). The genetic variants of *TBX21* studied here, and the variants described in gnomAD (<http://gnomad.broadinstitute.org/>) or in our in-house database were introduced into pCMV6-WT *TBX21* by site-directed mutagenesis PCR with the CloneAmp HiFi PCR Premix (Takara Bio). *TBX21* WT plasmids or plasmids containing variants were used to transfect HEK293T cells in the presence of Lipofectamine 2000 reagent (Thermo Fisher Scientific) to achieve overexpression. The WT or mutant (Mut) *TBX21* was overexpressed in *in vitro*-expanded T cells, HVS-T cells, or NK-92 cells, as previously described (Martínez-Barricarte et al., 2016). In brief, the *TBX21* plasmid was subcloned into pLZRSires- Δ NGFR (Addgene). We then used pLZRS containing the WT or Mut *TBX21* to transfect Phoenix A cells, and retroviruses were produced and concentrated with Retro-X (Takara Bio). Concentrated retrovirus preparations were used for retroviral transduction.

Immunoblotting

Proteins were solubilized in RIPA buffer containing 10 mM Tris-Cl (pH 8.0), 1 mM EDTA, 0.5 mM EGTA, 1% Triton X100, 0.1% sodium deoxycholate, 0.1% SDS and 150 mM NaCl supplemented with protease-inhibitor cocktail (Complete mini, Roche). Alternatively, nuclear proteins from HEK293T transfectants were purified with the NE-PER Nuclear Extraction kit in accordance with the manufacturer's procedures (Thermo Fisher Scientific). Proteins were quantified with the Bradford assay. Equal amounts of lysate (5 μ g to 50 μ g of) were mixed with SDS sample buffer and boiled for 5min at 95°C before being subjected to electrophoresis in 12% acrylamide SDS-PAGE gels. The following antibodies were used for immunoblotting: mouse anti-human T-bet 4B10 monoclonal Ab (BioxCell), rabbit anti-human T-bet polyclonal Ab

(Proteintech), anti-Flag-M2 HRP-conjugated Ab (Sigma-Aldrich), anti- α -tubulin HRP-conjugated Ab (Proteintech), anti-lamin A/C Ab (Santa Cruz), anti-GAPDH HRP-conjugated Ab (Santa Cruz), anti-STAT1 monoclonal Ab (BD Biosciences), sheep ECL anti-mouse IgG HRP-conjugated Ab (GE Healthcare), and ECL anti-rabbit IgG HRP-conjugated Ab (GE Healthcare).

Electrophoretic mobility shift assays (EMSA)

HEK293T cells were transfected with empty plasmid (EV), WT or mutant *TBX21* pCMV6 plasmids. After 2 days, nuclear extracts were obtained from the cells with the NE-PER Nuclear Extraction Kit (Thermo Fisher Scientific). EMSA was performed as previously described (Liu et al., 2011). In brief, ^{32}P was used to label consensus T-box responsive element (TBRE) duplexes of DNA oligos (WT oligo: 5'-gataatttcacacctaggtgtgaaatt-3', Mut Oligo as control: 5'-gataatttcacgtctaggtacgaaatt-3' and 5'-gataatttcgtacctagacgtgaaatt-3'). Unlabeled WT TBRE duplex was used as non-radioactive competitive probe. We mixed 10 μg of nuclear extract from each condition or 80 μg (8x) of nuclear extract from Mut *TBX21* transfectants with or without unlabeled probe, 2 μg mouse IgG1 control (BioxCell) or 2 μg mouse anti-T-bet 4B10 monoclonal Ab (BioxCell) and incubated for 30 min. ^{32}P -labeled WT or Mut TBRE duplex was then added and the mixture was incubated for 30 min on ice in the presence of poly-dIdC (Sigma-Aldrich). Samples were subjected to polyacrylamide gel electrophoresis. The gel was dried and placed against X-ray film for 2 days, after which the radioactive signal was read on a Typhoon platform.

Luciferase reporter assays

HEK293T cells were transfected with the indicated expression plasmids, firefly luciferase plasmids under the control of WT or Mut *TBRE* (Janesick et al., 2012), as previously described, or with human *IFNG* promoters in a pGL4.10 backbone (-565 - +85 of *IFNG*), and with a constitutively expressed *Renilla* luciferase plasmid for normalization (pRL-SV40). Cells were transfected in the presence of Lipofectamine 2000 (Thermo Fisher Scientific) for 3 days. Luciferase levels were measured with Dual-Glo reagent, according to the manufacturer's protocol (Promega). Firefly luciferase values were normalized against *Renilla* luciferase values, and fold-induction is reported relative to controls transfected with empty plasmid.

Generation and analysis of T-bet-deficient NK-92 cells

T-bet-deficient NK-92 cells were generated according to a protocol described elsewhere (Sanjana et al., 2014). We used oligonucleotides for gRNA9 and gRNA15 (gRNA9_Forward: 5'-caccgtccaacaatgtgaccaggt-3', gRNA_Reverse: 5'-aaacacctgggtcacattgttgac-3'; gRNA15_Forward: 5'-caccgcccactcaccgtccctgct-3', gRNA15_reverse: 5'-aaacagcagggacggtgagtgcggc-3'). DNA duplex was annealed from the oligonucleotides above, and was inserted into pLenti-CRISPR-V2 plasmids (Addgene). We then used pLenti-CRISPR plasmids, VSV-G envelope, and psPAX2 plasmids to transfect HEK293T cells in the presence of Lipofectamine 2000. Supernatants containing lentiviruses were harvested and concentrated with Lenti-X concentrator (Takara Bio). We resuspended 10^6 NK-92 cells with 20x concentrated lentiviruses for gRNA9, gRNA15 or empty plasmid, in the presence of proleukin IL-2 (200 U/mL). After incubation for 2 days, we added 3.75 μ g/mL puromycin to the culture for the selection of stably transduced NK-92 cells. After a further two weeks, cells were harvested for the Surveyor Nuclease Assay (Integrated DNA Tech) and a three-primer PCR-based screening system

(Harayama and Riezman, 2017) to confirm successful DNA editing. Cells were plated at a density of 0.7 cells in 200 μ L per well in a U-bottomed 96-well plate. Two weeks later, single-cell clones were screened with a three-primer PCR-based system, with Phire Direct PCR Master Mix (Thermo Fisher Scientific). The primers used for this screening assay were gRNA9_Forward: 5'-agccctaccctaattcct-3', gRNA9_Reverse: 5'-ggcatctattcctgggacc-4', gRNA9_Reverse_in: 5'-ctttgaagagcaggtcctacct-3' and gRNA15_Forward: 5'-GCCTGAATATGACCCCCGTC-3', gRNA15_Reverse: 5'-caccactaccaccactaaagc-3'; gRNA15_Forward_in: 5'-acagatgatcatcaccaagca-3'. Single-cell clones with biallelic disruptions were selected for validation by RT-qPCR and western blotting. EV-transduced single-cell clones were randomly picked as controls. Cells were then transduced with retroviruses generated from pLZRS-ires- Δ CD271 plasmids containing EV, WT, Mut or K314R *TBX21*, as described above (Martínez-Barricarte et al., 2016). Stably transduced cells were isolated with anti-CD271 antibody-coated beads (Miltenyi Biotec). Cells were stimulated with 50 pg/mL IL-12 (R&D) and 10 ng/mL IL-18 (InvivoGen), or were left unstimulated, and all cells were incubated for one day. The IFN- γ content of the supernatants was determined by ELISA. Intracellular IFN- γ production was measured with flow cytometry with intracellular staining (ICS). In brief, cells were fixed and permeabilized (BioLegend), and were subjected to ICS staining with FcBlock (Miltenyi Biotec), anti-T-bet BV421 (BioLegend) and anti-IFN- γ PE (BioLegend) before their use for ICS flow cytometry analysis.

Cytokine determinations in *TBX21*-transduced primary CD4⁺ T cells

PMBCs from three healthy donors were stained with FcBlock (Miltenyi Biotec), anti-CD4-APC-Cy7, anti-CD45RA-Alexa488, anti-CCR7-Alexa647 and Live-Dead exclusion Aqua. Naïve

CD4⁺ T cells were isolated by FACS. Cells were stimulated with anti-CD3/CD28 Ab Dynabeads (Thermo Fisher Scientific) at a 1:1 cell:bead ratio under T_{H0} or T_{H2} (recombinant human IL-4 12.5 ng/mL, R&D) polarizing conditions, in the presence of 100 U/mL proleukin IL-2. Fresh medium (X-vivo 15, 5% human AB serum) and cytokines were added every 3 days. After 7 days, cells were restimulated with Dynabeads at a 1:2 ratio (bead:cell). One day after restimulation, cells were transduced with retroviruses generated from pLZRS-ires-ΔCD271 plasmids containing WT or Mut *TBX21*, as previously described (Martínez-Barricarte et al., 2016). Transduced cells were isolated with anti-CD271 antibody-coated beads (Miltenyi Biotec) 14 days after stimulation. Intracellular cytokine production was determined by ICS. In brief, cells were restimulated with 25 ng/mL phorbol 12-myristate 13-acetate (PMA) and 0.5 μM ionomycin for 6 h in the presence of GolgiPlug (BD Biosciences). Cells were stained with Zombie-NIR live-dead exclusion dye (BioLegend), FcBlock (Miltenyi Biotec), and FITC-conjugated anti-CD271 antibody (BioLegend). Cells were then fixed, permeabilized and subjected to ICS staining with anti-TNF-α-BV510 (BioLegend), anti-IFN-γ-PERCP/Cy5.5 (BioLegend), anti-IL-4-PE, anti-IL-13-APC antibodies, followed by flow cytometry analysis with an Aurora cytometer (Cytex).

HVS-T cell analysis

We plated 200,000 HVS-T cells from healthy donors or P in a 96-well U-bottomed plate at a density of 1x10⁶ cells/mL. The plate was incubated for 2 days, and the culture supernatants and cells were harvested for ELISA or RT-qPCR for *IFNG* and *TNF*. HVS-T cells from P were transduced with retroviruses generated from pLZRS-ires-ΔCD271 plasmids containing WT *TBX21* or EV, as previously described (Martínez-Barricarte et al., 2016). After incubation for 5 days, the HVS-T cells were stimulated with 25 ng/mL PMA and 500 nM ionomycin or were left

untreated; they were then incubated in the presence of GolgiPlug (BD Biosciences) for 6-8 h. Cells were stained with Zombie-NIR live-dead dye (BioLegend), FcBlock (Miltenyi Biotec), anti-CD4-BV750 (BD Biosciences), anti-CD3-BV650 (BD Biosciences), anti-CD8a-Pacific Blue (BioLegend), and anti-CD271-FITC (BioLegend) antibodies, fixed and permeabilized for ICS staining with anti-T-bet-PE (BioLegend), anti-IFN- γ -BV711 (BioLegend), anti-TNF- α -BV510 (BioLegend), anti-IL-13-APC (BioLegend), anti-IL-10-PE-Dazzle594 (BioLegend) antibodies. ICS analysis was performed on an Aurora cytometer (Cytex).

Functional analysis of expanded T-bet-deficient CD4⁺ T cells *in vitro*

CD4⁺ T cells were isolated from PBMCs from five healthy donors, IL-12R β 1-deficient (m/m) patients, the T-bet wt/m heterozygous father, and the T-bet m/m patient (P), with anti-CD4 antibody-coated beads (Miltenyi Biotec). They were then expanded with anti-CD3/CD28 antibody-coated Dynabeads (Thermo Fisher Scientific) at a 1:1 (cell:bead) ratio under T_H0 or T_H1 (2.5 ng/mL IL-12 R&D and anti-human IL-4 neutralizing Ab InVivoMab, BioXcell) conditions, in the presence of 100 U/mL proleukin IL-2 and anti-human IL-10 neutralizing Ab (Thermo Fisher Scientific). Medium (X-vivo15 5% human AB serum) and cytokine cocktails were refreshed every 3 – 4 days. After 7 days, the culture consisted of >95% CD4⁺ T cells. Cells were restimulated with anti-CD3/CD28 Ab-coated Dynabeads every 7-8 days. P's CD4⁺ T cells were transduced with retroviruses obtained from pLZRS-ires- Δ CD271 plasmids with or without WT *TBX21* or EV, as previously described (Martínez-Barricarte et al., 2016). Six days after transduction, cells were restimulated with 25 ng/mL PMA and 500 nM ionomycin in the presence of GolgiPlug (BD Biosciences) for 6 h. Cells were stained with Zombie NIR Live-Dead exclusion reagents (BioLegend), anti-CD271-FITC antibody and were then fixed and permeabilized. They were

stained with anti-TNF- α -BV510, anti-IL-13-APC, anti-IL-4-PE, anti-IL-17A-BV785, anti-IL-10-PE-Dazzle594, anti-IL-5-BV421 and anti-IFN- γ -PerCp-Cy5.5 antibodies and subjected to flow cytometry in an Aurora cytometer (Cytex). Three weeks after their initial expansion, transduced CD271⁺ CD4⁺ T cells from P were isolated with anti-CD271 antibody-coated beads (Miltenyi Biotec). The cells isolated, and expanded CD4⁺ T_H0 cells from healthy donors or T-bet wt/m individuals were restimulated with anti-CD3/CD28 antibody-coated beads in the absence of cytokine for 16 h or 48 h. Cytokine levels were determined in 13-Legendplex assays (BioLegend) on culture supernatants from cultures restimulated for 48 h. Total RNA was extracted from cells restimulated for 16 h for RNA-seq analysis (Qiagen). In brief, 100 ng of total RNA was used to generate RNA-Seq libraries with the Illumina TruSeq stranded mRNA LT kit (Cat# RS-122-2101). Libraries prepared with unique barcodes were pooled at equal molar ratios. The pool was denatured and sequenced on an Illumina NextSeq 500 sequencer with high-output V2 reagents and NextSeq Control Software v1.4 to generate 75 bp single reads, according to the manufacturer's protocol (Illumina, Cat# 15048776).

RNA-seq FASTQ files were obtained, and inspected by fastqc for quality control of the raw data. The sequencing reads of each FASTQ file were then mapped to the GENCODE human reference genome GRCh37.p13 (Frankish et al., 2019) with STAR aligner v2.6 (Dobin et al., 2013), and the quality of each mapped alignment in the BAM file was evaluated by RSeQC (Wang et al., 2012). Reads were quantified to generate gene-level read counts from the read alignment, with featureCounts v1.6.0 (Liao et al., 2014), based on GENCODE GRCh37.p13 gene annotation. The gene-level read counts were then normalized and log₂-transformed by DESeq2 (Love et al., 2014), to obtain the gene expression value for all genes and all samples. An analysis of the differential expression of all genes and immune genes was performed to compare gene expression in the four

TBET samples (TBET_HET, TBET_HOM, TBET_HOM_EV, and TBET_HOM_WT) with that in five control samples, with each sample having two technical replicates. The 1,984 immune-related genes were identified from the immune system process gene set in the Molecular Signature Database (MSigDB) (Liberzon et al., 2015). By applying the trimmed mean of M values (TMM), normalization and gene-wise generalized linear model regression were performed in edgeR (Robinson et al., 2010). The genes displaying significant differential expression were selected on the basis of a p -value ≤ 0.05 and a FDR ≤ 0.05 . The differential gene expression data were plotted as a heatmap by ComplexHeatmap (Gu et al., 2016), and genes and samples were clustered on the basis of complete linkage and Euclidean distance of gene expression values.

Omni-ATAC-seq on CD4⁺ T cells and analysis

CD4⁺ T cells derived from healthy donors, IL-12R β 1 m/m patients, T-bet wt/m individuals and the T-bet m/m patient (P) were expanded under T_H0 conditions, as described above. Nine days after the retroviral transduction of CD4⁺ T cells from P, as described above, CD271⁺ cells were isolated with anti-CD271 antibody-coated beads (Miltenyi Biotec). Omni-ATAC-seq library preparation was performed as previously described (Corces et al., 2017). In brief, 50,000 cells from three healthy donors, two IL-12R β 1 m/m patients, technical duplicates for a T-bet wt/m individual, the T-bet m/m P and P cells complemented with EV or WT *TBX21* were harvested, washed with 50 μ l cold PBS, and centrifuged to obtain a pellet. Pellets were lysed with 50 μ l cold lysis buffer consisting of 48.5 μ l resuspension buffer (10 mM Tris-HCl pH 7.5, 10 mM NaCl, 3 mM MgCl₂ in water), 0.5 μ l 10% NP-40, 0.5 μ l 10% Tween-20, and 0.5 μ l 1% digitonin. Lysates were incubated on ice and then washed with 0.1% Tween-20 resuspension buffer. Lysates were centrifuged and the nuclei in the pellet were subjected to Tn5 transposition with 50 μ L of a mixture

of 25 μ L 2 x TD buffer, 16.5 μ L PBS, 0.5 μ L 10% Tween-20, 0.5 μ L 1% digitonin, 2.5 μ L Tn5 transposase, 5 μ L nuclease-free water at 37 °C in a thermomixer operating at 1,000 rpm for 30 min. DNA fragments were extracted with the MinElute PCR purification kit and eluted in 30 μ L EB buffer (Qiagen). We used 10 μ L of eluted DNA for the amplification of DNA fragments with the NEBNext PCR master mix (New England BioLab), over six cycles, with the Ad1_forward and 15 indexed Ad2_reverse primers, as previously described (Buenrostro et al., 2013, 2015). The partially amplified library was subjected to quantitative PCR analysis with the Ad1 and Ad2 primers, Sybr Green reagents and NEBNext PCR master mix for 25 cycles. Additional PCR cycles were performed, based on 1/3 the maximal fluorescence for each sample, as previously described (Buenrostro et al., 2013, 2015). A left-sided isolation of PCR products was performed with AMPure beads (Beckman Coulter). DNA was quantified with a Qubit fluorimeter. Equal amounts of each sample were pooled and subjected to paired-end sequencing on a NextSeq high-output sequencer generating 75 bp reads.

The ATAC-seq reads were aligned with the hg19 genome from the Bsgenome.Hsapiens.UCSC.hg19 Bioconductor package (version 1.4.0) with Rsubread's align method in paired-end mode, with fragments between 1 and 5,000 base pairs long considered correctly paired (Liao et al., 2014). Normalized, fragment signal bigWigs were created with the rtracklayer package. Peak calls were made with MACS2 software in BAMPE mode (Feng et al., 2012; Zhang et al., 2008) and peak summits were used in MEME-ChIP software the identification of known and novel motifs (Ma et al., 2014). Differential ATAC-seq signals were identified with the DESeq2 package (Love et al., 2014; Ross-Innes et al.). Fragment length distribution plots and nucleosome-free/mono-nucleosome meta-TSS plots were produced with the soGGi package (de

Santiago and Carroll, 2018). Heatmaps of ChIP-seq and ATAC-seq signals were created from the normalized bigWigs signal with DeepTools2 software (Ramírez et al., 2016).

T-bet ChIP-seq data (SRR332104) and its input control (SRR332102) were retrieved as unaligned sequences from the European Nucleotide Archive (Kanhere et al., 2012). Sequences were aligned with the hg19 genome from the Bsgenome.Hsapiens.UCSC.hg19 Bioconductor package (version 1.4.0) with Rsubread's align method, with predicted fragment lengths calculated with the ChIPQC package (Carroll et al., 2014; Liao et al., 2014; de Santiago and Carroll, 2018). Normalized, fragment-extended bigWigs signals were created with the rtracklayer package.

EPIC DNA methylation arrays and quantification of DNA methylation

CD4⁺ T cells derived from healthy donors, a T-bet wt/m individual and the T-bet m/m P were expanded under T_{H0} conditions, as described above. Seventeen days after the retroviral transduction of CD4⁺ T cells from P as described above, CD271⁺ cells were isolated with anti-CD271 antibody-coated beads (Miltenyi Biotec). DNA from non-transduced or CD271⁺ isolated CD4⁺ T cells was extracted with a DNA mini kit (Qiagen). DNA was subjected to bisulfite conversion with the EZ DNA Methylation Kit (ZymoResearch). We quantified the DNA in all samples by performing EPIC arrays (Illumina), following the manufacturer's instructions. Technical replicates were included for several samples during EPIC processing, to ensure that the measurements were reliable. All microarrays were scanned with the Illumina HiScan system. Data files were processed and converted to beta-values, corresponding to the percentage CpG methylation for a given CpG site. We wrote scripts to filter all loci, retaining those with higher levels of methylation in TBET_HOM and TBET_HOM_EV than the maximum methylation level in controls and lower levels of methylation in TBET_HOM_WT than in controls (group 1) and

those with lower levels of methylation in TBET_HOM and TBET_HOM_EV than the minimum level of methylation in controls and higher levels of methylation in TBET_HOM_WT than the minimum level in controls (group 2). We then measured and plotted the difference in CpG methylation between the patient and controls, by subtracting the mean methylation level for the five controls from that for TBET_HOM and comparing the value obtained with the level of restored CpG methylation by subtracting the level of methylation in TBET_HOM_WT from the methylation in TBET_HOM_EV. On the plot, red dots represent the loci with higher levels of methylation in the patient than in controls, and green dots represent loci with lower levels of methylation in the patient than in controls. Dot size is proportional to the fold difference in methylation in patients relative to the mean value for controls. The genes of our interest are highlighted on the scatter plot.

Immunophenotyping of leukocytes

Metal-conjugated mAbs were obtained from Fluidigm according to the manufacturer's instructions. The following antibodies were included in the staining panel: anti-CD45-89Y, anti-CD57-113In, anti-CD11c-115In, anti-CD33-141Pr, anti-CD19-142Nd, anti-CD45RA-143Nd, anti-CD141-144Nd, anti-CD4-145Nd, anti-CD8-146Nd, anti-CD20-147Sm, anti-CD16-148Nd, anti-CD127-149Sm, anti-CD1c-150Nd, anti-CD123-151Eu, anti-CD66b-152Sm, anti-PD-1-153Eu, anti-CD86-154Sm, anti-CD27-155Gd, anti-CCR5-156Gd, anti-CD117-158Gd, anti-CD24-159Tb, anti-CD14-160Gd, anti-CD56-161Dy, anti-gdTCR-162Dy, anti-DRTH2-163Dy, anti-CLEC12A-164Dy, anti-CCR6-165Ho, anti-CD25-166Er, anti-CCR7-167Er, anti-CD3-168Er, anti-CX3CR1-169Tm, anti-CD38-170Er, anti-CD161-171Yb, anti-CD209-172Yb, anti-CXCR3-173Yb, anti-HLA-DR-174Yb, anti-CCR4-176Yb, anti-CD11b-209Bi. PBMCs from five healthy

donors, two IL-12R β 1-deficient patients, P and P's parents were included in this experiment. In total, 20,000 DNA⁺CD45⁺CD66b⁻ events from individual CyTOF data files containing information for all markers except for CD45 and CD66b were deconvoluted into clusters by viSNE (Amir el et al., 2013). We also deconvoluted 5,000 memory CD4⁺ T cells (DNA⁺CD45⁺CD66b⁻CD123⁻CD3⁺CD20⁻CD56⁻ γ δ TCR⁺CD4⁺CD8⁻CD45RA⁻) into viSNE plots based on 21 surface markers (113ln_CD57, 115ln_CD11c, 149sm_CD127, 150Nd_CD1c, 153Eu_PD-1, 154Sm_CD86, 155Gd_CD27, 156Gd_CCR5, 158Gd_CD117, 159Tb_CD24, 163Dy_CRTH2, 165Ho_CCR6, 166Er_CD25, 167Er_CCR7, 169Tm_CX3CR1, 170Er_CD38, 171Yb_CD161, 173Yb_CXCR3, 174Yb_HLA-DR, 176Yb_CCR4, 209Bi_CD11b). Analyses were performed by manually gating populations for NK cells, naïve and memory subsets of CD4⁺ and CD8⁺ T cells, innate lymphoid cells (ILCs), Tregs and dendritic cell subsets. For T helper cell analysis, we included an additional four healthy donors from a separate experiment (same staining panel) in the analysis. Manual gating was used for TH analysis.

Immunophenotyping for MAIT, invariant NKT cells, V δ 2 and V δ 1 cells was performed with a flow cytometry staining panel containing FcBlock (Miltenyi Biotec), Zombie-NIR live-dead exclusion dye (BioLegend), anti-CD3-Alexa532 (Thermo Fisher Scientific), anti- γ δ TCR-FITC (Thermo Fisher Scientific), anti-V δ 2-APC-Fire750 (BioLegend), anti-CD56-BV605 (BioLegend), anti-CD4-BV750 (BD Biosciences), anti-CD8a-BV510 (BioLegend), anti-V α 7.2-BV711 (BioLegend), anti-V α 24-J α 18-PE-Cy7 (BioLegend), anti-V δ 1-Vioblue (Miltenyi Biotec), anti-CD161-PE (BioLegend) and anti-V β 11-APC (Miltenyi Biotec) antibodies. Cells were analyzed with an Aurora cytometer (Cytex). Immunophenotyping for innate lymphoid cells and NK cells was confirmed separately with a conventional flow cytometry. In brief, biotinylated anti-human anti-CD1a (HI149), anti-CD3 (OKT3), anti-CD5 (UCHT2), anti-CD14 (61D3), anti-CD19

(HIB19), anti-CD34 (4H11), anti-CD123 (6H6), anti-CD203c (FR3-16A11), anti-CD303 (AC144), anti-TCR $\alpha\beta$ (IP26), anti-TCR $\gamma\delta$ (B1) and anti-Fc ϵ RI α (AER-37) antibodies were used in combination with streptavidin BUV661; conjugated anti-CD62L-FITC (Dreg-56), anti-CD94-PerCP-Vio700 (REA113), anti-TCRV α 24J α 18-PE (6B11), anti-CD26-PE-CF594 (M-A261), anti-CD127-PE-Cy7 (eBioRDR5), anti-CRTH2-Alexa Fluor 647 (BM16), anti-CD161-Alexa Fluor 700 (HP-3G10), anti-EOMES-APC-eFluor 780 (WD1928), anti-NKp46-BV421 (9E2/NKp46), anti-CD45RA-BV570 (HI100), anti-CD117-BV605 (104D2), anti-ROR γ t-BV650 (Q21-559), anti-CD7-BV711(M-T701), anti-CD16-BUV496 (3G8), anti-CD25-BUV563 (2A3), anti-CD56-BUV737 (NCAM16.2) and anti-CD45-BUV805 (HI30); anti- T-bet-BV786 (O4-46), anti-GATA3-BUV395 (L50-823) antibodies were purchased from BioLegend, Thermo Fisher Scientific, BD Biosciences, or Miltenyi Biotec. Fc receptors were blocked with IgG from human serum (Sigma-Aldrich). Surface membrane staining was performed in Brilliant Stain Buffer (BD Biosciences). Transcription factors were stained with the Foxp3 staining buffer set (Thermo Fisher Scientific) according to the manufacturer's instructions. The fixable viability dye eFluor 506 (Thermo Fisher Scientific) was used to exclude dead cells. Samples were acquired on a Symphony A5 cytometer (BD Biosciences) with FACSDiva 8 software and were analyzed with FlowJo 10 (BD Biosciences).

Immunophenotyping was confirmed separately for the T- and B-cell subsets by conventional flow cytometry. In brief, PBMCs from healthy controls and P were labeled with mAbs against CD3, CD4, CD8, CD45RA, CCR7, CD127, CD25, CXCR5, CXCR3, CCR6, PD-1, and CD56. The CD4⁺ and CD8⁺ T-cell subsets were separated into naïve (T_{Naive}: CCR7⁺CD45RA⁺), central memory (T_{CM}: CCR7⁺CD45RA⁻), effector memory (T_{EM}: CCR7⁻CD45RA⁻), and terminally differentiated effector memory cells (T_{EMRA}: CCR7⁻CD45RA⁺) after

initial gating on CD8⁻CD4⁺ or CD8⁺CD4⁻ cells. Proportions of regulatory T cells (CD4⁺CD127^{lo}CD25^{hi}), total memory (CD4⁺CD45RA⁻), and circulating Tfh (cTfh; CD4⁺CD45RA⁻CXCR5⁺) cells, and subsets of total memory and cTfh cells defined on the basis of CXCR3 and CCR6 expression (Th1: CCR6⁻CXCR3⁺, Th17: CCR6⁺CXCR3⁻, Th1*/Th1-17: CCR6⁺CXCR3⁺, Th2: CCR6⁻CXCR3⁻) were also determined.

Single-cell (sc) RNA-seq and analysis

We performed scRNA-seq on PBMCs obtained from the *TBX21* wt/m heterozygous father and the *TBX21* m/m patient. PBMCs were quickly thawed at 37°C and gently resuspended by serial additions of DMEM + 10% heat-inactivated (HI) FBS, according to the recommendations from the 10x Genomics “Sample preparation Fresh Frozen Human PBMC” protocol Rev C. Cells were centrifuged at 400 x g for 5 min, washed with DMEM + 10% HI-FBS, and cells were then counted and viability was assessed with the LIVE/DEAD™ Viability kit (Thermo Fisher Scientific) according to the manufacturer’s guidelines. Following centrifugation at 400 x g for 5 min, cells were resuspended at a concentration of 1000 cells/μl in PBS + 0.04% BSA and loaded onto a 10 x Genomics Chromium chip for single-cell capture. Reverse transcription and library preparation were performed with Chromium Single Cell 3’ Reagent Kits (v2) in accordance with the manufacturer’s guidelines, and library quality was assessed with a Bioanalyzer DNA chip. Each library was sequenced on two lanes of an Illumina HiSeq 4000 sequencer in a 28 bp/98 bp paired-end configuration.

The sequence-read quality of individual sequencing lanes was assessed with BVAtools (<https://bitbucket.org/muggic/bvatools>). Cell Ranger v3.0.1 was used to aggregate the sequences from two lanes/samples, to map reads to the hg38 human reference genome assembly, for filtering,

and counting barcodes and UMIs; a list of UMI counts was thus obtained for each gene and each cell. Cells outside the [5%,95%] interval for these metrics or with >10% mitochondrial genes were excluded. The DoubletFinder package was used to identify and filter out cell doublets (McGinnis et al., 2019). After the removal of dead cells and doublets, 10,409 cells for the T-bet wt/m heterozygous father and 11,741 cells for the T-bet m/m P were analyzed together with the Seurat v3 R package (Stuart et al., 2019), and cell clustering was performed by the Uniform Manifold Approximation and Projection dimension reduction method (Becht et al., 2019), using the most variable genes, but excluding mitochondrial and ribosomal protein genes. This analysis identified eight distinct cell clusters; the marker genes for each cluster were identified with Seurat and used to determine cell types. Differential expression was analyzed by comparing UMI gene counts between the patient and the control for each cluster, with the MAST approach (Finak et al., 2015). Genes with a p -value $< 10^{-25}$ for differential expression were analyzed in more detail. For each selected gene, cells in which the expression of the gene was detectable were counted for the index case and the control in each cluster, to reduce the dropout bias inherent to droplet scRNA approaches. The number of cells expressing the gene was normalized according to the number of cells in each cluster and the fold-difference in expression was calculated by comparing the index case and the control. For the figures, cluster annotations and the levels of expression of genes of interest were projected onto the UMAP clustering, but with the cells of the patient and the control shown separately.

Stimulation of NK cells *ex vivo*

PBMCs from five healthy donors including a travel control, the T-bet wt/m mother, the T-bet wt/wt brother and the T-bet m/m P were left untreated or stimulated with IL-12 (Miltenyi

Biotech), IL-15 (Miltenyi Biotec) and IL-18 (MBL/CliniSciences) for 18 h. Cells were treated with GolgiPlug and GolgiStop (BD Biosciences), and stained with anti-CD107a-PE antibody (Thermo Fisher Scientific) 4 h before harvest. Cells were harvested and stained with eFluor506 live-dead reagents (Thermo Fisher) and then with surface Abs, including anti-CD1a-FITC (BioLegend), anti-CD3-FITC (Thermo Fisher Scientific), anti-CD5-FITC (Thermo Fisher Scientific), anti-CD14-FITC (Miltenyi Biotec), anti-CD19-FITC (BioLegend), anti-CD34-FITC (BioLegend), anti-CD123-FITC (BioLegend), anti-CD203c (BioLegend), anti-CD303-FITC (BioLegend), anti-FcεRIα-FITC (BioLegend), anti-TCRαβ-FITC (Thermo Fisher Scientific), anti-TCRγδ-FITC (BioLegend), anti-CD94-PerCP-Vio700 (Miltenyi Biotec), anti-CD127-PE-Cy7 (Thermo Fisher Scientific), anti-NKp46-APC (BD Biosciences), anti-CD7-BV711 (BD Biosciences), anti-CD56-BV786 (BD Biosciences), anti-CD16-BUV737 (BD Biosciences), and anti-CD45-BUV805 (BD Biosciences) antibodies. All the markers targeted by FITC-conjugated Abs were considered to be Lineage-specific markers (Lin). Cells were fixed and permeabilized (Thermo Fisher Scientific) and subjected to intracellular staining with anti-granzyme B-PE-CF594 (BD Biosciences), anti-EOMES-APC-eFluor780 (Thermo Fisher Scientific), anti-perforin-BV421 (BD Biosciences), anti-TNF-α-BV605 (BioLegend) and anti-IFN-γ-BUV395 (BD Biosciences) antibodies. ICS and surface staining were analyzed with an LSRFortessa flow cytometer (BD Biosciences).

CD4⁺ T-cell isolation and functional characterization *ex vivo* and T_H differentiation *in vitro*

PBMCs from healthy donors and P were incubated with mAbs against CD4, CD45RA, CCR7, CXCR5, CD127 and CD25. Naïve and memory CD4⁺ T cells were isolated by first excluding Tregs (CD25^{hi}CD127^{lo}) and then sorting CD4⁺CD45RA⁺CCR7⁺CXCR5⁻ and CD4⁺CD45RA⁻CCR7[±] cells, respectively. Isolated naïve and memory CD4⁺ T cells were then

cultured in 96-well round-bottomed well plates (30-40 x10³ cells/well) with T-cell activation and expansion (TAE) beads (anti-CD2/CD3/CD28; Miltenyi Biotech) alone (T_H0) or under T_H1 (50 ng/mL IL-12), T_H2 (100 U/mL, IL-4), T_H9 (2.5 ng/mL TGF-β, 100 U/mL IL-4), or T_H17 (2.5 ng/mL TGF-β, 50 ng/mL IL-1-β, 50 ng/mL IL-6, 50 ng/mL IL-21, 50 ng/mL IL-23, 50 ng/mL PGE2) polarizing conditions. After 5 days, supernatants were harvested and the production of IL-4, IL-5, IL-9, IL-10, IL-13, IL-17A, IL-17F, IFN-γ and TNF-β was assessed with cytometric bead arrays (Becton Dickinson); IL-22 secretion was measured by ELISA (eBioscience). For cytokine expression, activated CD4⁺ T cells were restimulated with PMA (100 ng/mL)/ionomycin (750 ng/mL) for 6 h, with brefeldin A (10 μg/mL) added after two hours. Cells were then fixed and the intracellular expression of IL-4, IL-9, IL-13, IL-10, IL-17A, IL-17F, IL-22, IL-21 and IFN-γ was determined.

Stimulation of PBMCs with live *M. bovis*-BCG or PMA/ionomycin

Ten healthy donors and four BCG-vaccinated healthy donors were recruited at the Rockefeller University (New York, USA). Three local controls, one IL-12Rβ1 m/m patient and the T-bet m/m P and his members of his family were recruited at Necker Hospital (Paris, France). PBMCs from these individuals were isolated and cryopreserved under the same conditions. We plated 200,000 cells per well in 96-well U-bottomed plates at a density of 1 x 10⁶ cells/ml. PBMCs from the T-bet m/m P, his T-bet wt/m mother, T-bet wt/wt brother, and the IL-12Rβ1-deficient patient were analyzed in technical duplicates. For each sample, cells were plated in the presence or absence of live *M. bovis*-BCG at a MOI=1 or 20, and in the presence and absence of recombinant IL-12 (500 pg/mL, R&D) or recombinant IL-23 (10 ng/mL, R&D). Golgiplug (BD Biosciences) was added to each well after 40 h of stimulation. Cells were also stimulated with 25 ng/mL PMA

and 500 nM ionomycin. Eight hours later, supernatants were harvested for cytokine determinations in a 13-plex Legendplex assay (BioLegend), and cells were collected by centrifugation for FACS staining. Cells were stained with the Zombie NIR Viability kit (BioLegend) and were then surface-stained with Abs including FcBlock (Miltenyi Biotec), anti-CD3-Alexa532 (Thermo Fisher Scientific), anti- $\gamma\delta$ TCR-FITC (Thermo Fisher Scientific), anti-V δ 2 TCR-APCFire750 (BioLegend), anti-CD56-BV605 (BioLegend), anti-CD4-BV750 (BD Biosciences), anti-CD8a-Pacific Blue (BioLegend), anti-V α 7.2 TCR-APC (BioLegend), anti-V α 24-J α 18 (iNKT)-PE/Cy7 (BioLegend), and anti-CD20-BV785 (BioLegend) antibodies. Cells were then fixed and permeabilized for staining for intracellular proteins with antibodies including FcBlock (Miltenyi Biotec), anti-IFN- γ -BV711 (BioLegend), anti-TNF- α -BV510 (BioLegend), anti-T-bet-PE (BioLegend), and anti-IL-10-PE/Dazzle594 (BioLegend) antibodies. Samples were then analyzed on an Aurora cytometer (Cytex). Flow data were analyzed with Cytobank. T-bet⁺ IFN- γ ⁺ double-positive cells were gated manually from the live single-lymphocyte population. These T-bet⁺ IFN- γ ⁺ double-positive cells were clustered with the viSNE algorithm, with CD3-Alexa532, $\gamma\delta$ TCR-FITC, V δ 2 TCR-APCFire750, CD56-BV605, CD4-BV750, CD8a-Pacific Blue, V α 7.2 TCR-APC, V α 24-J α 18 (iNKT)-PE/Cy7, CD20-BV785, TNF- α -BV510 and IL-10-PE/Dazzle594 (Amir et al., 2013). Automated viSNE clusters were plotted with tSNE1 and tSNE2. Clusters were then overlaid on manually gated immune cell subsets for illustration.

V δ 2 $\gamma\delta$ T cell stimulation

Lysates of *M. bovis*-BCG was prepared and provided by Dr. Carl F. Nathan. PBMCs from healthy donors, local control donors, BCG-vaccinated healthy donors, IL-12R β 1 m/m patients, the T-bet m/m P and his relatives were resuspended at a density of 1×10^6 cells/mL. We plated 200 μ L

cells per well for each condition, in a 96-well U-bottomed plate. We added BCG lysate to each well at a final concentration of 5 $\mu\text{g}/\text{mL}$. Recombinant IL-2 (Roche) was added to a final concentration of 10 U/mL. Fresh medium and IL-2 were added to the culture every three to four days. Eleven days after stimulation, the cells were fully confluent in the 96-well plate. Cells were then transferred to a 48-well plate and each well was topped up to 500 μL per well with medium. After 14 days of stimulation, the cells were stained with FcBlock (Miltenyi Biotec), Zombie-NIR live/dead (BioLegend), anti-CD3-Alexa532 (Thermo Fisher Scientific), anti- $\gamma\delta$ TCR-FITC (Thermo Fisher Scientific), anti-V δ 2 TCR-APCFire750 (BioLegend), anti-CD56-BV605 (BioLegend), anti-CD4-BV750 (BD Biosciences), anti-CD8a-BV510 (BioLegend), anti- β 11 TCR-APC (Miltenyi Biotec), anti-CD161-PE (BioLegend), anti- V α 7.2 TCR-BV711 (BioLegend), anti- V α 24-J α 18 (iNKT)-PE/Cy7 (BioLegend), anti-V δ 1-Vioblue (Miltenyi Biotec), anti-CD16-BV650 (BioLegend), anti-CD20-BV785 (BioLegend), anti- $\alpha\beta$ TCR-Alexa700 (BioLegend) antibodies and analyzed by flow cytometry on an Aurora cytometer (Cytex).

Isolation and screening of CD4⁺ T cell lines

The T-cell clone experiment was performed as previously described (Geiger et al., 2009). In brief, CCR6⁺ and CCR6⁻ CD4⁺ memory T cells were sorted from CD14⁻ PBMCs with a FACS Aria (BD Biosciences), excluding CD45RA⁺CCR7⁺ naïve cells, and CD25⁺, CD19⁺, and CD8⁺ cells. Sorted T cells (500 cells/well) were polyclonally stimulated with 1 $\mu\text{g}/\text{mL}$ PHA (Remel) in the presence of irradiated (45 Gy) allogeneic feeder cells (10^4 per well) and IL-2 (500 IU/mL) in RPMI complete medium. After expansion for at least 20 days, the T-cell lines were analyzed by surface or intracellular staining with the following monoclonal antibodies: anti-CCR6-PE (BD Biosciences; clone: 11A9); anti-CXCR3-APC (BD Biosciences; clone: 1C6); anti-IFN- γ -FITC or

anti-IFN- γ -PE (BD Biosciences, clone: B27); anti-IL-17A-eFluor660 FITC (eBiosciences, clone: eBio64DEC17); anti-IL-4-PE (BD Biosciences, clone: MP4-25D2); anti-IL-22-PerCP-eFluor-710 (Thermo Fisher Scientific, clone: 22URTI). For identification of the antigen-responding T-cell clones, the T-cell lines were also screened by culturing thoroughly washed cells (2.5×10^5 cells/well) with autologous irradiated B cells (2.5×10^4 cells/well), with or without a three-hour pulse of the following antigens: *M. tuberculosis* peptide pool (0.5 $\mu\text{g}/\text{mL}/\text{peptide}$, comprising 207 15-mer peptides), BCG peptide pool (0.5 $\mu\text{g}/\text{mL}/\text{peptide}$, comprising 211 15-mer peptides), HCMV peptide pool (0.5 $\mu\text{g}/\text{mL}/\text{peptide}$, comprising 76 15-20-mer peptides), EBV peptide pool (0.5 $\mu\text{g}/\text{mL}/\text{peptide}$, comprising 46 15-20-mer peptides), Influenza virus HA peptide pool (2 $\mu\text{g}/\text{mL}/\text{peptide}$, comprising 351 15-mer peptides), *Candida albicans* peptide pool (0.5 $\mu\text{g}/\text{mL}/\text{peptide}$, comprising 252 15-mer peptides) or tetanus toxoid peptide pool (1 $\mu\text{g}/\text{mL}/\text{peptide}$, comprising 125 15-20-mer peptides). These peptide pools were kindly provided by Cecilia Lindestam Arlehamn and Alessandro Sette at the La Jolla Institute for Immunology (Lindestam Arlehamn et al., 2016). Proliferation was assessed on day 4, after incubation for 16 h with 1 $\mu\text{Ci}/\text{mL}$ [^3H]-thymidine (GE Healthcare). The concentrations of cytokines in the culture supernatants produced by the antigen-responding T-cell clones were measured after 48 h of stimulation with cytometric bead arrays (eBioscience).

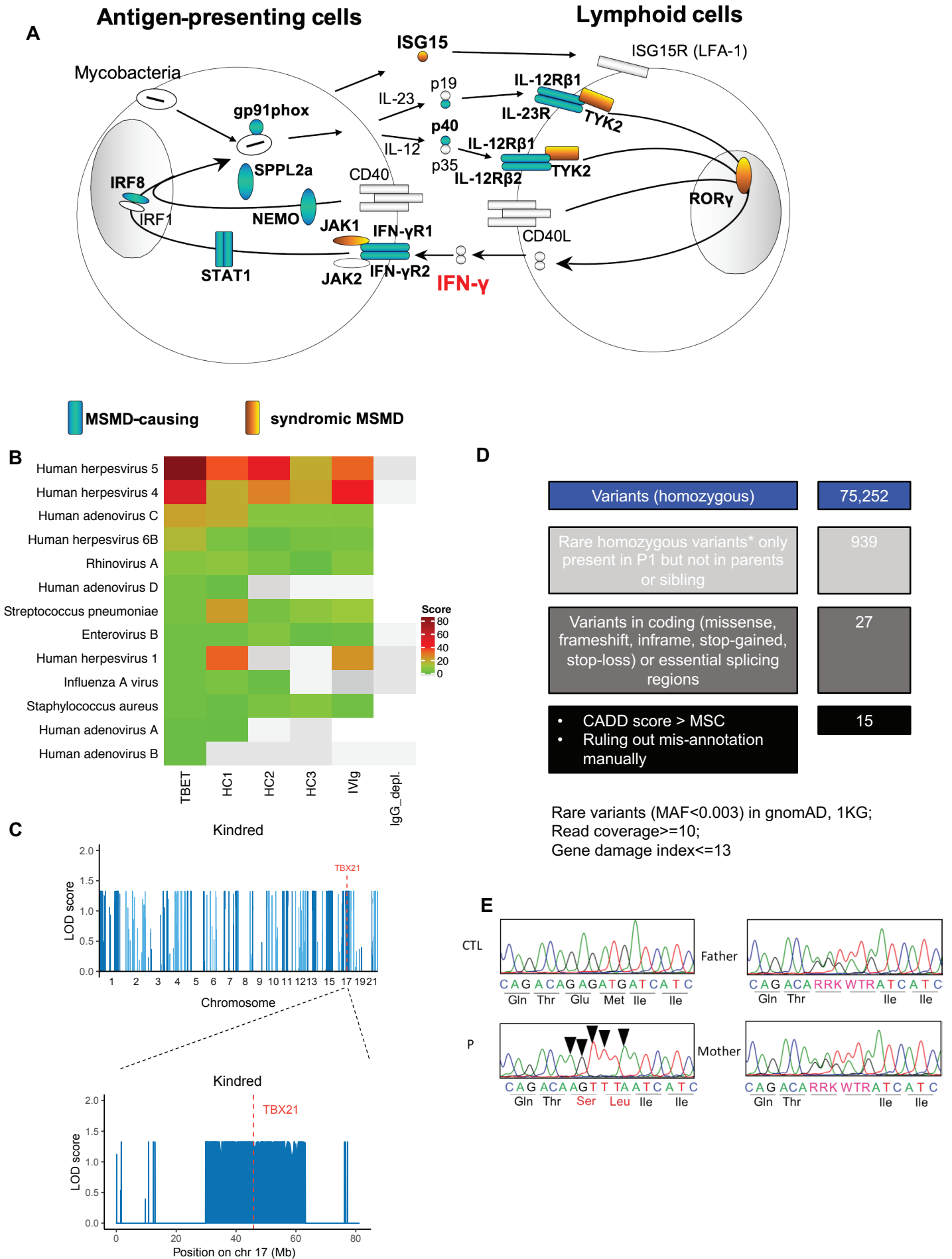


Figure S1

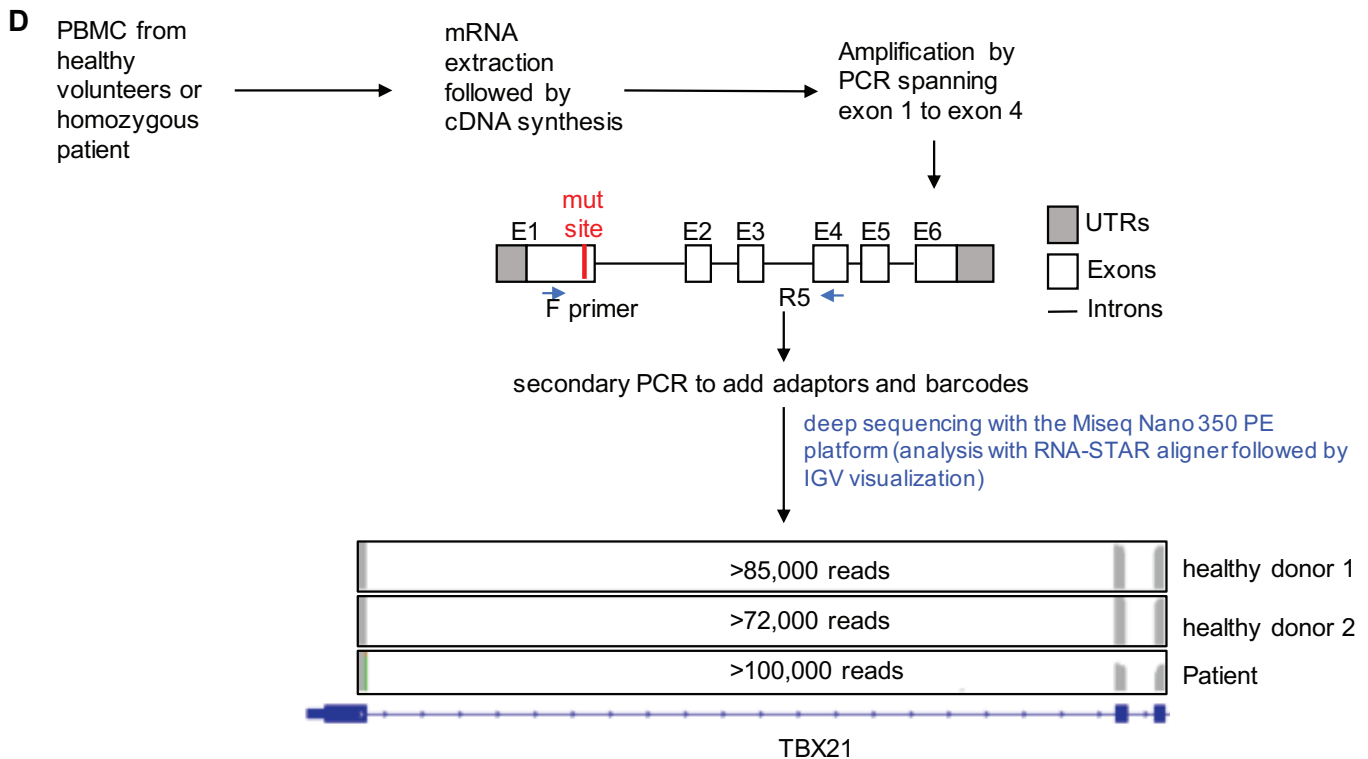
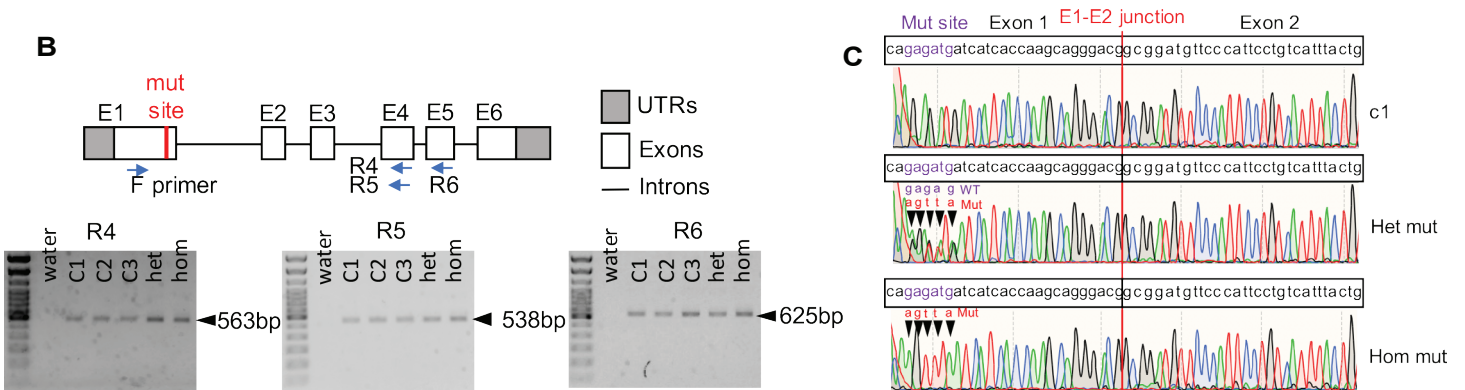
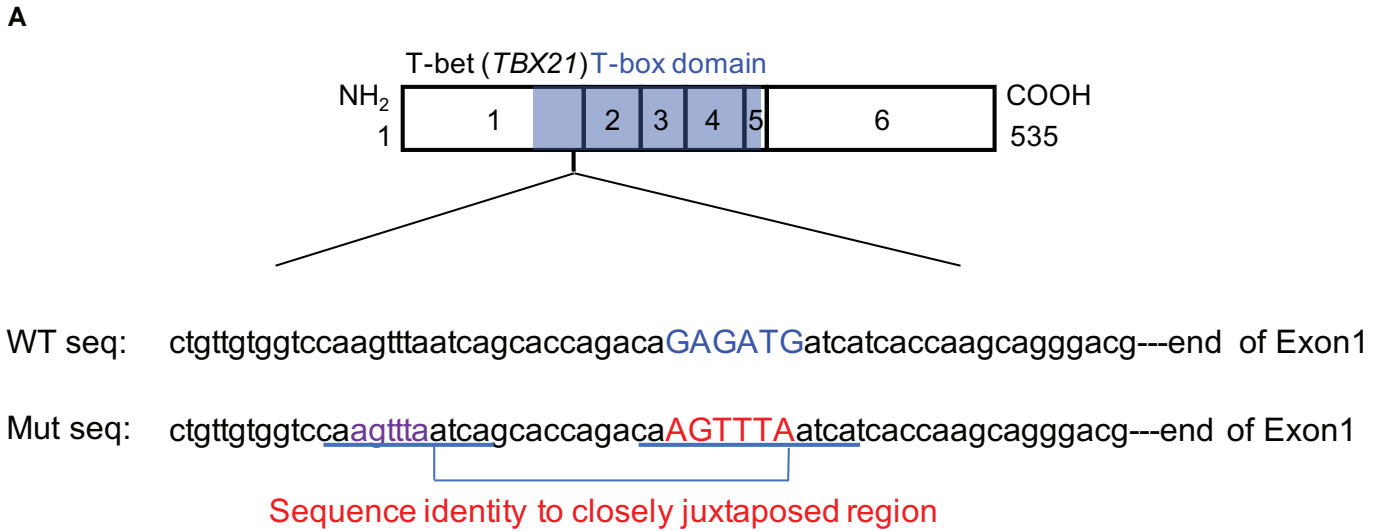


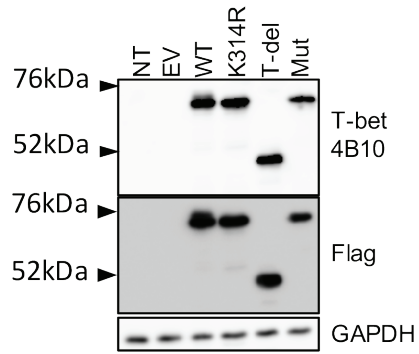
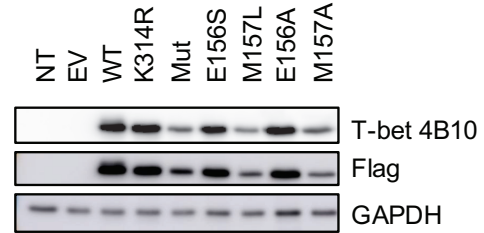
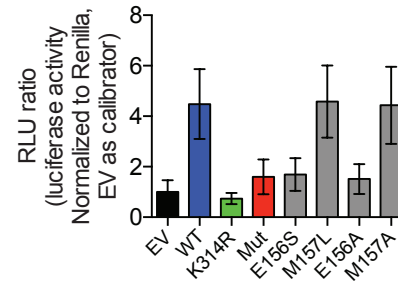
Figure S2

A**T-box family paralogs**

sp|O43435|TBX1_HUMAN
 sp|Q13207|TBX2_HUMAN
 sp|O15119|TBX3_HUMAN
 sp|P57082|TBX4_HUMAN
 sp|Q99593|TBX5_HUMAN
 sp|O95947|TBX6_HUMAN
 sp|O75333|TBX10_HUMAN
 sp|Q96SF7|TBX15_HUMAN
 sp|O95935|TBX18_HUMAN
 sp|O60806|TBX19_HUMAN
 sp|Q9UMR3|TBX20_HUMAN
 sp|Q9Y458|TBX22_HUMAN
 sp|O95936|EOMES_HUMAN
 sp|Q8IWI9|MGAP_HUMAN
 sp|O15178|TBXT_HUMAN
 sp|Q16650|TBR1_HUMAN
 sp|Q9UL17|TBX21_HUMAN

Amino acids

G**T**EMIVTK
 G**T**EMVITK
 G**T**EMVITK
 G**T**EM**I**ITK
 G**T**EM**I**ITK
 G**T**EM**I**ITK
 G**T**EMIVTK
 G**T**EM**I**ITK
 G**T**EM**I**ITK
 G**T**EM**I**ITK
 G**T**EM**I**ITK
 T**N**EMIVTK
 G**T**EM**I**ITK
 G**T**EM**I**ITK
 Q**T**EM**I**ITK
 S**T**EM**I**ITK
 T**N**EMIVTK
 Q**T**EM**I**ITK
 Q**T**EM**I**ITK
 . ** : : **

B**C****D**

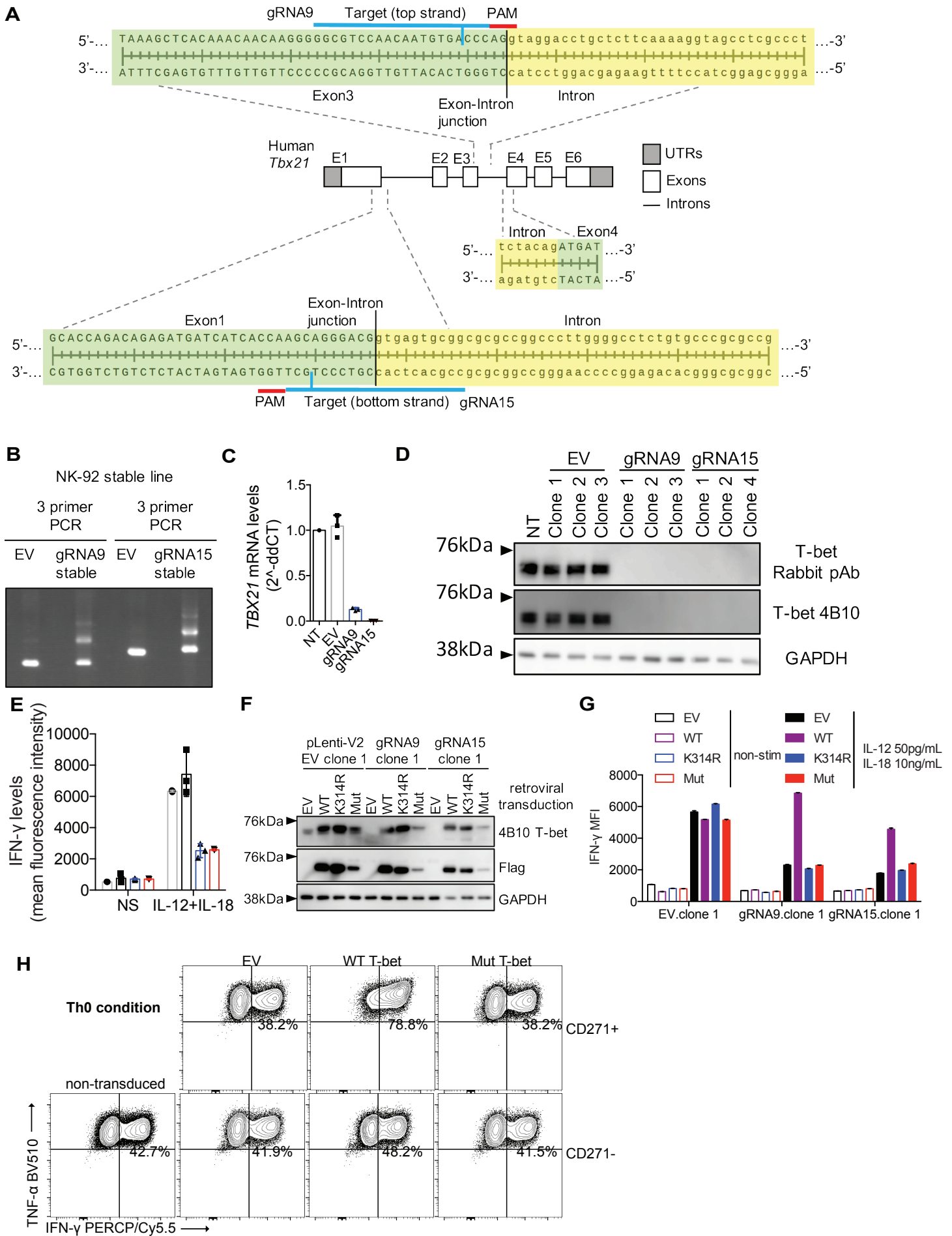


Figure S4

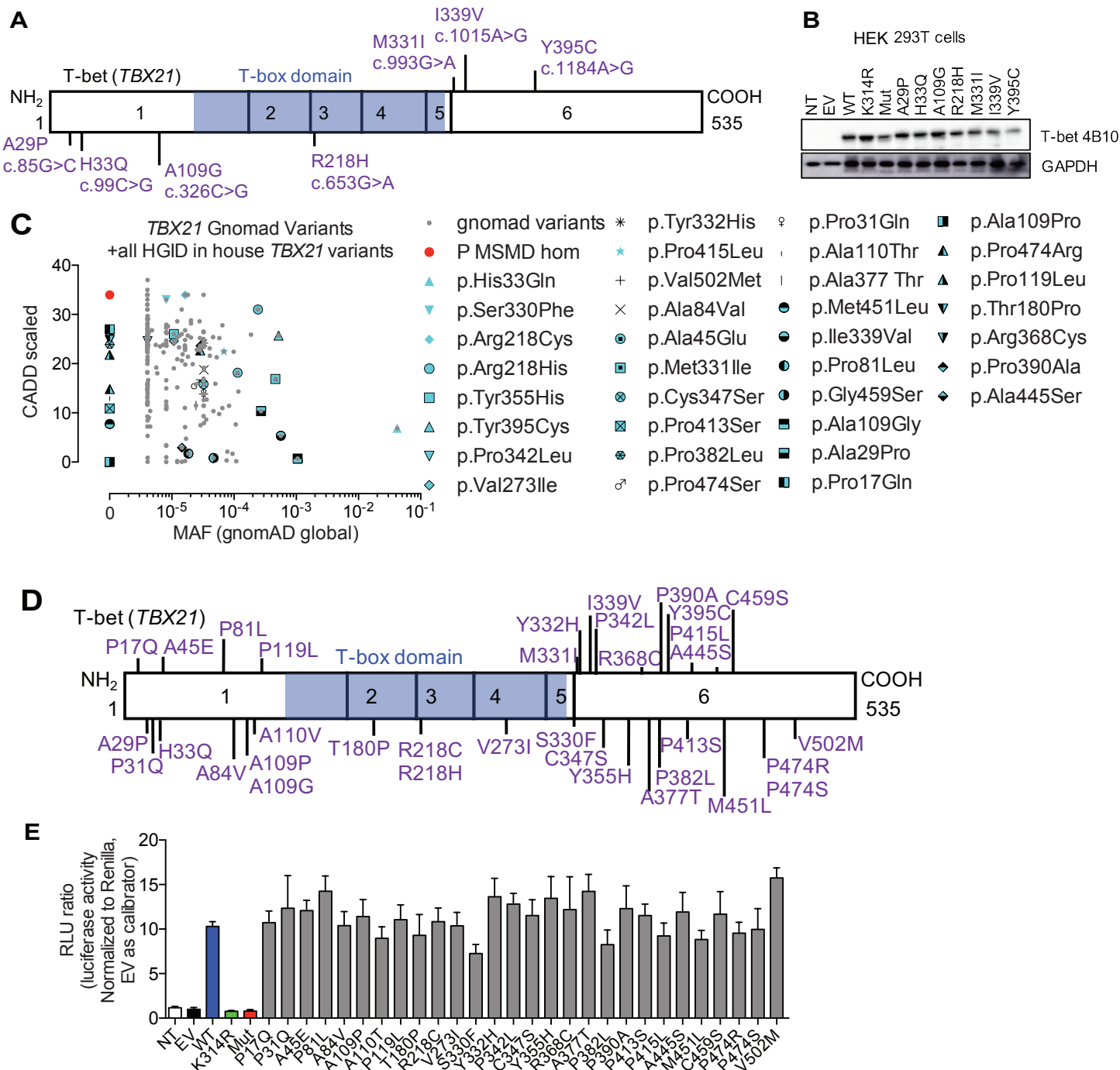


Figure S5

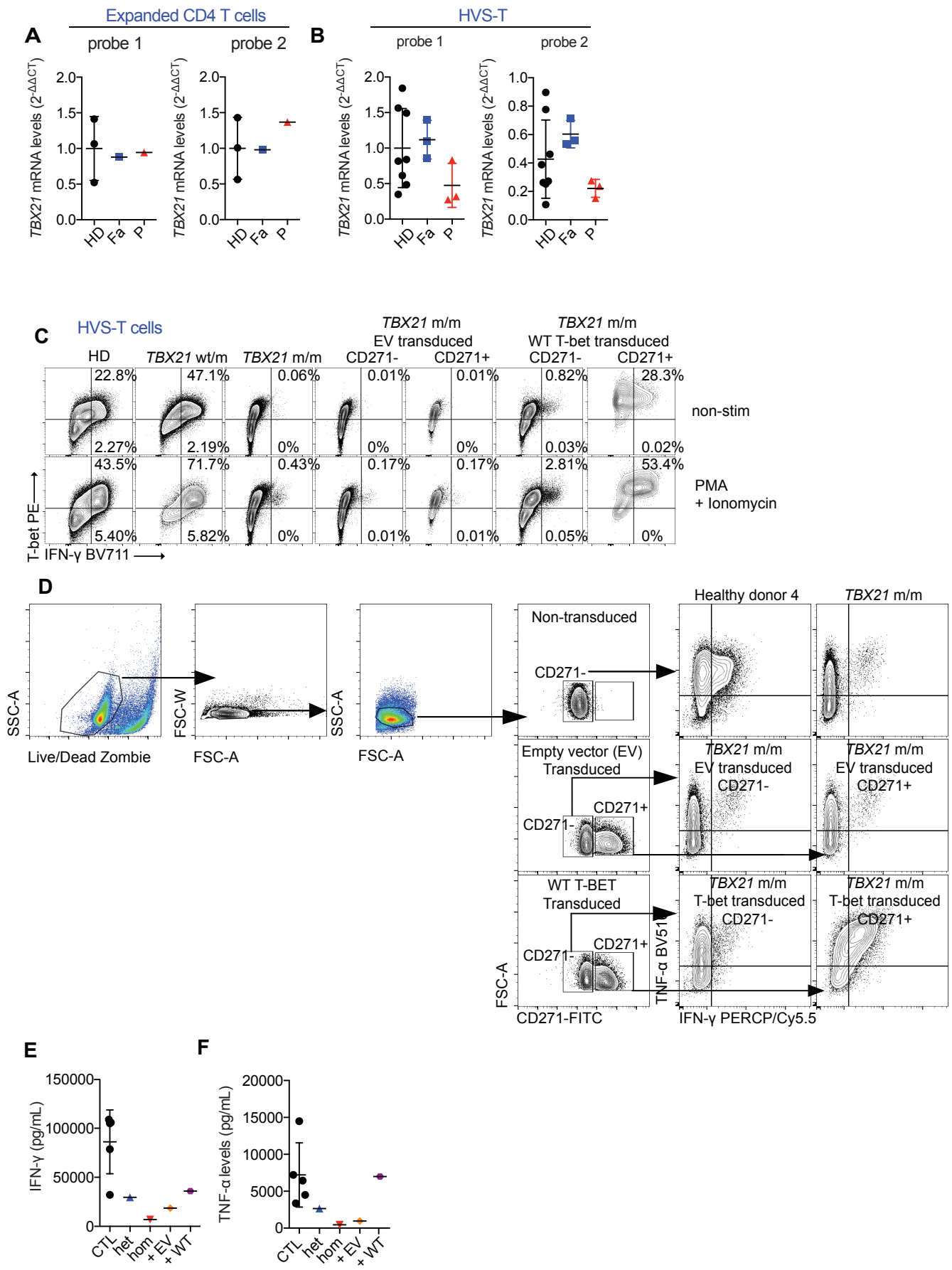


Figure S6

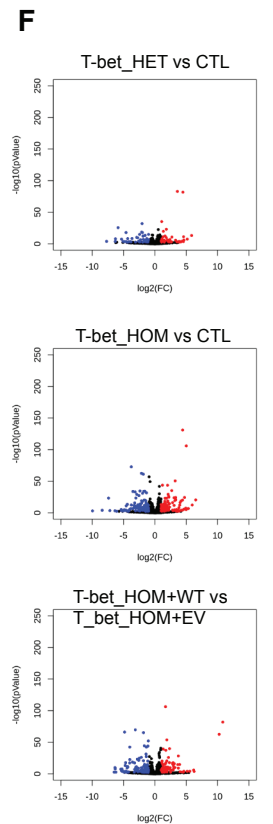
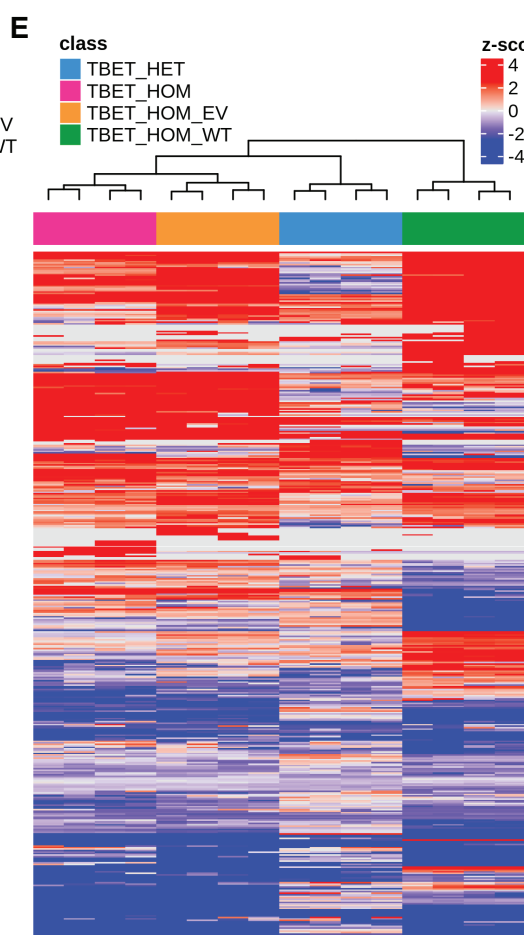
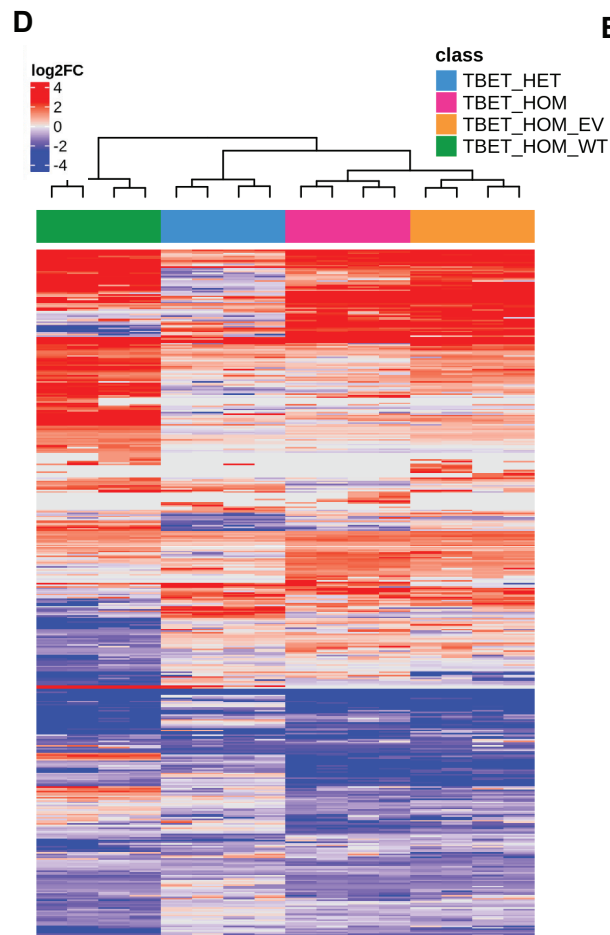
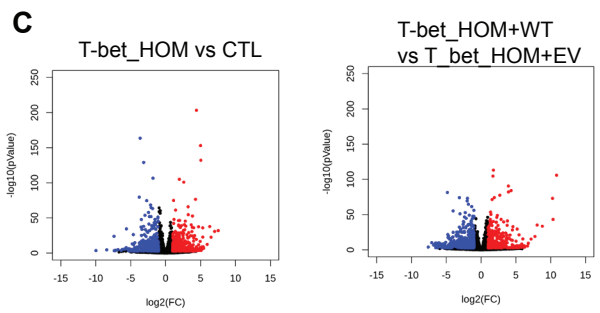
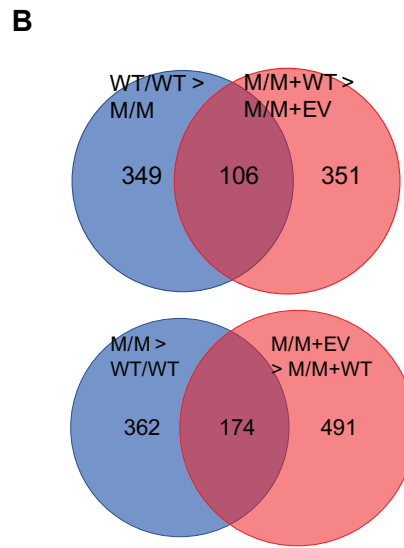
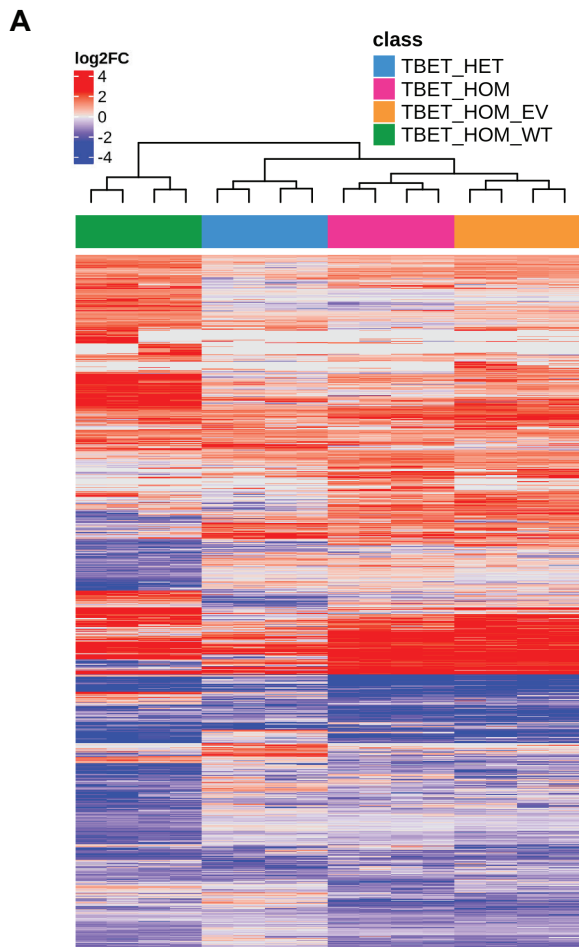


Figure S7

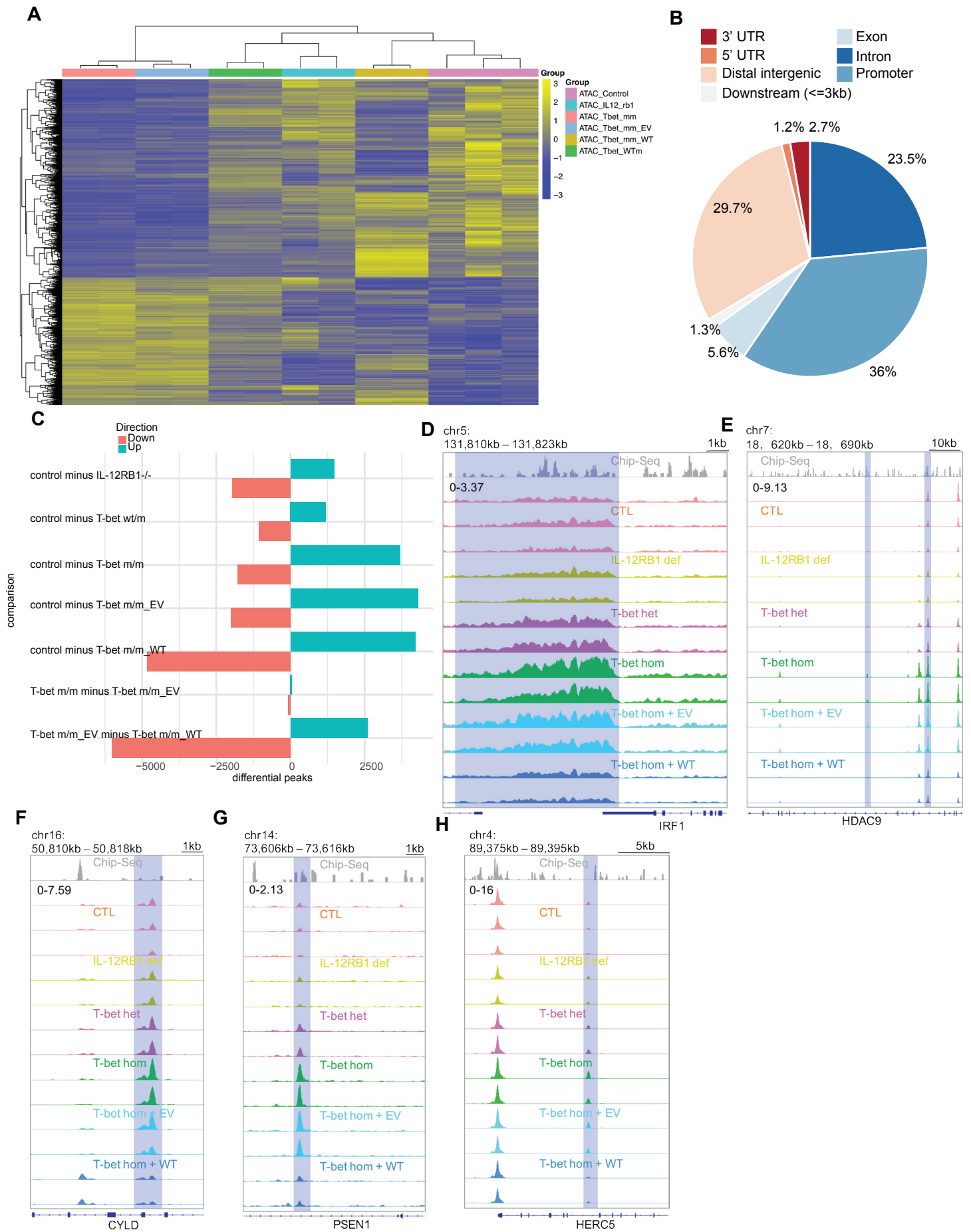
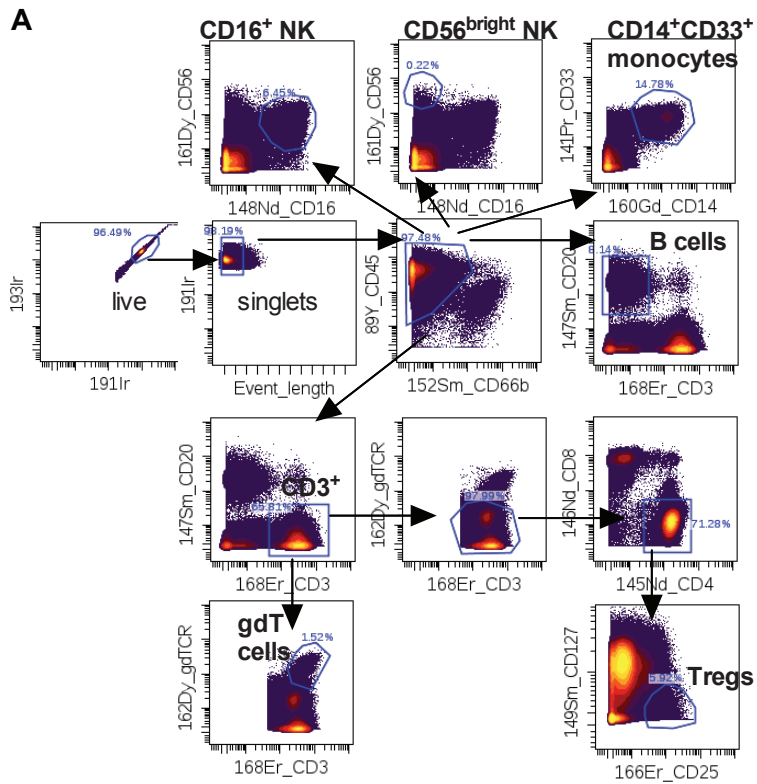




Figure S9



B
gated on CD45⁺CD66b⁻ live singlets

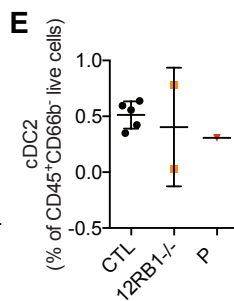
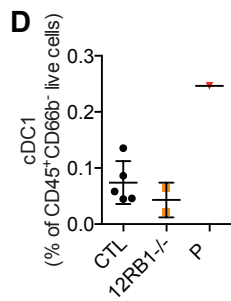
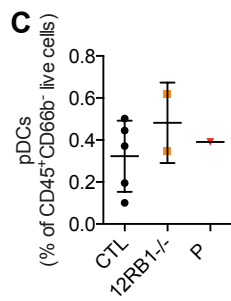
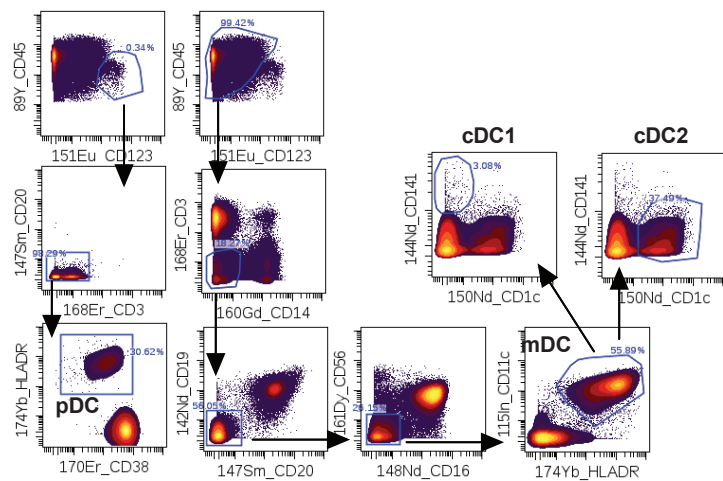


Figure S10

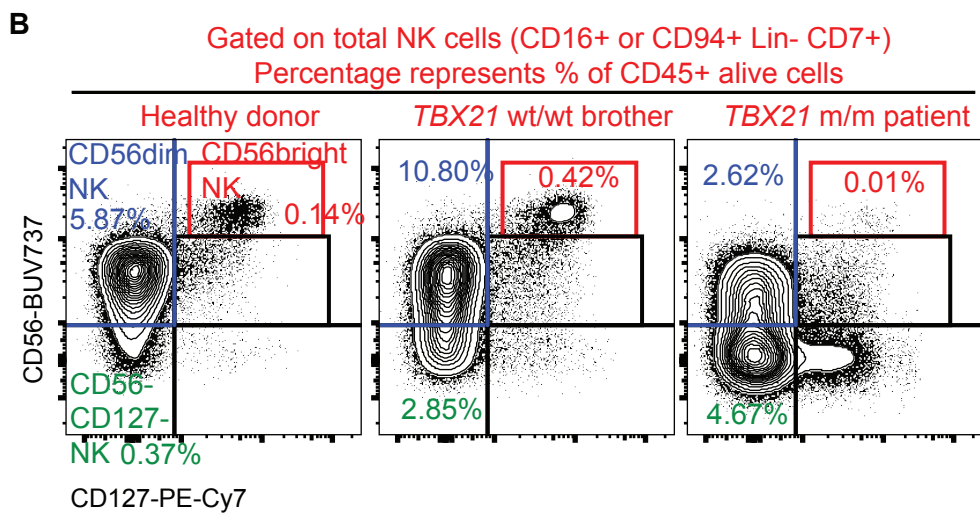
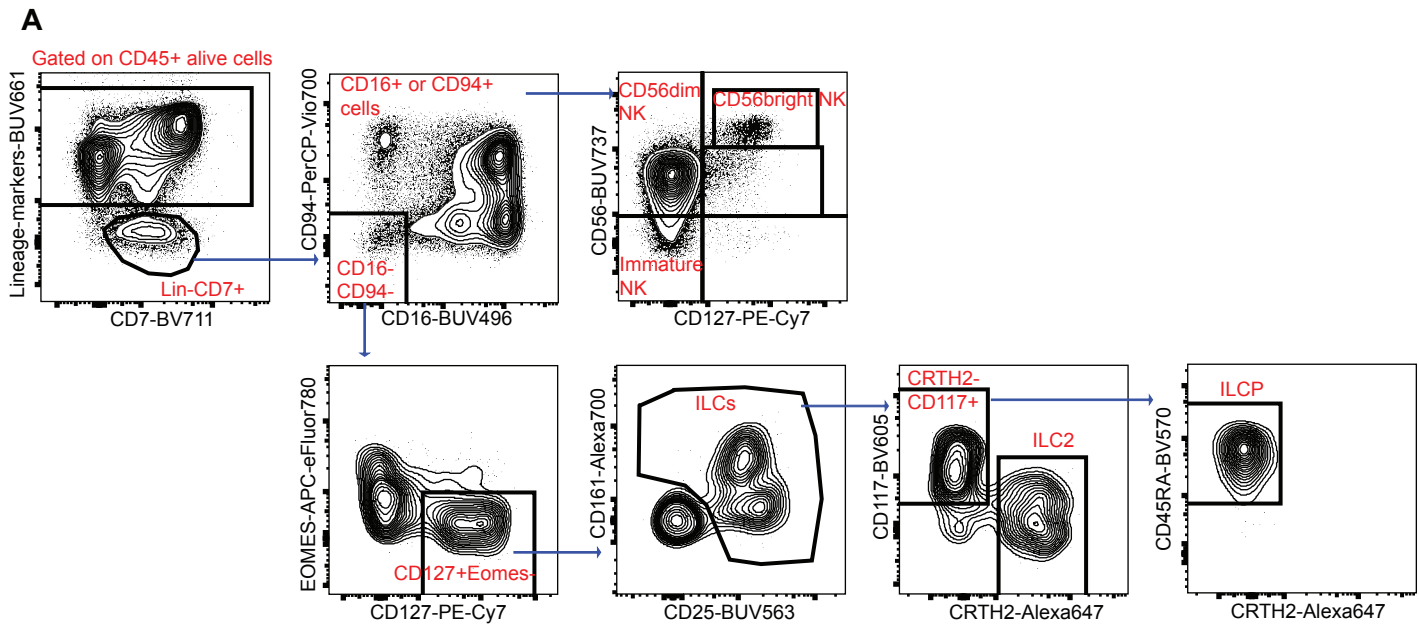


Figure S11

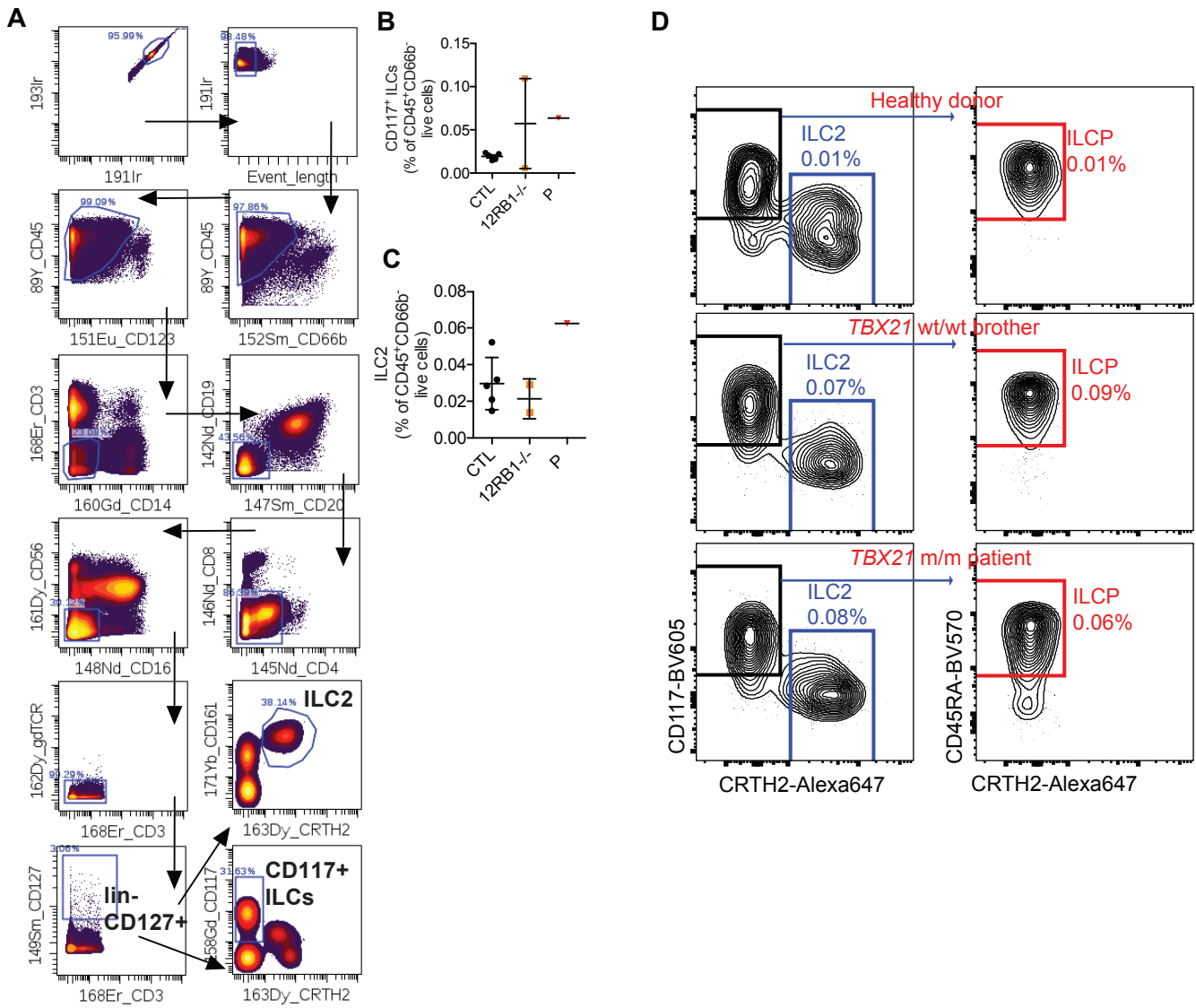


Figure S12

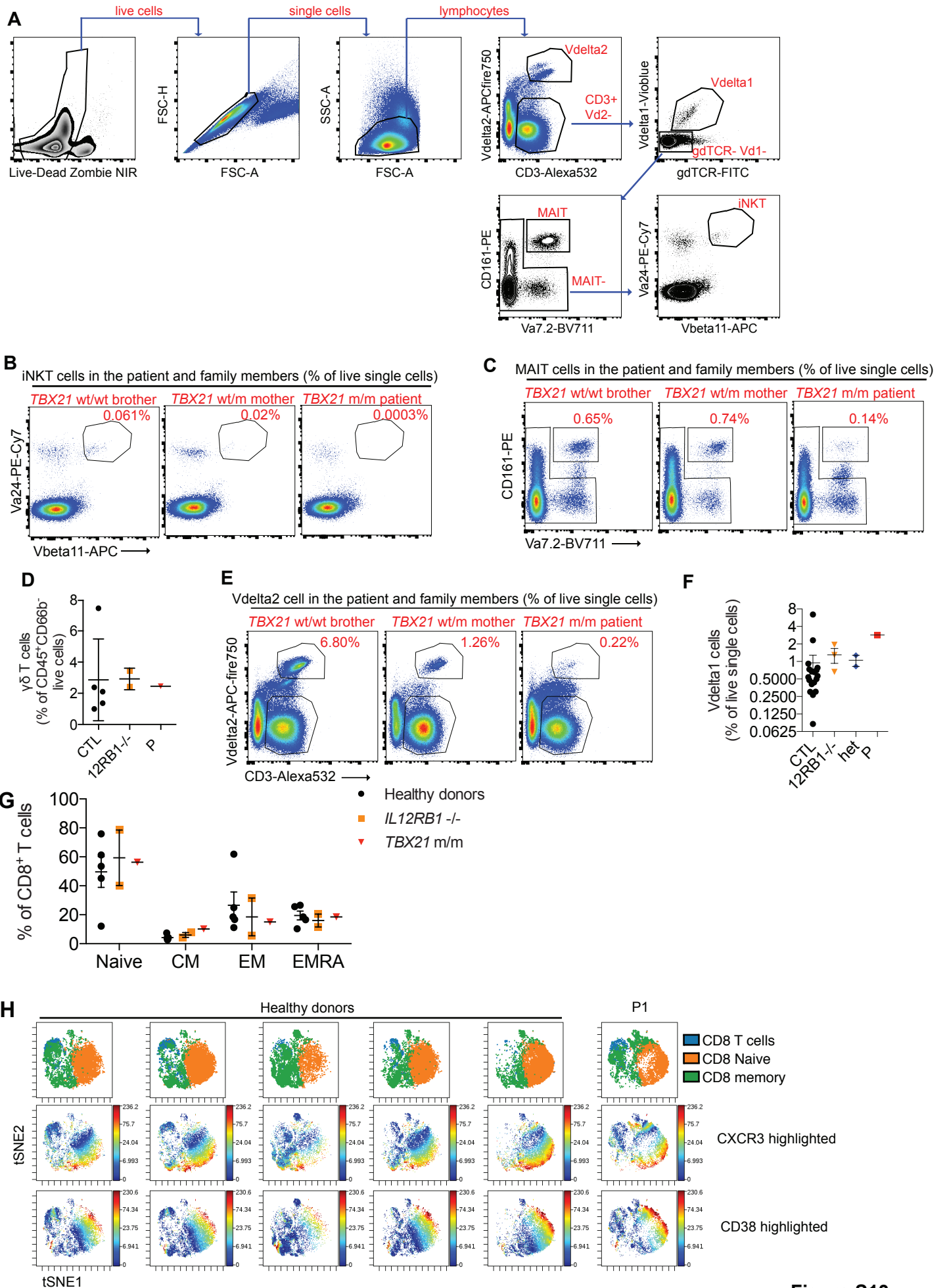


Figure S13

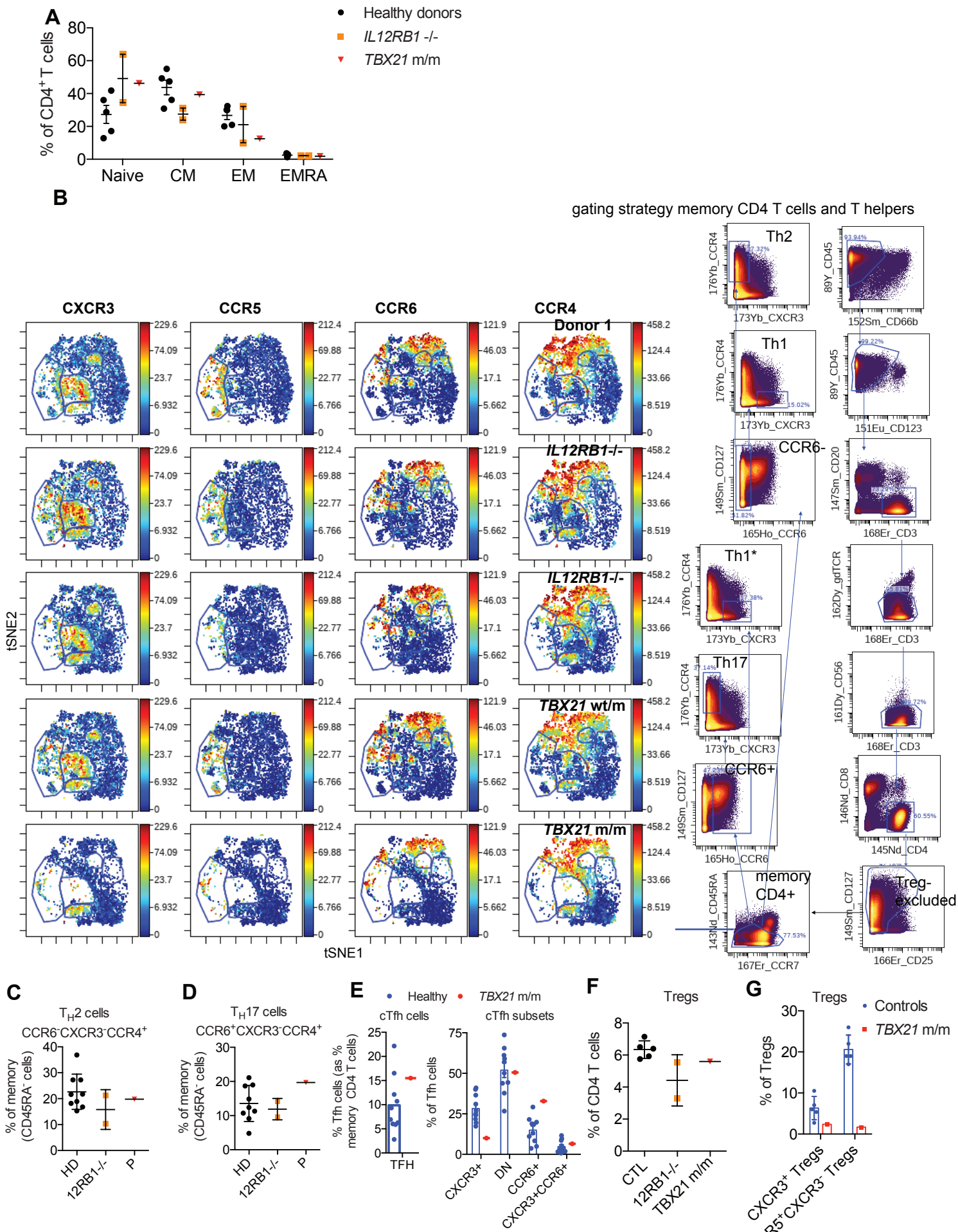


Figure S14

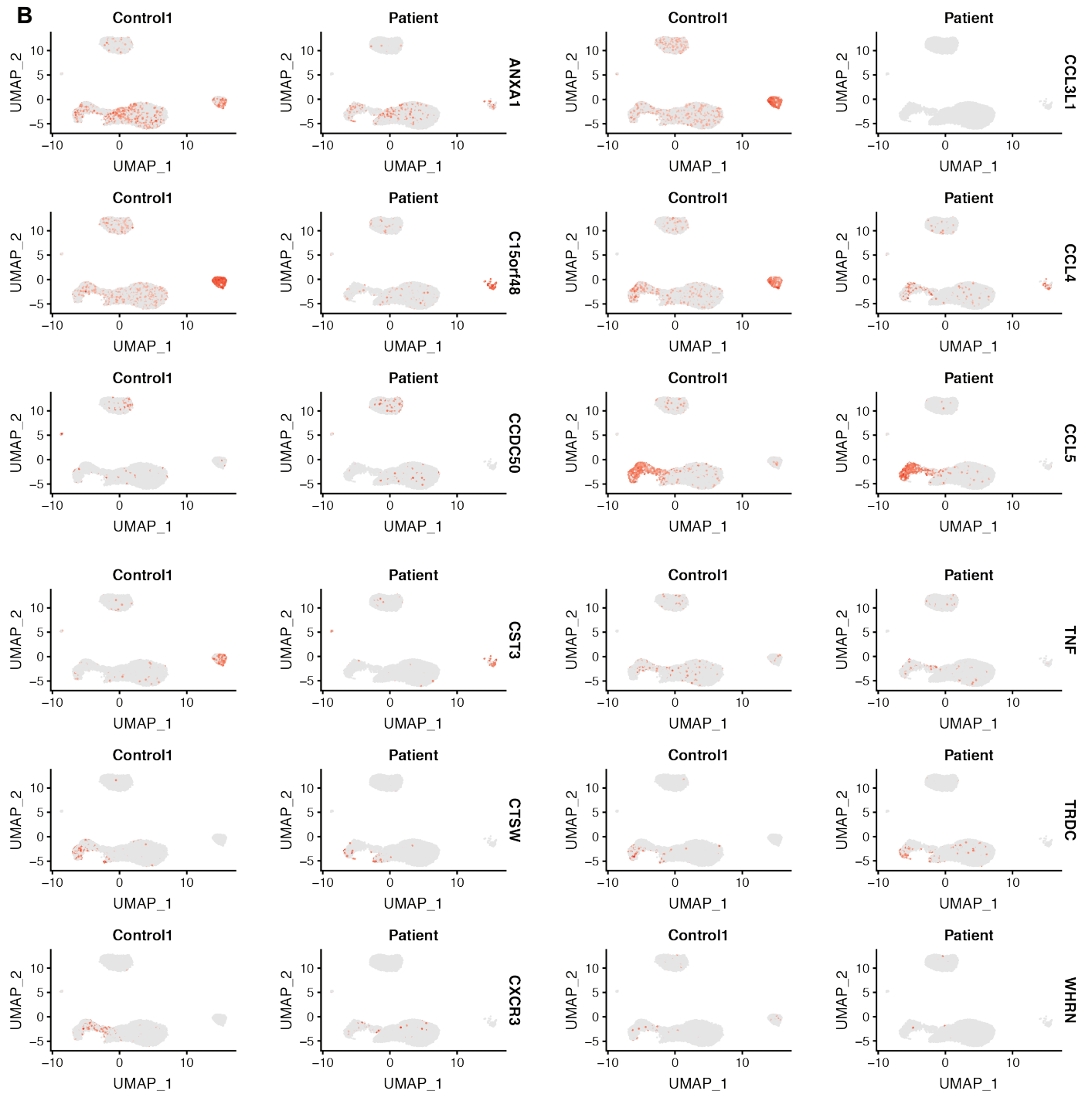
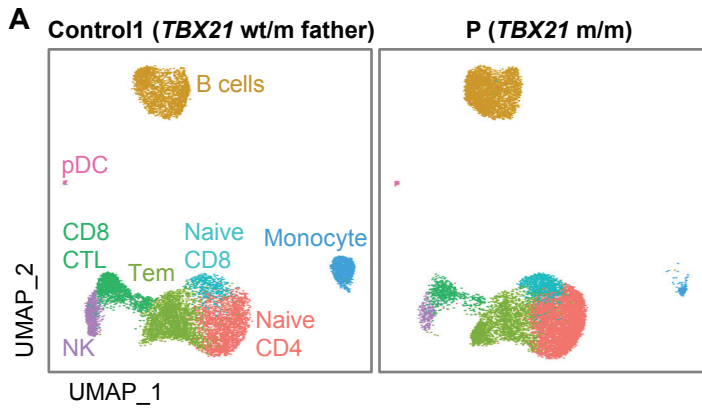


Figure S15

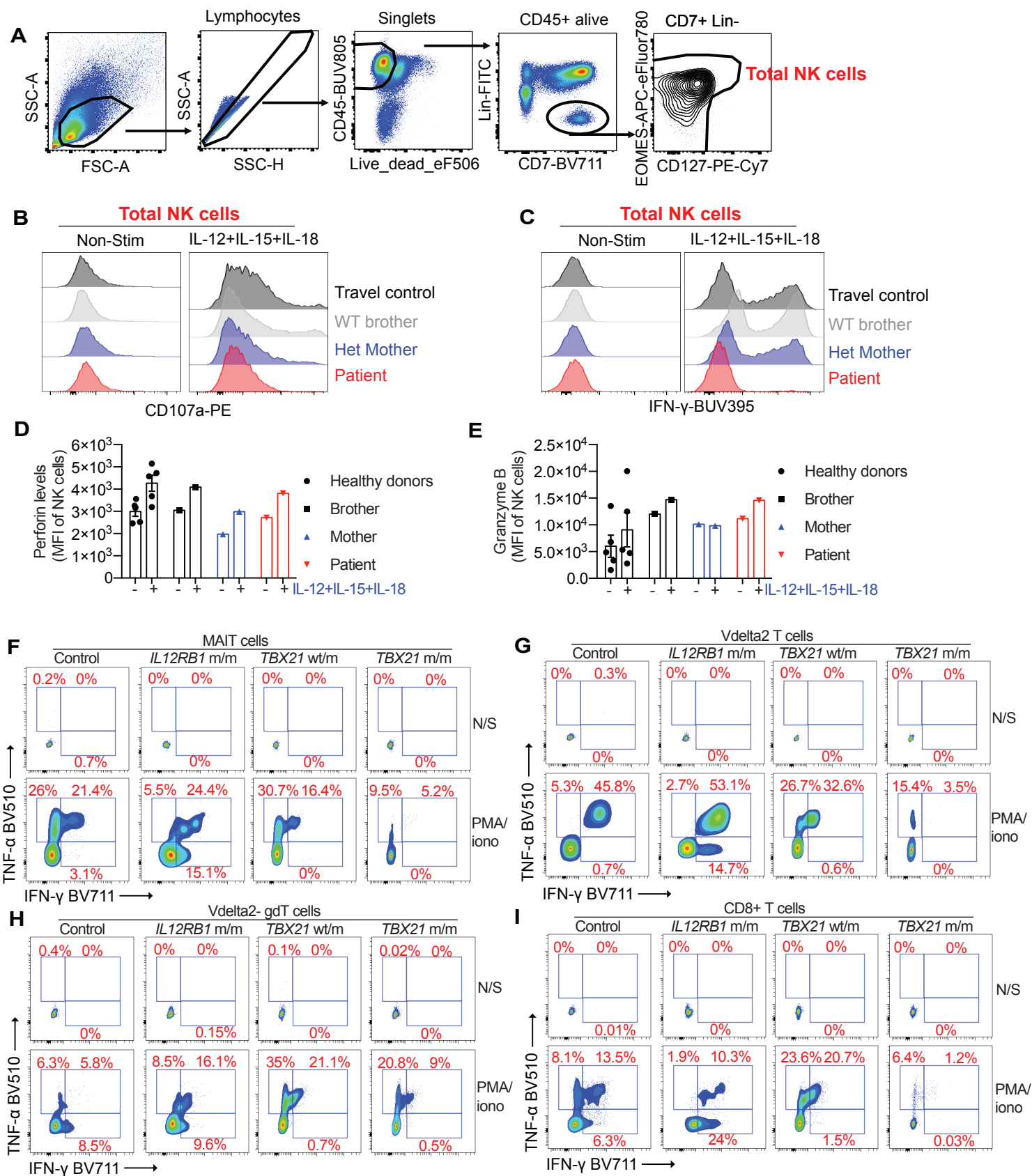


Figure S16

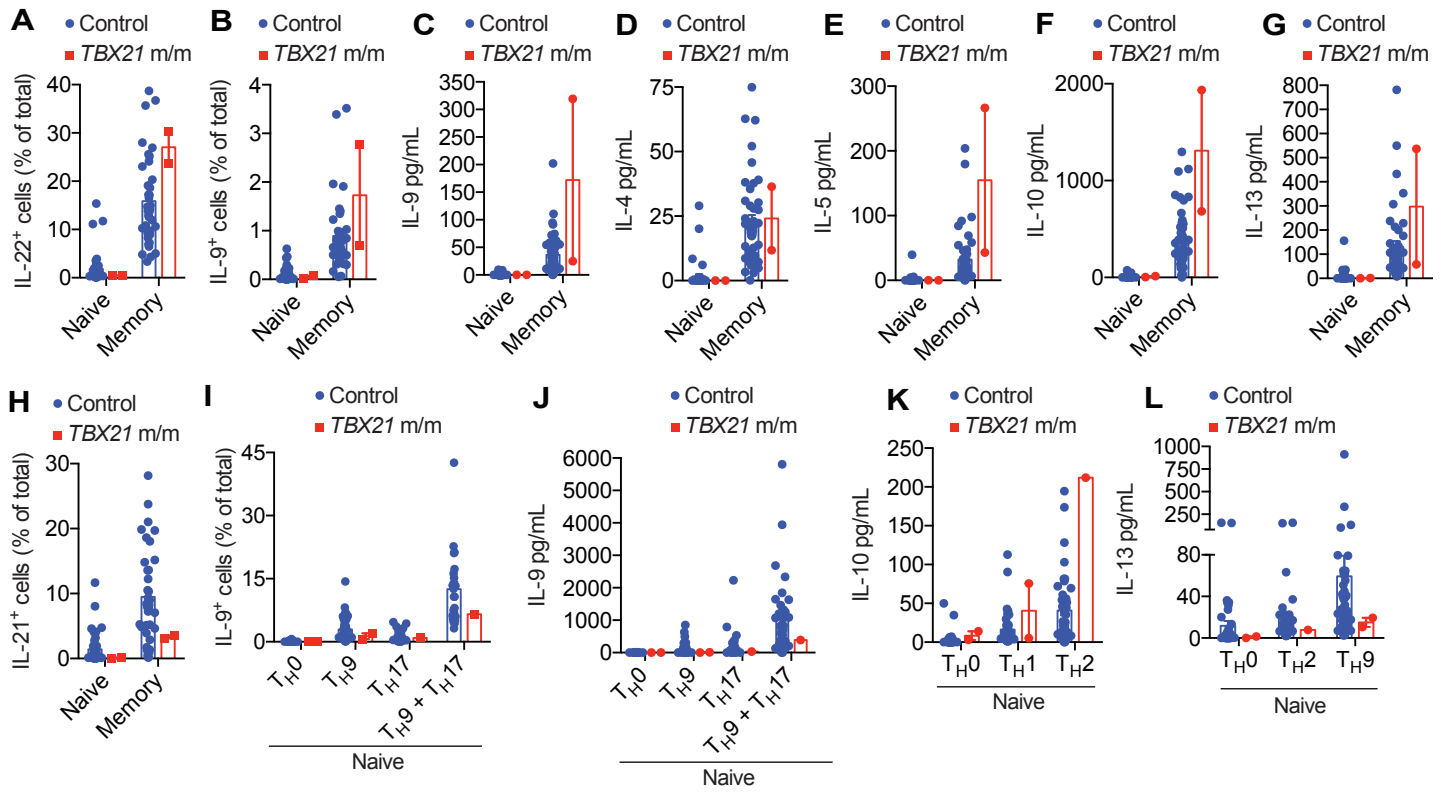


Figure S17

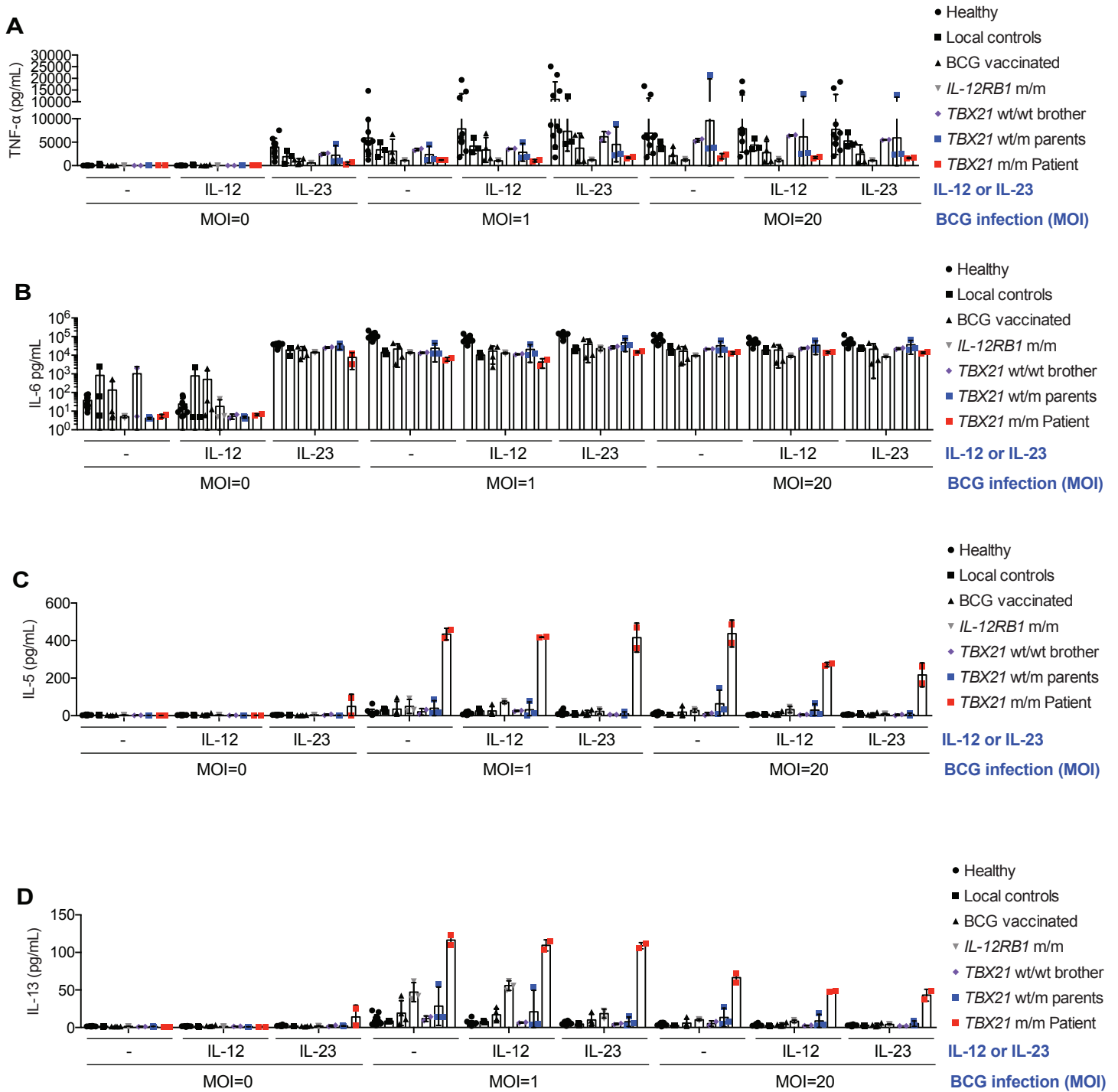


Figure S18

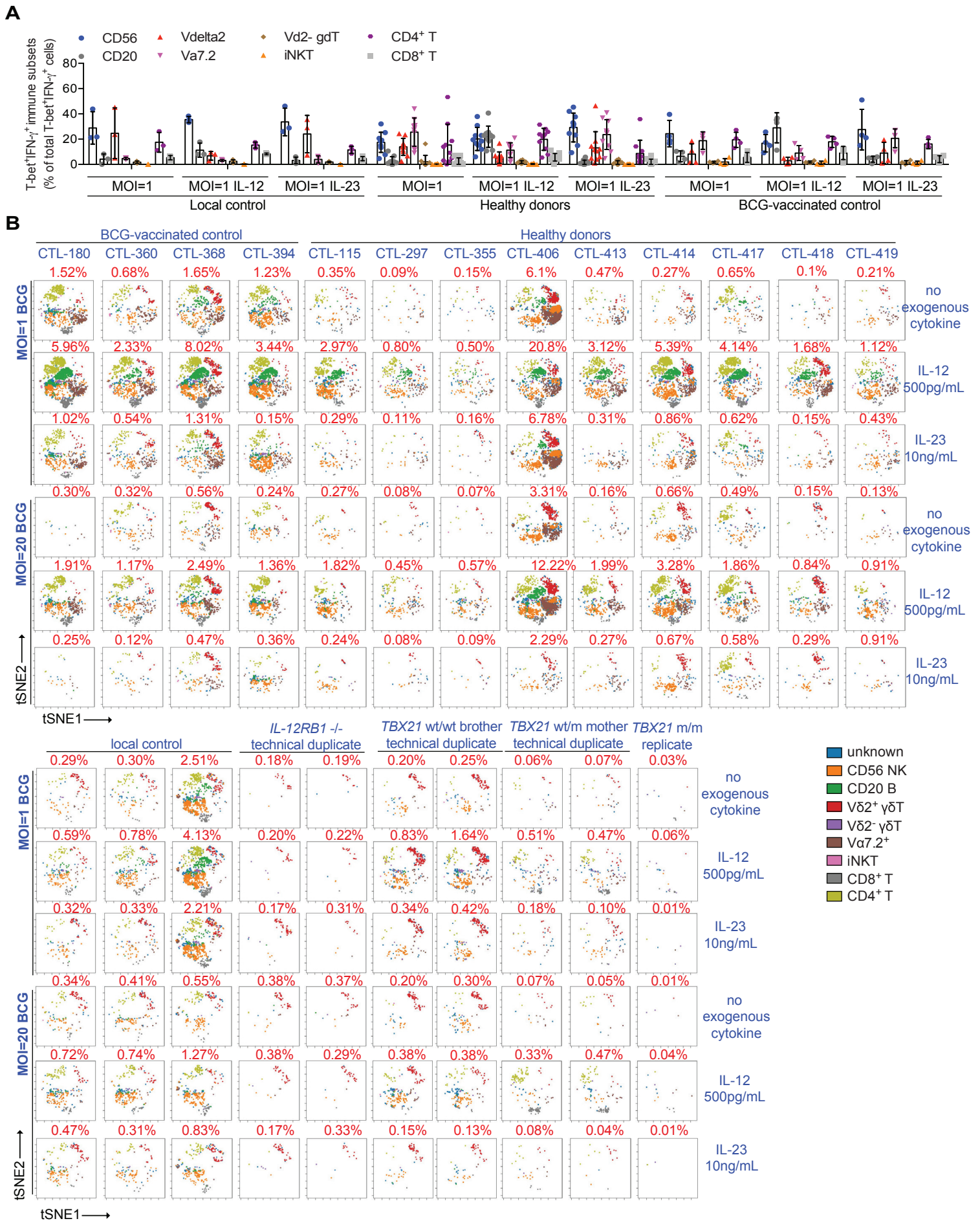


Figure S20

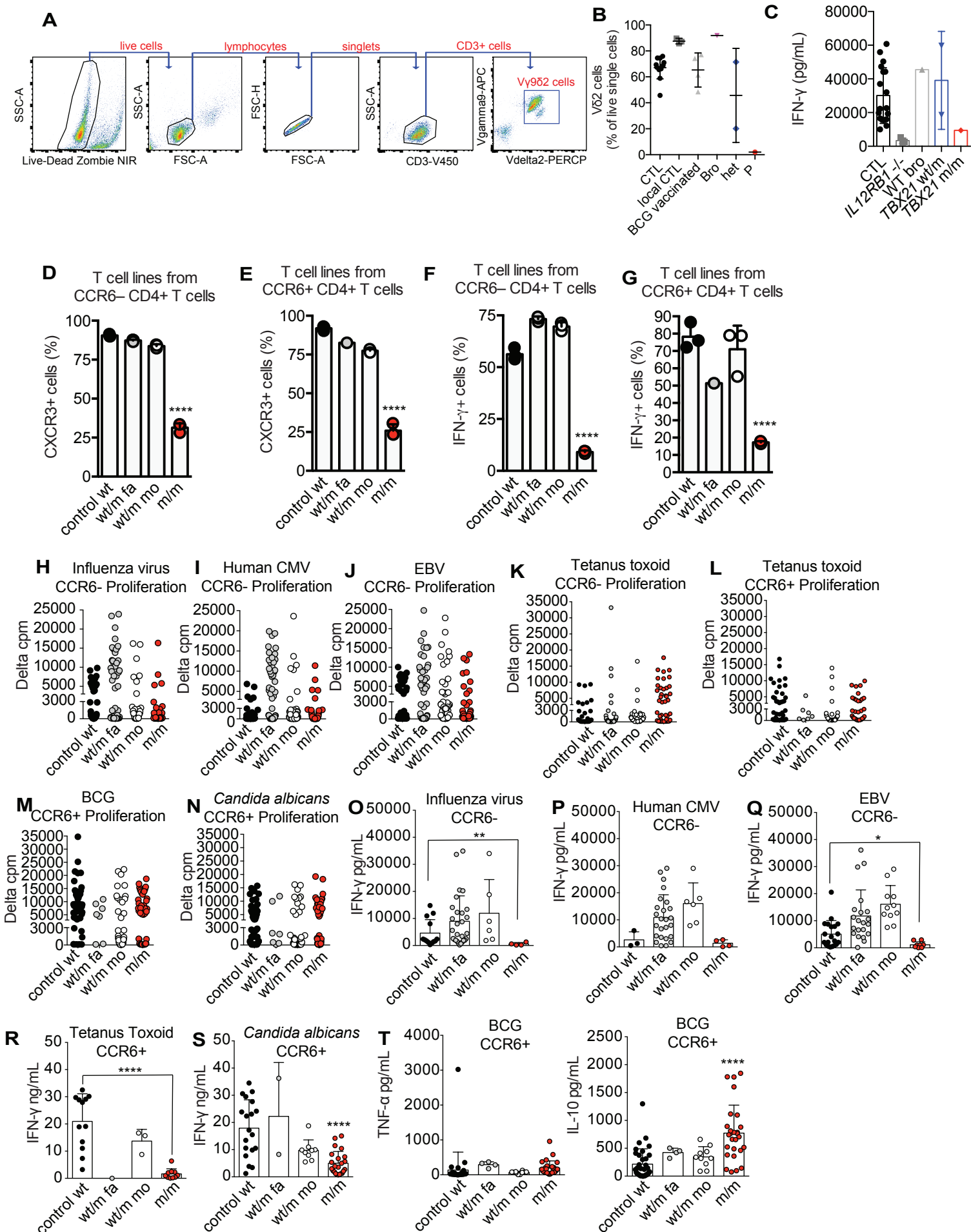


Figure S21

Figure legends for Supplementary Figures

Figure S1. Clinical and genetic features of a patient with MSMD, Related to Figure 1. (A)

Schematic view of the 15 MSMD-causing genes within myeloid and lymphoid cells in the context of host antimycobacterial immunity. (B) Serum IgG against various viral peptides or peptides derived from bacteria or other pathogens was tested by phage immunoprecipitation-sequencing. Serum samples from an unrelated healthy three-year-old boy (HC1), two healthy adults (HC2 and HC3), a *TBX21* m/m patient P, IgG-depleted serum and intravenous immunoglobulin (IVIg) were assayed. The heatmap (left) shows the counts of peptides significantly enriched for a given species with less than a continuous seven-residue subsequence, the estimated size of a linear epitope, in common. The species for which the patient had a score greater than our set threshold (>3) are shown. Count values above the set threshold are shown in on a color scale from green (≥ 4) to red (≥ 40) and dark-red (≥ 80). (C) Whole-genome linkage (WGL) analysis of the kindred. Genomic regions with LOD scores (LOD score >1.3 and size >500 kb) are shown for each chromosome. The linked region of chromosome 17 containing *TBX21* is indicated. (D) Homozygous genetic variants in P were filtered based on: 1) their presence in P but not in siblings or parents, 2) predicted changes in the amino-acid composition of the encoded protein, 3) Rarity in the general population and major ethnic groups (MAF < 0.003 , <http://gnomad.broadinstitute.org> and 1000 Genomes), 4) CADD score $> MSC$. (E) genomic DNA from P and his parents was subjected to Sanger sequencing to confirm the *TBX21* variant.

Figure S2. The *TBX21* variant led to the substitution of two amino acids, Related to Figure 1. (A) Comparison between the WT and Mut sequence of the region in which the variant is located in exon 1 of *TBX21*. An alignment of the WT and Mut sequences revealed a juxtaposed region with a sequence identical to that of the variant sequence. (B and C) The cDNAs generated from EBV-B cells derived from three healthy donors, *TBX21* wt/m heterozygous individuals (heterozygous) and the *TBX21* m/m patient (homozygous) were used as templates for the amplification of a region spanning the mutant site. Three sets of primers were used for this purpose (F forward primer and R4/R5/R6 reverse primers), as indicated. Agarose gel electrophoresis was performed to characterize these PCR products (B). PCR products were subjected to Sanger sequencing for genotyping (C). (D) RNA was extracted from PBMCs from two healthy donors and P and used for cDNA synthesis with random hexamers. The region spanning exons 1 to 4 was amplified from the cDNA by PCR. The PCR products were barcoded and an adaptor was added for Nano MiSeq sequencing. Sequencing reads passing quality controls were aligned with the reference genome, with RNA-STAR aligner. The sequence alignment for the junction between exons 1 and 2 of *TBX21* is shown with Integrative Genome Viewer.

Figure S3. Overexpression of the mutant *TBX21* cDNA, Related to Figure 1. (A) Alignment of peptide fragments from human T-box domain-containing transcription factors. (B) pCMV6 plasmids containing EV, WT T-bet (WT), the K314R variant of T-bet (K314R), T-bet with a deletion of the T-box domain (T-del), and mutant T-bet (Mut) were used to transfect HEK293T cells. Cells were harvested and lysed, and the lysates were subjected to immunoblotting. T-bet expression was characterized with anti-T-bet 4B10 monoclonal Ab and anti-Flag Ab. Anti-

GAPDH antibody was used as an endogenous control. **(C)** Mutations of individual residues in the T-bet cDNA (E156S, M157L, E156A, and E157A) were generated in pCMV6 plasmids by site-directed mutagenesis. The plasmids were used to transfect HEK293T cells for overexpression. T-bet levels were measured by immunoblotting with anti-T-bet 4B10 Ab and anti-Flag Ab. Anti-GAPDH Ab was used as endogenous control. **(D)** The plasmids described in **(C)** were used to transfect HEK293T cells, together with the WT-TBRE firefly luciferase and *Renilla* luciferase pRL-SV40 plasmids. After 3 days, the luciferase signal was detected in a Dual-Glo assay. The bars represent the mean and the standard deviation. Dots represent individual samples or technical replicates.

Figure S4. Overexpression of the mutant *TBX21* cDNA does not induce IFN- γ production, Related to Figure 1. **(A)** Schematic diagram of the CRISPR/Cas9 design for disrupting the exon-intron junctions of *TBX21*. gRNA9 was designed to disrupt the end of exon 1 and gRNA15 was designed to disrupt the end of exon 3. **(B)** Lentiviruses generated from empty vector, gRNA9 or gRNA15-containing pLenti-Crispr-V2 plasmids were used to transduce NK-92 cells. Stably transduced cells were genotyped with a three-primer PCR protocol. **(C and D)** Three EV-transduced, gRNA9- or gRNA15-transduced single-cell clones with a stable KO were selected based on the genotyping described in **(B)**. We determined the levels of *TBX21* mRNA **(C)** by reverse transcription-quantitative PCR (RT-qPCR). mRNA levels were normalized by the $2^{-\Delta\Delta CT}$ method. T-bet protein levels were determined by immunoblotting **(D)**. **(E)** Single-cell CRISPR/Cas9-edited NK-92 clones were stimulated with 50 pg/mL IL-12 and 10 ng/mL IL-18 or were left untreated (NS). Intracellular IFN- γ production was determined by ICS flow cytometry. **(F)** T-bet-deficient or EV-transduced NK-92 single-cell clones were transduced with

retroviruses generated from pLZRS-ires- Δ NGFR plasmids containing no insert (EV), or the WT, K314R or Mut *TBX21* cDNA with a C-terminal Flag-tag as previously described. T-bet proteins levels were determined by immunoblotting. GAPDH levels were determined as an endogenous control. **(G)** NK-92 cells transduced as described in (F) were stimulated with 50 pg/mL IL-12 and 10 ng/mL IL-18 or were left untreated. Intracellular IFN- γ production was determined by ICS flow cytometry. **(H)** Naïve CD4⁺ T cells were expanded under T_H0 conditions, and were then transduced with retroviruses generated from pLZRS-ires- Δ NGFR plasmids containing no insert (EV), or the WT, or Mut *TBX21* cDNA with a C-terminal Flag-tag. Transduced cells were positive for the bicistronic marker CD271. Cells were surface-stained for CD271 and intracellularly stained for IFN- γ and TNF- α and subjected to flow cytometry analysis. Bars represent the mean and the standard deviation. Dots represent individual samples or technical replicates.

Figure S5. Variants of *TBX21* common in the general population and all variants from in-house cohorts were functionally neutral, Related to Figure 1. **(A)** Schematic representation of all variants found in the homozygous state at least once in the gnomAD database (<http://gnomad.broadinstitute.org>). **(B)** Overexpression of seven variants of *TBX21* (shown in A) for which at least one homozygous individual has been identified in the general population. The variants indicated were overexpressed by transfecting HEK293T cells with pCMV6 plasmids containing the variants concerned. Protein levels were assessed by western blotting. **(C)** All variants (including the only homozygous variant and 28 heterozygous variants) from the HGID in-house database, excluding the H33Q allele already tested in (B), are represented on the CADD-MAF graph. The minor allele frequency (MAF) in the general population is shown on

the *x*-axis. The CADD score is shown on the *y*-axis. **(D)** A schematic representation of all variants from our in-house cohorts is shown in (C). **(E)** All in-house *TBX21* variants were tested for transcriptional activity in the WT-TBRE luciferase reporter assay. pCMV6 plasmids containing variants were used to transfect cells, together with the TBRE luciferase reporter plasmid, and the pRL-SV40 *Renilla* plasmid for luciferase activity measurement. Bars represent the mean and standard deviation. Dots represent technical replicates.

Figure S6. The T-bet variant in patient-derived cells is loss-of-function, Related to Figure 2.

(A) CD4⁺ T cells from healthy donors (HD), the heterozygous father (Fa) or the patient (P) were expanded with anti-CD3/CD28 antibody-coated beads. They were subjected to RT-qPCR for *TBX21* with two different probes. Data are displayed as $2^{-\Delta\Delta C_t}$ after normalization relative to *GUS* (endogenous control) expression, using the control mean as a calibrator. **(B)** *TBX21* expression was assessed in immortalized T cells from healthy donors (HD), the heterozygous father (Fa) or the patient (P) by RT-qPCR. **(C)** P-derived HVS-T cells (*TBX21* m/m) were retrovirally transduced with EV or WT *TBX21* containing a bicistronic CD271 surface marker. Along with HD and heterozygous *TBX21* wt/m HVS-T cells, they were analyzed for intracellular T-bet and IFN- γ production by flow cytometry ICS in the presence or absence of P/I stimulation. **(D)** Isolated CD4⁺ T cells from a healthy donor, a *TBX21* wt/m parent and the *TBX21* homozygous m/m P were expanded with anti-CD3/CD28 antibody-coated beads under T_{H0} or T_{H1} conditions. After 7d, EV or WT T-bet plasmids were used to transduce P's cells in the presence of a bicistronic CD271 surface reporter. Cells were subjected to ICS for IFN- γ and TNF- α in response to P/I restimulation. The gating strategy for the experiment is shown. **(E and F)** Cells transduced as in (D) were isolated with anti-CD271 antibody-coated beads by MACS.

Together with non-transduced cells, they were restimulated with anti-CD3/CD28 antibody-coated beads, and their culture supernatants were subjected to ELISA for IFN- γ (E) and TNF- α (F). Bars represent the mean and the standard deviation. Dots represent individual samples or technical replicates.

Figure S7. The production of T helper effectors in T-bet deficiency is T-bet-dependent, Related to Figure 2. (A) Expanded CD4⁺ T_{H0} cells from healthy donors, a T-bet heterozygous parent (TBET_HET), the T-bet homozygous P (TBET_HOM), P's cells complemented with empty vector (TBET_HOM_EV) or P's cells complemented with WT T-bet (TBET_HOM_WT) were restimulated with anti-CD3/CD28 antibody-coated beads for 16 h. RNA was extracted from these cells and subjected to RNA-seq analysis. Genome-wide transcriptome profile of all genes differentially expressed relative to the mean value for of healthy donors, represented as a heat map. (B) Transcriptomic analysis, as in (A), revealed target genes up- or downregulated in conditions of T-bet deficiency (WT/WT-control > or < M/M- homozygous deficiency), this differential regulation being abolished by WT T-bet complementation (M/M+EV > or < M/M+WT). The numbers of differentially regulated targets with T-bet-dependent expression are shown. (C) Volcano plots of transcriptomic profile comparing T-bet_HOM with CTL, and T-bet_HOM+WT with T-bet_HOM+EV. (D and E) Transcriptomic profile of immune genes displaying differential expression relative to the control (healthy donors), shown as a heat map for fold-change in expression (D) and Z-score (E). (F) Volcano plots of the transcriptomic profiles of immune genes comparing T-bet_HOM with CTL, and T-bet_HOM+WT with T-bet_HOM+EV.

Figure S8. Changes in chromatin accessibility in CD4⁺ T cells in conditions of T-bet deficiency, Related to Figure 3. (A) Expanded CD4 T_H0 cells from healthy donors (control), IL-12Rβ1-deficient MSMD patients (IL12_rb1), a T-bet-heterozygous parent (Tbet_WTm), the T-bet-homozygous P (Tbet_mm), P's cells complemented with empty vector (Tbet_mm_EV) or P's cells complemented with WT T-bet (Tbet_mm_WT) in the absence of stimulation were used to prepare an omni-ATAC-seq library. The library was then subjected to omni-ATAC-seq. Heat map of the genome-wide omni-ATAC-seq peaks called. (B) A pie chart showing the genomic annotation of ATAC-seq peaks with respect to known RefSeq genes. (C) Number of chromatin peak accessibility changes, as determined by comparisons of the indicated groups of samples. (D - H) Regions of immune genes in which chromatin accessibility was downregulated in conditions of T-bet deficiency, including regions within *IRF1* (D), *HDAC9* (E), *CYLD* (F), *PSENI* (G) and *HERC5* (H).

Figure S9. Regions of immune genes in which chromatin accessibility was downregulated in conditions of T-bet deficiency, Related to Figure 3. (A - I) Chromatin accessibilities of regions within *IL23R* (A), *IRF8* (B), *GZMB* (C), *KLRD1* (D), *RUNX3* (E), *SLAMF7* (F), *CCL5* (G), *IRF4* (H) and *RBPJ* (I).

Figure S10. T-bet deficiency results in a normal dendritic cell distribution, Related to Figure 4. (A) PBMCs were immunophenotyped with CyTOF. The gating strategy for different immune subsets is indicated. (B) Gating strategy for dendritic cell subsets, including plasmacytoid dendritic cells (pDC), conventional dendritic cells of type 1 and type 2 (cDC1 and cDC2), based on CyTOF data. (C - E) Percentages of pDCs (C), cDC1 cells (D) and cDC2 (E) cells. Bars represent the mean and the standard deviation. Dots represent individual samples.

Figure S11. T-bet deficiency impairs NK cell maturation, Related to Figure 4. (A) CD117⁺ ILCs, consisting principally of ILC precursors (ILCP) and type 2 ILC (ILC2) cells, were gated manually on conventional flow cytometry. PBMCs from P or a healthy donor control were subjected to FACS immunophenotyping of innate lymphoid cells (ILCs) and NK cells. The gating strategy is shown. (B) Total NK cells (CD16⁺ or CD94⁺Lin⁻CD7⁺ cells) were plotted with CD56 against CD127 for manual gating on different NK cell subsets.

Figure S12. T-bet deficiency does not affect ILC homeostasis in human PBMCs, Related to Figure 4. (A) CD117⁺ ILCs, consisting primarily of ILC precursors (ILCP) and type 2 ILC (ILC2) cells, were gated manually on CyTOF data. (B and C) Percentage of CD117⁺ ILCs (B) and ILC2 cells (C) in healthy donors (CTL), IL-12Rβ1-deficient MSMD patients (12RB1^{-/-}) and the T-bet-deficient patient (P). (D) Immunophenotyping of ILC2 and ILCP cells, analyzed by fluorescence flow cytometry, as in Fig. S11. Plot of ILC2 and ILCP, and the percentage of ILC2 and ILCP (within live CD45⁺ cells) in a healthy donor, the T-bet deficient patient and his healthy brother. Bars represent the mean and the standard deviation. Dots represent individual samples.

Figure S13. T-bet deficiency results in the impaired development of iNKT, MAIT and Vδ2⁺ cells, but normal Vδ1⁺ γδT cell development, Related to Figure 4. (A) PBMCs from healthy donors, IL-12Rβ1 deficient MSMD patients, the *TBX21* wt/m heterozygous parents, and the *TBX21* m/m patient were stained with surface markers for lymphocytes involved innate immunity (MAIT and iNKT cells) or both adaptive and innate immunity (γδT cells, in particular Vδ1 and Vδ2 cells). The gating strategy for flow cytometry is shown. (B and C) iNKT (B) and

MAIT (C) cells are shown for the T-bet-deficient patient and his family members. **(D)** Percentages of total $\gamma\delta$ T cells, gated on CyTOF data. **(E)** $V\delta 2^+$ $\gamma\delta$ T cells in the T-bet deficient patient and his family members. **(F)** Percentages of $V\delta 1$ $\gamma\delta$ T cells in healthy donors (CTL), IL-12R $\beta 1$ -deficient MSMD patients (12RB1 $^{-/-}$), the T-bet-deficient patient (P), and P's healthy heterozygous parents (het). **(G)** Naïve (CD45RA $^+$ CCR7 $^+$), central memory (CM, CD45RA $^-$ CCR7 $^+$), effector memory (EM, CD45RA $^-$ CCR7 $^-$) and effector memory T cells (T_{EMRA} , CD45RA $^+$ CCR7 $^-$) were manually gated from CD8 $^+$ T cells on CyTOF data. The percentages of these cells are shown. **(H)** Total CD8 $^+$ T cells were clustered by viSNE, based on a selection of surface markers. Manual gating of naïve and memory subsets overlaid on clusters of CD8 $^+$ T cells. CXCR3 and CD38 expression are indicated on this plot. Bars represent the mean and the standard deviation (A and G) or the mean and the standard error of the mean (D). Dots represent individual samples.

Figure S14. Preserved T_H2 , T_H17 and circulating T_{FH} memory $CD4^+$ T cells and normal Treg cells in T-bet deficiency, Related to Figure 4. **(A)** Naïve (CD45RA $^+$ CCR7 $^+$), central memory (CM, CD45RA $^-$ CCR7 $^+$), effector memory (EM, CD45RA $^-$ CCR7 $^-$) and effector memory T cells (T_{EMRA} , CD45RA $^+$ CCR7 $^-$) were manually gated from CD4 $^+$ T cells on the basis of CyTOF data. The percentages of these cells are shown. **(B)** Memory CD4 $^+$ T cells (CD45RA $^-$) were gated out manually, and further subjected to viSNE deconvolution with T-cell chemokine markers for 5,000 randomly selected events. Expression of CXCR3, CCR5, CCR6 and CCR4. The gating strategy for memory CD4 $^+$ T cells and T_H1 , T_H2 , T_H17 and T_H1^* cells is shown. **(C and D)** Percentages of T_H2 (CCR6 $^-$ CXCR3 $^-$ CCR4 $^+$) **(C)** and T_H17 cells (CCR6 $^+$ CXCR3 $^-$ CCR4 $^+$) **(D)** among memory CD4 $^+$ T cells. **(E)** Frequencies of the circulating follicular T helper (cT_{FH})

cells and their subsets (CXCR3⁺, double-negative as DN, CCR6⁺, or CXCR3⁺CCR6⁺ T_{FH}) from healthy donors and the T-bet-deficient patient (*TBX21* m/m). **(F)** Percentage of Tregs. **(G)** Percentages of CXCR3⁺ and CCR5⁺CXCR3⁻ Tregs. Bars represent the mean and the standard deviation (A, C, D, and F) or the mean and the standard error of the mean (E and G). Dots represent individual samples.

Figure S15. Single-cell RNA-seq on human T-bet-deficient cells, Related to Figure 4. (A)

Single-cell RNA-seq UMAP clustering of PBMC from the index P (*TBX21* m/m) and his father (*TBX21* wt/m – Control 1). Major cell lineage clusters are labeled. **(B)** Cells expressing genes of interest are highlighted in red in UMAP clusters. *ANXA1*, *C15orf48*, *CCDC50*, *CST3*, *CTSW*, *CXCR3*, *CCL3L1*, *CCL4*, *CCL5*, *TNF*, *TRDC* and *WHRN* were selected as examples.

Figure S16. Ex vivo stimulation of the residual lymphocytes from the patient with T-bet

deficiency, Related to Figure 5. (A) PBMCs from the patient or controls (healthy donors, brother-*TBX21* wt/wt, mother-*TBX21* wt/m) were stimulated with IL-12, IL-15 and IL-18. The gating strategy for total NK cells is shown. **(B and C)** Intracellular staining of IFN- γ (B) and TNF- α (C) in total NK cells from a travel control, P, P's brother and P's heterozygous mother, as shown in (A), in the presence and absence of stimulation with IL-12, IL-15 and IL-18. **(D and E)** Intracellular staining of perforin and granzyme B in total NK cells from a travel control, P, P's brother and P's heterozygous mother, as shown in (A). Mean fluorescence intensity (MFI) for perforin (D) and granzyme B (E) for the various samples. **(F - I)** MAIT cells (CD56⁻CD20⁻CD3⁺V δ 2⁻V α 7.2⁺), V δ 2 cells (CD56⁻CD20⁻CD3⁺V α 7.2⁻V δ 2⁺), V δ 2-negative $\gamma\delta$ T (CD56⁻CD20⁻CD3⁺V α 7.2⁻V δ 2⁻ $\gamma\delta$ TCR⁺) and CD8⁺ T cells (CD56⁻CD20⁻CD3⁺V α 7.2⁻V δ 2⁻ $\gamma\delta$ TCR⁺CD4⁻CD8⁺)

were gated from PBMCs prepared as in (A). Intracellular staining for IFN- γ and TNF- α in these MAIT cells (V α 7.2⁺) (F), V δ 2⁺ cells (V δ 2⁺) (G), V δ 2⁻ $\gamma\delta$ TCR⁺ T cells (H) and CD8⁺ T cells (I). Dots represent individual samples. Bars represent the mean and the standard error of the mean.

Figure S17. *Ex vivo* and *in vitro* stimulation of CD4⁺ T cells in conditions of T-bet

deficiency, Related to Figure 5. (A - H) Naïve and memory CD4⁺ T cells were sorted by FACS and activated/expanded. Intracellular staining of IL-22 (A), IL-9 (B) and IL-21 (H). Production of IL-9 (C), IL-4 (D), IL-5 (E), IL-10 (F) and IL-13 (G), as measured in culture supernatants. **(I and J)** Naïve CD4⁺ T cells were isolated by FACS and subjected to activation under T_H0, T_H9, T_H17 or T_H9 conditions combined with T_H17 conditions. The production of IL-9 was assessed intracellularly (I) and in culture supernatants (J). **(K)** Naïve CD4⁺ T cells were isolated by FACS and subjected to activation under T_H0, T_H1 or T_H2 conditions IL-10 production, measured on culture supernatants. **(L)** Naïve CD4⁺ T cells were isolated by FACS isolated and subjected to activation under T_H0, T_H2 or T_H9 conditions. IL-13 production, as measured on culture supernatants. Dots represent individual samples. Bars represent the mean and the standard error of the mean.

Figure S18. T-bet deficiency leads to changes in cytokine production in response to *M.bovis*

BCG stimulation, Related to Figure 6. (A - D) PBMCs from healthy donors, local controls, BCG-vaccinated controls, IL-12R β 1-deficient MSMD patients (*IL12RB1* m/m), the T-bet-deficient patient (*TBX21* m/m), and his family members were stimulated with or without live *M. bovis* BCG in the presence and absence of IL-12 and IL-23. The production of TNF- α (A), IL-6

(B), IL-5 (C) and IL-13 (D) was assessed with Legendplex cytometric bead arrays. Dots represent individual samples. Bars represent the mean and the standard deviation.

Figure S19. T-bet deficiency leads to smaller numbers of T-bet⁺ IFN- γ ⁺ double-positive cells following stimulation with live *M. bovis* BCG, Related to Figure 6. (A) PBMCs from healthy donors, local controls, BCG-vaccinated controls, IL-12R β 1-deficient MSMD patients (*IL12RB1* m/m), the T-bet-deficient patient (*TBX21* m/m), and his family members were stimulated with live *M. bovis* BCG in the presence and absence of IL-12 and IL-23. The gating strategies for total CD56⁺ NK cells, CD20⁺ B cells, V δ 2⁺ γ δ T cells, V α 7.2⁺ MAIT cells, V δ 2⁻ γ δ T cells, iNKT cells, CD4⁺ T cells and CD8⁺ T cells are shown. The gating strategies for T-bet⁺ IFN- γ ⁺ double-positive CD56⁺ NK cells, CD20⁺ B cells, V δ 2⁺ γ δ T cells, V α 7.2⁺ MAIT cells, V δ 2⁻ γ δ T cells, iNKT cells, CD4⁺ T cells and CD8⁺ T cells are also shown. (B and C) Plots and percentages of T-bet⁺ IFN- γ ⁺ double-positive cells from the individuals indicated in response to live *M. bovis* BCG infection at a MOI=1 (B) and a MOI=20 (C) in the presence and absence of IL-12 or IL-23.

Figure S20. T-bet deficiency leads to defective V δ 2⁺ γ δ T and MAIT cells, resulting in susceptibility to mycobacteria, Related to Figure 6. (A) PBMCs from healthy donors, local controls, BCG-vaccinated controls, IL-12R β 1-deficient MSMD patients (*IL-12R β 1* m/m), the T-bet-deficient patient (T-bet m/m), and his family members were stimulated with live *M. bovis* BCG in the presence and absence of IL-12 and IL-23. The percentages of CD56⁺ NK cells, CD20⁺ B cells, V δ 2⁺ γ δ T cells, V α 7.2⁺ MAIT cells, V δ 2⁻ γ δ T cells, iNKT cells, CD4⁺ T cells and CD8⁺ T cells among T-bet⁺ IFN- γ ⁺ double-positive cells are shown for healthy donors, local controls and BCG-vaccinated controls. (B) T-bet⁺ IFN- γ ⁺ double-positive cells among PBMCs

from healthy donors, local controls, BCG-vaccinated controls, an IL-12R β 1-deficient MSMD patient (*IL12RB1*^{-/-}), the *TBX21* m/m patient and his family members in response to *M. bovis* BCG stimulation, deconvoluted into automated clusters by viSNE analysis. Clusters representing CD56⁺ NK cells, CD20⁺ B cells, V δ 2⁺ $\gamma\delta$ T cells, V α 7.2⁺ MAIT cells, V δ 2⁻ $\gamma\delta$ T cells, iNKT cells, CD4⁺ T cell and CD8⁺ T cells are shown. Dots represent individual samples. Bars represent the mean and the standard deviation.

Figure S21. Defective prolonged anti-BCG immunity in V δ 2 $\gamma\delta$ T but not memory CD4⁺ T cells in T-bet deficiency, Related to Figure 6. (A) PBMCs from healthy controls, IL-12R β 1-deficient patients, the T-bet wt/m parents (mother and father), the T-bet wt/wt brother, and the patient (T-bet m/m) were stimulated with lysates of *M. bovis* BCG for 14 days. The gating strategy for the analysis of V γ 9 δ 2 T cells, also known as V δ 2 cells, is shown. (B) Percentages of V γ 9 δ 2 T cells among live single cells in culture, as in (A). (C) IFN- γ production by the end of the two-week culture period, as in (A), was measured in Legendplex assays. (D - G) T-cell libraries from a healthy BCG-vaccinated donor (control wt), the T-bet wt/m parents (wt/m), and the T-bet m/m patient (m/m) were generated by the polyclonal stimulation of sorted memory CD4⁺ T cells (either CCR6⁻ or CCR6⁺). The proportions of CXCR3⁺ (D and E) and IFN- γ ⁺ (F and G) cells were determined by surface staining and ICS flow cytometry. (H - N) Libraries from CCR6⁻ (H - K) or CCR6⁺ (L - N) memory CD4⁺ T cells from a control (wt control), the T-bet wt/m parents (wt/m), and the T-bet m/m patient (m/m) were screened for antigen reactivity by culturing T cells with autologous antigen-presenting cells, with and without peptide pools derived from influenza virus (H), human CMV (I), EBV (J), tetanus toxoid (K and L), *M. bovis* BCG (M) and *C. albicans* (N). Proliferation was assessed by evaluating [³H]-thymidine

incorporation, and is expressed in delta cpm values. **(O - Q)** CCR6⁻ memory CD4⁺ T cell clones responsive to peptide pools from influenza virus (O), human CMV (P) or EBV (Q) were subjected to Luminex assays to assess the production of IFN- γ . **(R and S)** CCR6⁺ memory CD4⁺ T-cell clones responsive to peptide pools from tetanus toxoid (R) and *C. albicans* (S) were subjected to Luminex assays to assess the production of IFN- γ . **(T)** BCG-responsive T-cell clones, as in (M), were subjected to Luminex assays to assess the production of TNF- α and IL-10. Dots represent individual samples or T-cell clones. Bars represent the mean and the standard deviation. One-way ANOVA was used to analyze statistical significance for D, E, F, G, S and T. A non-parametric *t*-test comparing WT to m/m was used to analyze statistical significance for (O - R).

Table S1: Overview of diseases underlying isolated or syndromic Mendelian susceptibility to mycobacterial disease (MSMD)

Gene	Inheritance	Defect	Protein
<i>IL12RB1</i>	AR	Complete	E-
	AR	Complete	E+
<i>IL12B</i>	AR	Complete	E-
<i>IL23R</i>	AR	Complete	E+
<i>IL12RB2</i>	AR	Complete	E-
<i>SPPL2A</i>	AR	Complete	E- or E+
<i>IRF8</i>	AD	Partial	E+
	AR	Complete	E- or E+
<i>IFNGR1</i>	AR	Complete	E+
	AR	Complete	E-
	AD	Partial	E+++
	AR	Partial*	E+
	AR	Partial	E+
<i>IFNGR2</i>	AR	Complete	E+
	AR	Complete	E-
	AR	Partial	E+ of mutant protein
	AR	Partial	E+ of WT protein
	AD	Partial	E+
<i>STAT1</i>	AD	Partial	E+P-
	AD	Partial	E+B-
	AD	Partial	E+P-B-
	AR	Complete	E-
	AR	Partial	E+

<i>NEMO (IKBKG)</i>	XR	Partial	E+
<i>CYBB</i>	XR	Partial*	E+
<i>TYK2 P1104A</i>	AR	Partial	E+
<i>TYK2</i>	AR	Complete	E-
<i>JAK1</i>	AR	Partial	E-
<i>RORC</i>	AR	Complete	E-
<i>ISG15</i>	AR	Complete	E-

MSMD genetic etiologies may have autosomal recessive (AR), autosomal dominant (AD), or X-linked recessive (XR) inheritance. Defects can be complete (C) or partial (P). Protein expression (E) of the mutant can be abolished (E-), normal or weaker than normal (E+), or stronger than normal (E+++). The mutant protein may be able or unable to undergo phosphorylation (P-) or to bind to DNA (B-). * Impaired function in specific cell types.

	No. of patients diagnosed	$\alpha\beta$ CD4 ⁺ T	$\alpha\beta$ CD8 ⁺ T	MAIT	B cell/Ig	DC	NK	iNKT	Mycobacterial infection
CD8 deficiency (<i>CD8A</i>)	3	NI	A		NI				No (OMIM#186910) (Dumontet et al., 2015; de la Calle-Martin et al., 2001; Mancebo et al., 2008).
MHC class I deficiency (<i>TAP1</i> , <i>TAP2</i> , <i>TAPBP</i> , <i>B2M</i>)	~30	NI	↓↓↓↓		NI				No (OMIM#170260, OMIM#170261, OMIM#601962, OMIM#109700) (Ardeniz et al., 2015; Chen et al., 1996; Colonna et al., 1992; Furukawa et al., 1999; Gao et al., 2016; Hanalioglu et al., 2017; Hanna and Etzioni, 2014; De La Salle et al., 1994; Law-Ping-Man et al., 2018; Maeda et al., 1985; Moins-Teisserenc et al., 1999; Sophie et al., 2012; Wani et al., 2006; Yabe et al., 2002).
TCR α deficiency	1	A	A		NI				No (OMIM#615387) (Morgan et al., 2011).
MHC class II deficiency (<i>CIITA</i> , <i>RFXANK</i> , <i>RFX5</i> , <i>RFXAP</i>)	>200	↓↓↓↓	NI		↓↓				Generally no (OMIM#209920) (Bontron et al., 1997; Durand et al., 1997; Dziembowska et al., 2002; Ghaderi et al., 2006; Hanna and Etzioni, 2014; Lennon-Duménil

									et al., 2001; Lisowska-Groszpiere et al., 1994; Mach et al., 1998; Nagarajan et al., 2000; Nekrep et al., 2002; Ouederni et al., 2011; Peijnenburg et al., 1999; Steimle et al., 1993, 1995; Swanberg et al., 2005; Villard et al., 1997a, 1997b, 2001, 2002; Wiszniewski et al., 2000, 2003). One case of <i>M. avium</i> infection reported (Dimitrova et al., 2014).
MCM4 deficiency (<i>MCM4</i>)	~24	NI	NI		NI		IIII		No (OMIM#602638) (Casey et al., 2012; Eidenschenk et al., 2006; Gineau et al., 2012; Hughes et al., 2012).
GINS1 deficiency (<i>GINS1</i>)	5	NI	NI		NI		IIII		No (OMIM#610608) (Cottineau et al., 2017).
ROR γ /ROR γ T deficiency	7	↓	NI	A				A	Yes (OMIM#602943) (Okada et al., 2015).
AD IRF8 deficiency	4					II to A	II		Yes (OMIM#601565) (Hambleton et al., 2011; Salem et al., 2014).
SPPL2A deficiency (<i>SPPL2A</i>)	2					II			Yes (Kong et al., 2018).

SAP deficiency	>300							↓↓↓↓	No (OMIM#308240) reviewed in (Tangye et al., 2017).
WASP deficiency	Many							A	Generally No (OMIM#300392) reviewed in (Locci et al., 2009; Massaad et al., 2013). Two cases of mycobacterial infection reported (Pacharn et al., 2017; Yasutomi et al., 2015).

Abbreviations: A absent, ↓ reduced, ↑ elevated, NI normal

Table S2. Mycobacterial diseases in primary immunodeficiency disorders in humans leading to the selective depletion of one or more populations of $\alpha\beta$ T cells, NK cells, MAIT cells or dendritic cell subsets.

Gene	Chr	Position	Ref	Alt	Consequence	Function category	Comments
<i>TSEN15</i>	1	184041317	G	A	p.Arg127Gln	Nucleic acid binding	MAF=0.00336 in Middle Eastern population (Joseph Gleeson cohort). MAF<0.003 in all other ethnic groups in public databases.
<i>EPHA1</i>	7	143098636	C	G	p.Met71Ile	Angiogenesis, GTPase activation, ephrin receptor signaling pathway	MAF<0.003 in all ethnic groups in public databases.
<i>AKR1D1</i>	7	137776608	T	C	p.Ile119Thr	Androgen metabolism, bile acid synthesis	MAF<0.003 in all ethnic groups in public databases.
<i>ABCA2</i>	9	139908757	TGGGTC AGCTCC GAGCAC C	T	p.Arg1362_Thr1367del	Cholesterol homeostasis, lipid metabolism	MAF<0.003 in all ethnic groups in public databases.
<i>PDE2A</i>	11	72297209	C	T	p.Glu363Lys	GPCR signaling, cAMP-regulation	MAF<0.003 in all ethnic groups in public databases.
<i>PSMD9</i>	12	122326874	A	C	p.Lys38Gln	Insulin secretion, bHLH transcription factor binding	MAF<0.003 in all ethnic groups in public databases.
<i>GCN1L1</i>	12	120568996	G	A	p.Ala2519Val	Amino acid starvation, cadherin	MAF<0.003 in all ethnic groups in

						binding, regulation of translation	public databases.
<i>ATP6V0A2</i>	12	124228405	G	A	p.Arg371His	Iron homeostasis, ATP hydrolysis coupled proton transport	MAF<0.003 in all ethnic groups in public databases.
<i>CIB2</i>	15	78416081	C	T	p.Asp18Asn	Calcium homeostasis	MAF<0.003 in all ethnic groups in public databases.
<i>ERN1</i>	17	62121392	C	T	p.Glu964Lys	JUN kinase activation, cell cycle arrest, insulin metabolism	Another patient with a different phenotype in laboratory cohort is homozygous e for the same variant.
<i>TBX21</i>	17	45811289	ATG	A	p.Glu156_Met 157SerLeu	T-helper regulation, T-cell differentiation	Private variant, and highly related to interferon gamma immunity
<i>AOC2</i>	17	40997583	G	T	p.Gly314Cys	Amine metabolism, catecholamine metabolism, visual perception	>2% Ashkenazi Jews carry a LOF premature stop variant in <i>AOC2</i> (Variant: 17-40996783-G-A).
<i>AKAP1</i>	17	55182923	T	G	p.Val33Gly	Blood coagulation, protein kinase A regulation	>6.4% of Africans carry a LOF premature stop variant

							of <i>AKAP1</i> (Variant: 17-55198645-C-CT)
<i>ARHGAP27</i>	17	43506940	G	A	p.Arg236Cys	GTPase regulation, receptor-mediated endocytosis	Another patient with a different phenotype in laboratory cohort is homozygous for the same variant.
<i>RHBDD3</i>	22	29656330	G	C	p.Ser323Cys	Liver development, MAPK cascade, serine-type endopeptidase activity	>0.79% of the general population (all gnomAD) carry a LOF premature stop variant of <i>RHBDD3</i> (Variant: 22-29656431-C-T)

Table S3. Homozygous candidate variants that might cause MSMD and reactive airway disease in the patient.

Target Gene	Distance	Rank	P-Value (percentile)	Sphere	Degrees of separation
<i>TBX21</i>	1.11111	7	0.00042	0	1
<i>EPHA1</i>	4.44444	602	0.03597	2	2
<i>PSMD9</i>	4.44444	1040	0.06214	3	2
<i>ERN1</i>	4.72222	2132	0.12738	4	2
<i>ABCA2</i>	10.41667	7835	0.46812	5	3
<i>GCN1L1</i>	10.41667	7193	0.42977	5	3
<i>ARHGAP27</i>	11.98582	10149	0.60638	6	3
<i>PDE2A</i>	18.11722	14155	0.84573	7	4
<i>CIB2</i>	19.29372	14797	0.88409	7	3
<i>ATP6V0A2</i>	19.68254	15112	0.90291	7	4
<i>TSEN15</i>	19.88576	15163	0.90596	7	4
<i>AKR1D1</i>	27.3569	16308	0.97437	7	4

Table S4. Connectome analysis of the distance of *TBX21*, *EPHA1*, *PSMD9*, *ABCA2*, *GCN1L1*, *ERN1*, *ARHGAP27*, *PDE2A*, *CIB2*, *ATP6V0A2*, *TSEN15*, and *AKR1D1* to *IFNG* as the anchor gene.

	In human T-bet deficiency	In mouse T-bet deficiency
CD56^{bright} NK cells	↓ 25-fold in frequency	↓60-fold in frequency in periphery (Townsend et al., 2004)
CD16⁺CD56^{dim} NK cells	↓ 15-fold in frequency	
Invariant NKT cells	↓ 200-fold in frequency	↓18-fold in frequency in liver (Townsend et al., 2004)
MAIT cells	↓ 14-fold in frequency Low levels of IFN- γ production in the remaining cells**	Not known
T_H1 CD4⁺ T cells	↓ 9-fold in frequency Low levels of IFN- γ production in the remaining cells**	↓ in frequency (Szabo et al., 2002)
T_H1* CD4⁺ T cells	Normal in frequency	Not known
Vδ2 $\gamma\delta$T cells	↓ 8-fold in frequency Low levels of IFN- γ production in the remaining cells**	Not present in mice
Vδ1 $\gamma\delta$T cells	Normal in frequency Normal IFN- γ production in V δ 1-containing $\gamma\delta$ T cells (V δ 2 ⁻ $\gamma\delta$ T cells) **	Not known
T_H2 CD4⁺ T cells	Normal in frequency	↑ T _H 2 differentiation and cytokine production during experimental inoculation (Finotto et al., 2002)
T_H17 CD4⁺ T cells	Normal in frequency	↑ T _H 17 differentiation and cytokine production during experimental inoculation (Lazarevic et al., 2011)
CD8⁺ T cells	Normal in frequency Low levels of IFN- γ production**	Normal in frequency (Tang et al.) Low levels of IFN- γ production (Bettelli et al., 2004; Intlekofer et al., 2007; Pearce et al., 2003; Sullivan et al., 2003)
ILC2	Normal in frequency	↑ ILC2 and ↑ activity of ILC2 in the spleen, lymph nodes and gut mucosa (Garrido-Mesa et al., 2019)
ILCP	Normal in frequency	Not known
ILC1	Cannot be studied as present at too low a frequency in peripheral blood	↓ in frequency (Daussy et al., 2014)
ILC3	Cannot be studied as present at too low a frequency in peripheral blood	↓ in frequency (Rankin et al., 2013)

mDC and pDC subsets	Normal in frequency	Normal in frequency (Lugo-Villarino et al., 2003)
----------------------------	---------------------	---

**In response to PMA-ionomycin stimulation

Table S8. Comparison of the development and function of various immune lineages of human and murine T-bet-deficient cells.

	Mice or Rats (T-bet KO or cKO or silencing)	Human T-bet deficiency (P)
Susceptibility to infections	<ul style="list-style-type: none"> ➤ ↑ <i>Leishmania major</i> and <i>L. donovani</i> (Rosas et al., 2006; Szabo et al., 2002) ➤ ↑ <i>Toxoplasma gondii</i> colonization at secondary sites of infection (Harms Pritchard et al., 2015) ➤ ↑ Attenuated rabies virus CNS infection (Lebrun et al., 2015) ➤ ↑ <i>Staphylococcus aureus</i> sepsis and arthritis (Hultgren et al., 2004) ➤ ↑ Genital HSV-2 (Svensson et al., 2005) ➤ ↑ <i>Mycobacterium tuberculosis</i> (Sullivan et al., 2005) ➤ ↑ <i>M. avium complex</i> (MAC) (Matsuyama et al., 2014) ➤ ↑ <i>Salmonella</i> infection (Ravindran et al., 2005) ➤ ↑ <i>M. pulmonis</i> colonization (Bakshi et al., 2006) ➤ ↑ Chronic LCMV infection (Kao et al., 2011) ➤ ↑ <i>Plasmodium berghei</i> parasitemia (Oakley et al., 2013) ➤ ↓ <i>Plasmodium berghei</i> experimental cerebral malaria (Oakley et al., 2013) ➤ ↓ <i>Plasmodium yoelii</i> 17XNL infection ➤ ↓ <i>T. spiralis</i> infection in intestines (Oakley et al., 2014) ➤ ↓ <i>T. spiralis</i> infection in intestines (Alcaide et al., 2007) 	<ul style="list-style-type: none"> ➤ ↑ BCG infection ➤ Mild chronic CMV viremia (this publication)

Table S9. Comparison of the infectious phenotypes of T-bet deficiency between humans and rodents.

Legends to the supplemental tables

Table S1. Overview of diseases underlying isolated or syndromic Mendelian susceptibility to mycobacterial disease (MSMD).

Table S2. Mycobacterial diseases in primary immunodeficiency disorders in humans leading to the selective depletion of one or more populations of $\alpha\beta$ T cells, NK cells, MAIT cells or dendritic cell subsets.

Table S3. Homozygous candidate variants that might cause MSMD and reactive airway disease in P.

Table S4. Connectome analysis of the distances of *TBX21*, *EPHA1*, *PSMD9*, *ABCA2*, *GCNIL1*, *ERN1*, *ARHGAP27*, *PDE2A*, *CIB2*, *ATP6V0A2*, *TSEN15*, and *AKR1D1* to *IFNG*, the anchor gene.

Table S5. RNA-seq analysis of expanded CD4 T_H0 cells from healthy donors, a T-bet heterozygous parent (TBET_HET), the T-bet homozygous P (TBET_HOM), P complemented with empty vector (TBET_HOM_EV) or P complemented with WT T-bet (TBET_HOM_WT) were restimulated with anti-CD3/CD28 Ab-coated beads for 16 h. Lists of DEG_Status, DEG_FoldChange and DEG_ZScore identifying differentially regulated target genes genome-wide. Slim_DEG identifies differentially regulated target immune genes.

Table S6. Chromatin accessibility of 1649 loci opening in a T-bet-dependent manner and 666 loci closing in a T-bet-dependent manner.

Table S7. Beta-value for the differential methylation of CpG sites between T-bet m/m (Hom) and controls (CTL) abolished by WT T-bet complementation.

Table S8. Comparison of the development and function of various immune lineages of human and murine T-bet-deficient cells.

Table S9. Comparison of the infectious phenotypes of human T-bet deficiency in humans and rodents.

Reference

Abecasis, G.R., Cherny, S.S., Cookson, W.O., and Cardon, L.R. (2002). Merlin—rapid analysis of dense genetic maps using sparse gene flow trees. *Nat. Genet.* *30*, 97–101.

Alcaide, P., Jones, T.G., Lord, G.M., Glimcher, L.H., Hallgren, J., Arinobu, Y., Akashi, K., Paterson, A.M., Gurish, M.A., and Luscinskas, F.W. (2007). Dendritic cell expression of the transcription factor T-bet regulates mast cell progenitor homing to mucosal tissue. *J Exp Med* *204*, 431–439.

Amir el, A.D., Davis, K.L., Tadmor, M.D., Simonds, E.F., Levine, J.H., Bendall, S.C., Shenfeld, D.K., Krishnaswamy, S., Nolan, G.P., and Pe'er, D. (2013). viSNE enables visualization of high dimensional single-cell data and reveals phenotypic heterogeneity of leukemia. *Nat Biotechnol* *31*, 545–552.

Ardeniz, Ö., Unger, S., Onay, H., Ammann, S., Keck, C., Cianga, C., Gerçeker, B., Martin, B., Fuchs, I., Salzer, U., et al. (2015). β 2-Microglobulin deficiency causes a complex immunodeficiency of the innate and adaptive immune system. *J. Allergy Clin. Immunol.* *136*, 392–401.

Bakshi, C.S., Malik, M., Carrico, P.M., and Sellati, T.J. (2006). T-bet deficiency facilitates airway colonization by *Mycoplasma pulmonis* in a murine model of asthma. *J Immunol* *177*, 1786–1795.

Becht, E., McInnes, L., Healy, J., Dutertre, C.-A., Kwok, I.W.H., Ng, L.G., Ginhoux, F., and Newell, E.W. (2019). Dimensionality reduction for visualizing single-cell data using UMAP. *Nat. Biotechnol.* *37*, 38–44.

Bettelli, E., Sullivan, B., Szabo, S.J., Sobel, R.A., Glimcher, L.H., and Kuchroo, V.K. (2004). Loss of T-bet, but not STAT1, prevents the development of experimental autoimmune

encephalomyelitis. *J Exp Med* 200, 79–87.

Bontron, S., Steimle, V., Ucla, C., Eibl, M.M., and Mach, B. (1997). Two novel mutations in the MHC class II transactivator CIITA in a second patient from MHC class II deficiency complementation group A. *Hum. Genet.* 99, 541–546.

Buenrostro, J.D., Giresi, P.G., Zaba, L.C., Chang, H.Y., and Greenleaf, W.J. (2013).

Transposition of native chromatin for fast and sensitive epigenomic profiling of open chromatin, DNA-binding proteins and nucleosome position. *Nat Methods* 10, 1213–1218.

Buenrostro, J.D., Wu, B., Chang, H.Y., and Greenleaf, W.J. (2015). ATAC-seq: A Method for Assaying Chromatin Accessibility Genome-Wide. *Curr Protoc Mol Biol* 109, 21 29 1-9.

Carroll, T.S., Liang, Z., Salama, R., Stark, R., and de Santiago, I. (2014). Impact of artifact removal on ChIP quality metrics in ChIP-seq and ChIP-exo data. *Front. Genet.* 5, 75.

Casey, J.P., Nobbs, M., McGettigan, P., Lynch, S., and Ennis, S. (2012). Recessive mutations in MCM4/PRKDC cause a novel syndrome involving a primary immunodeficiency and a disorder of DNA repair. *J. Med. Genet.* 49, 242–245.

Chen, H.L., Gabrilovich, D., Tampé, R., Girgis, K.R., Nadaf, S., and Carbone, D.P. (1996). A functionally defective allele of TAP1 results in loss of MHC class I antigen presentation in a human lung cancer. *Nat. Genet.*

Colonna, M., Bresnahan, M., Bahram, S., Strominger, J.L., and Spies, T. (1992). Allelic variants of the human putative peptide transporter involved in antigen processing. *Proc. Natl. Acad. Sci. U. S. A.* 89, 3932–3936.

Corces, M.R., Trevino, A.E., Hamilton, E.G., Greenside, P.G., Sinnott-Armstrong, N.A., Vesuna, S., Satpathy, A.T., Rubin, A.J., Montine, K.S., Wu, B., et al. (2017). An improved ATAC-seq protocol reduces background and enables interrogation of frozen tissues. *Nat.*

Methods *14*, 959–962.

Cottineau, J., Kottemann, M.C., Lach, F.P., Kang, Y.-H., Vély, F., Deenick, E.K., Lazarov, T., Gineau, L., Wang, Y., Farina, A., et al. (2017). Inherited GINS1 deficiency underlies growth retardation along with neutropenia and NK cell deficiency. *J. Clin. Invest.* *127*, 1991–2006.

Daussy, C., Faure, F., Mayol, K., Viel, S., Gasteiger, G., Charrier, E., Bienvenu, J., Henry, T., Debien, E., Hasan, U.A., et al. (2014). T-bet and Eomes instruct the development of two distinct natural killer cell lineages in the liver and in the bone marrow. *J. Exp. Med.*

Depristo, M.A., Banks, E., Poplin, R., Garimella, K. V., Maguire, J.R., Hartl, C., Philippakis, A.A., Del Angel, G., Rivas, M.A., Hanna, M., et al. (2011). A framework for variation discovery and genotyping using next-generation DNA sequencing data. *Nat. Genet.*

Dimitrova, D., Ong, P.Y., O’Gorman, M.R.G., and Church, J.A. (2014). Major Histocompatibility Complex Class II Deficiency Complicated by *Mycobacterium avium* Complex in a Boy of Mixed Ethnicity. *J. Clin. Immunol.*

Dobin, A., Davis, C.A., Schlesinger, F., Drenkow, J., Zaleski, C., Jha, S., Batut, P., Chaisson, M., and Gingeras, T.R. (2013). STAR: ultrafast universal RNA-seq aligner. *Bioinformatics* *29*, 15–21.

Dumontet, E., Osman, J., Guillemont-Lambert, N., Cros, G., Moshous, D., and Picard, C. (2015). Recurrent Respiratory Infections Revealing CD8 α Deficiency. *J. Clin. Immunol.* *35*, 692–695.

Durand, B., Sperisen, P., Emery, P., Barras, E., Zufferey, M., Mach, B., and Reith, W. (1997). RFXAP, a novel subunit of the RFX DNA binding complex is mutated in MHC class II deficiency. *EMBO J.* *16*, 1045–1055.

Dziembowska, M., Fondaneche, M.-C., Vedrenne, J., Barbieri, G., Wiszniewski, W., Picard, C., Cant, A.J., Steimle, V., Charron, D., Alca-Loridan, C., et al. (2002). Three novel mutations of the

CIITA gene in MHC class II-deficient patients with a severe immunodeficiency.

Immunogenetics 53, 821–829.

Eidenschenk, C., Dunne, J., Jouanguy, E., Fourlinnie, C., Gineau, L., Bacq, D., McMahon, C., Smith, O., Casanova, J.-L., Abel, L., et al. (2006). A Novel Primary Immunodeficiency with Specific Natural-Killer Cell Deficiency Maps to the Centromeric Region of Chromosome 8. *Am. J. Hum. Genet.*

Feng, J., Liu, T., Qin, B., Zhang, Y., and Liu, X.S. (2012). Identifying ChIP-seq enrichment using MACS. *Nat. Protoc.* 7, 1728–1740.

Finak, G., McDavid, A., Yajima, M., Deng, J., Gersuk, V., Shalek, A.K., Slichter, C.K., Miller, H.W., McElrath, M.J., Prlic, M., et al. (2015). MAST: a flexible statistical framework for assessing transcriptional changes and characterizing heterogeneity in single-cell RNA sequencing data. *Genome Biol.* 16, 278.

Finotto, S., Neurath, M.F., Glickman, J.N., Qin, S., Lehr, H.A., Green, F.H., Ackerman, K., Haley, K., Galle, P.R., Szabo, S.J., et al. (2002). Development of spontaneous airway changes consistent with human asthma in mice lacking T-bet. *Science* (80-.). 295, 336–338.

Frankish, A., Diekhans, M., Ferreira, A.-M., Johnson, R., Jungreis, I., Loveland, J., Mudge, J.M., Sisu, C., Wright, J., Armstrong, J., et al. (2019). GENCODE reference annotation for the human and mouse genomes. *Nucleic Acids Res.* 47, D766–D773.

Furukawa, H., Murata, S., Yabe, T., Shimbara, N., Keicho, N., Kashiwase, K., Watanabe, K., Ishikawa, Y., Akaza, T., Tadokoro, K., et al. (1999). Splice acceptor site mutation of the transporter associated with antigen processing-1 gene in human bare lymphocyte syndrome. *J. Clin. Invest.* 103, 755–758.

Gao, Y., Arkwright, P.D., Carter, R., Cazaly, A., Harrison, R.J., Mant, A., Cant, A.J., Gadola, S.,

Elliott, T.J., Khakoo, S.I., et al. (2016). Bone marrow transplantation for MHC class I deficiency corrects T-cell immunity but dissociates natural killer cell repertoire formation from function. *J. Allergy Clin. Immunol.* *138*, 1733-1736.e2.

Garrido-Mesa, N., Schroeder, J.-H., Stolarczyk, E., Gallagher, A.L., Lo, J.W., Bailey, C., Campbell, L., Sexl, V., MacDonald, T.T., Howard, J.K., et al. (2019). T-bet controls intestinal mucosa immune responses via repression of type 2 innate lymphoid cell function. *Mucosal Immunol.* *12*, 51–63.

Geiger, R., Duhon, T., Lanzavecchia, A., and Sallusto, F. (2009). Human naive and memory CD4⁺ T cell repertoires specific for naturally processed antigens analyzed using libraries of amplified T cells. *J. Exp. Med.* *206*, 1525–1534.

Ghaderi, M., Gambelunghe, G., Tortoioli, C., Brozzetti, A., Jatta, K., Gharizadeh, B., De Bellis, A., Giraldi, F.P., Terzolo, M., Betterle, C., et al. (2006). MHC2TA single nucleotide polymorphism and genetic risk for autoimmune adrenal insufficiency. *J. Clin. Endocrinol. Metab.*

Gineau, L., Cognet, C., Kara, N., Lach, F.P., Dunne, J., Veturi, U., Picard, C., Trouillet, C., Eidenschenk, C., Aoufouchi, S., et al. (2012). Partial MCM4 deficiency in patients with growth retardation, adrenal insufficiency, and natural killer cell deficiency. *J. Clin. Invest.* *122*, 821–832.

Gu, Z., Eils, R., and Schlesner, M. (2016). Complex heatmaps reveal patterns and correlations in multidimensional genomic data. *Bioinformatics* *32*, 2847–2849.

Hambleton, S., Salem, S., Bustamante, J., Bigley, V., Boisson-Dupuis, S., Azevedo, J., Fortin, A., Haniffa, M., Ceron-Gutierrez, L., Bacon, C.M., et al. (2011). IRF8 Mutations and Human Dendritic-Cell Immunodeficiency. *N. Engl. J. Med.*

Hanalioglu, D., Ayvaz, D.C., Ozgur, T.T., van der Burg, M., Sanal, O., and Tezcan, I. (2017). A

novel mutation in TAP1 gene leading to MHC class I deficiency: Report of two cases and review of the literature. *Clin. Immunol.* *178*, 74–78.

Hanna, S., and Etzioni, A. (2014). MHC class I and II deficiencies. *J. Allergy Clin. Immunol.*

Harayama, T., and Riezman, H. (2017). Detection of genome-edited mutant clones by a simple competition-based PCR method. *PLoS One* *12*, e0179165.

Harms Pritchard, G., Hall, A.O., Christian, D.A., Wagage, S., Fang, Q., Muallem, G., John, B., Glatman Zaretsky, A., Dunn, W.G., Perrigoue, J., et al. (2015). Diverse roles for T-bet in the effector responses required for resistance to infection. *J Immunol* *194*, 1131–1140.

Hernandez, N., Melki, I., Jing, H., Habib, T., Huang, S.S.Y., Danielson, J., Kula, T., Drutman, S., Belkaya, S., Rattina, V., et al. (2018). Life-threatening influenza pneumonitis in a child with inherited IRF9 deficiency. *J. Exp. Med.* *215*, 2567–2585.

Hughes, C.R., Guasti, L., Meimaridou, E., Chuang, C.-H., Schimenti, J.C., King, P.J., Costigan, C., Clark, A.J.L., and Metherell, L.A. (2012). MCM4 mutation causes adrenal failure, short stature, and natural killer cell deficiency in humans. *J. Clin. Invest.* *122*, 814–820.

Hultgren, O.H., Verdrengh, M., and Tarkowski, A. (2004). T-box transcription-factor-deficient mice display increased joint pathology and failure of infection control during staphylococcal arthritis. *Microbes Infect* *6*, 529–535.

Intlekofer, A.M., Takemoto, N., Kao, C., Banerjee, A., Schambach, F., Northrop, J.K., Shen, H., Wherry, E.J., and Reiner, S.L. (2007). Requirement for T-bet in the aberrant differentiation of unhelped memory CD8⁺ T cells. *J Exp Med* *204*, 2015–2021.

Janesick, A., Shiotsugu, J., Taketani, M., and Blumberg, B. (2012). RIPPLY3 is a retinoic acid-inducible repressor required for setting the borders of the pre-placodal ectoderm. *Development* *139*, 1213–1224.

Kanhere, A., Hertweck, A., Bhatia, U., Gökmen, M.R., Perucha, E., Jackson, I., Lord, G.M., and Jenner, R.G. (2012). T-bet and GATA3 orchestrate Th1 and Th2 differentiation through lineage-specific targeting of distal regulatory elements. *Nat. Commun.* 3, 1268.

Kao, C., Oestreich, K.J., Paley, M.A., Crawford, A., Angelosanto, J.M., Ali, M.A., Intlekofer, A.M., Boss, J.M., Reiner, S.L., Weinmann, A.S., et al. (2011). Transcription factor T-bet represses expression of the inhibitory receptor PD-1 and sustains virus-specific CD8⁺ T cell responses during chronic infection. *Nat Immunol* 12, 663–671.

Kong, X.F., Martinez-Barricarte, R., Kennedy, J., Mele, F., Lazarov, T., Deenick, E.K., Ma, C.S., Breton, G., Lucero, K.B., Langlais, D., et al. (2018). Disruption of an antimycobacterial circuit between dendritic and helper T cells in human SPPL2a deficiency. *Nat Immunol* 19, 973–985.

de la Calle-Martin, O., Hernandez, M., Ordi, J., Casamitjana, N., Arostegui, J.I., Caragol, I., Ferrando, M., Labrador, M., Rodriguez-Sanchez, J.L., and Espanol, T. (2001). Familial CD8 deficiency due to a mutation in the CD8 alpha gene. *J. Clin. Invest.* 108, 117–123.

De La Salle, H., Hanau, D., Fricker, D., Urlacher, A., Kelly, A., Salamero, J., Powis, S.H., Donato, L., Bausinger, H., Laforet, M., et al. (1994). Homozygous human TAP peptide transporter mutation in HLA class I deficiency. *Science* (80-).

Law-Ping-Man, S., Toutain, F., Rieux-Laucat, F., Picard, C., Kammerer-Jacquet, S., Magérus-Chatinet, A., Dupuy, A., and Adamski, H. (2018). Chronic granulomatous skin lesions leading to a diagnosis of TAP1 deficiency syndrome. *Pediatr. Dermatol.* 35, e375–e377.

Lazarevic, V., Chen, X., Shim, J.H., Hwang, E.S., Jang, E., Bolm, A.N., Oukka, M., Kuchroo, V.K., and Glimcher, L.H. (2011). T-bet represses TH 17 differentiation by preventing Runx1-mediated activation of the gene encoding ROR γ t. *Nat. Immunol.*

Lebrun, A., Portocarrero, C., Kean, R.B., Barkhouse, D.A., Faber, M., and Hooper, D.C. (2015). T-bet Is Required for the Rapid Clearance of Attenuated Rabies Virus from Central Nervous System Tissue. *J Immunol* *195*, 4358–4368.

Lennon-Duménil, A.M., Barbouche, M.R., Vedrenne, J., Prod'Homme, T., Béjaoui, M., Ghariani, S., Charron, D., Fellous, M., Dellagi, K., and Alcaïde-Loridan, C. (2001). Uncoordinated HLA-D gene expression in a RFXANK-defective patient with MHC class II deficiency. *J. Immunol.*

Li, H., and Durbin, R. (2009). Fast and accurate short read alignment with Burrows-Wheeler transform. *Bioinformatics* *25*, 1754–1760.

Li, H., Handsaker, B., Wysoker, A., Fennell, T., Ruan, J., Homer, N., Marth, G., Abecasis, G., Durbin, R., and 1000 Genome Project Data Processing Subgroup (2009). The Sequence Alignment/Map format and SAMtools. *Bioinformatics* *25*, 2078–2079.

Liao, Y., Smyth, G.K., and Shi, W. (2014). featureCounts: an efficient general purpose program for assigning sequence reads to genomic features. *Bioinformatics* *30*, 923–930.

Liberzon, A., Birger, C., Thorvaldsdóttir, H., Ghandi, M., Mesirov, J.P., and Tamayo, P. (2015). The Molecular Signatures Database Hallmark Gene Set Collection. *Cell Syst.* *1*, 417–425.

Lindestam Arlehamn, C.S., McKinney, D.M., Carpenter, C., Paul, S., Rozot, V., Makgotlho, E., Gregg, Y., van Rooyen, M., Ernst, J.D., Hatherill, M., et al. (2016). A Quantitative Analysis of Complexity of Human Pathogen-Specific CD4 T Cell Responses in Healthy *M. tuberculosis* Infected South Africans. *PLOS Pathog.* *12*, e1005760.

Lisowska-Grospierre, B., Fondaneche, M.C., Rols, M.P., Griscelli, C., and Fischer, A. (1994). Two complementation groups account for most cases of inherited MHC class II deficiency. *Hum. Mol. Genet.* *3*, 953–958.

Liu, L., Okada, S., Kong, X.-F., Kreins, A.Y., Cypowyj, S., Abhyankar, A., Toubiana, J., Itan, Y., Audry, M., Nitschke, P., et al. (2011). Gain-of-function human STAT1 mutations impair IL-17 immunity and underlie chronic mucocutaneous candidiasis. *J. Exp. Med.* *208*, 1635–1648.

Locci, M., Ghici, E.D., Marangoni, F., Bosticardo, M., Catucci, M., Aiuti, A., Cancrini, C., Marodi, L., Espanol, T., Bredius, R.G.M., et al. (2009). The Wiskott-Aldrich syndrome protein is required for iNKT cell maturation and function. *J. Exp. Med.* *206*, 735–742.

Love, M.I., Huber, W., and Anders, S. (2014). Moderated estimation of fold change and dispersion for RNA-seq data with DESeq2. *Genome Biol.* *15*, 550.

Lugo-Villarino, G., Maldonado-Lopez, R., Possemato, R., Penaranda, C., and Glimcher, L.H. (2003). T-bet is required for optimal production of IFN-gamma and antigen-specific T cell activation by dendritic cells. *Proc Natl Acad Sci U S A* *100*, 7749–7754.

Ma, W., Noble, W.S., and Bailey, T.L. (2014). Motif-based analysis of large nucleotide data sets using MEME-ChIP. *Nat. Protoc.* *9*, 1428–1450.

Mach, B., Reith, W., Masternak, K., Barras, E., Zufferey, M., Conrad, B., Corthals, G., Aebersold, R., Sanchez, J.-C., and Hochstrasser, D.F. (1998). A gene encoding a novel RFX-associated transactivator is mutated in the majority of MHC class II deficiency patients. *Nat. Genet.*

Maeda, H., Hirata, R., Chen, R.F., Suzaki, H., Kudoh, S., and Tohyama, H. (1985). Defective expression of HLA class I antigens: a case of the bare lymphocyte without immunodeficiency. *Immunogenetics* *21*, 549–558.

Mancebo, E., Moreno-Pelayo, M.A., Mencía, Á., de la Calle-Martín, O., Allende, L.M., Sivadurai, P., Kalaydjieva, L., Bertranpetit, J., Coto, E., Calleja-Antolín, S., et al. (2008). Gly111Ser mutation in CD8A gene causing CD8 immunodeficiency is found in Spanish

Gypsies. *Mol. Immunol.* *45*, 479–484.

Martínez-Barricarte, R., de Jong, S.J., Markle, J., de Paus, R., Boisson-Dupuis, S., Bustamante, J., van de Vosse, E., Fleckenstein, B., and Casanova, J.-L. (2016). Transduction of *Herpesvirus saimiri* -Transformed T Cells with Exogenous Genes of Interest. In *Current Protocols in Immunology*, (Hoboken, NJ, USA: John Wiley & Sons, Inc.), pp. 7.21C.1-7.21C.12.

Massaad, M.J., Ramesh, N., and Geha, R.S. (2013). Wiskott-Aldrich syndrome: a comprehensive review. *Ann. N. Y. Acad. Sci.* *1285*, 26–43.

Matsuyama, M., Ishii, Y., Yageta, Y., Ohtsuka, S., Ano, S., Matsuno, Y., Morishima, Y., Yoh, K., Takahashi, S., Ogawa, K., et al. (2014). Role of Th1/Th17 balance regulated by T-bet in a mouse model of *Mycobacterium avium* complex disease. *J Immunol* *192*, 1707–1717.

McGinnis, C.S., Murrow, L.M., and Gartner, Z.J. (2019). DoubletFinder: Doublet Detection in Single-Cell RNA Sequencing Data Using Artificial Nearest Neighbors. *Cell Syst.* *8*, 329-337.e4.

McKenna, A., Hanna, M., Banks, E., Sivachenko, A., Cibulskis, K., Kernytsky, A., Garimella, K., Altshuler, D., Gabriel, S., Daly, M., et al. (2010). The Genome Analysis Toolkit: A MapReduce framework for analyzing next-generation DNA sequencing data. *Genome Res.* *20*, 1297–1303.

Moins-Teisserenc, H., Gadola, S.D., Cella, M., Dunbar, P.R., Exley, A., Blake, N., Baycal, C., Lambert, J., Bigliardi, P., Willemsen, M., et al. (1999). Association of a syndrome resembling Wegener's granulomatosis with low surface expression of HLA class-I molecules. *Lancet*.

Morgan, N. V, Goddard, S., Cardno, T.S., McDonald, D., Rahman, F., Barge, D., Ciupek, A., Straatman-Iwanowska, A., Pasha, S., Guckian, M., et al. (2011). Mutation in the TCR α subunit constant gene (TRAC) leads to a human immunodeficiency disorder characterized by a lack of TCR $\alpha\beta$ ⁺ T cells. *J. Clin. Invest.* *121*, 695–702.

Nagarajan, U.M., Peijnenburg, A., Gobin, S.J., Boss, J.M., and van den elsen, P.J. (2000). Novel mutations within the RFX-B gene and partial rescue of MHC and related genes through exogenous class II transactivator in RFX-B-deficient cells. *J. Immunol.* *164*, 3666–3674.

Nekrep, N., Jabrane-Ferrat, N., Wolf, H.M., Eibl, M.M., Geyer, M., and Peterlin, B.M. (2002). Mutation in a winged-helix DNA-binding motif causes atypical bare lymphocyte syndrome. *Nat. Immunol.* *3*, 1075–1081.

Oakley, M.S., Sahu, B.R., Lotspeich-Cole, L., Solanki, N.R., Majam, V., Pham, P.T., Banerjee, R., Kozakai, Y., Derrick, S.C., Kumar, S., et al. (2013). The transcription factor T-bet regulates parasitemia and promotes pathogenesis during *Plasmodium berghei* ANKA murine malaria. *J Immunol* *191*, 4699–4708.

Oakley, M.S., Sahu, B.R., Lotspeich-Cole, L., Majam, V., Thao Pham, P., Sengupta Banerjee, A., Kozakai, Y., Morris, S.L., and Kumar, S. (2014). T-bet modulates the antibody response and immune protection during murine malaria. *Eur J Immunol* *44*, 2680–2691.

Okada, S., Markle, J.G., Deenick, E.K., Mele, F., Averbuch, D., Lagos, M., Alzahrani, M., Al-Muhsen, S., Halwani, R., Ma, C.S., et al. (2015). Impairment of immunity to *Candida* and *Mycobacterium* in humans with bi-allelic RORC mutations. *Science (80-)*. *349*, 606–613.

Ouederni, M., Vincent, Q.B., Frange, P., Touzot, F., Scerra, S., Bejaoui, M., Bousfiha, A., Levy, Y., Lisowska-Grospierre, B., Canioni, D., et al. (2011). Major histocompatibility complex class II expression deficiency caused by a RFXANK founder mutation: a survey of 35 patients. *Blood* *118*, 5108–5118.

Pacharn, P., Boonyawat, B., Tantemsapya, N., Visitsunthorn, N., and Jirapongsananuruk, O. (2017). A novel mutation of WAS gene in a boy with *Mycobacterium bovis* infection in spleen. *Asian Pacific J. Allergy Immunol.* *35*, 166–170.

Pearce, E.L., Mullen, A.C., Martins, G.A., Krawczyk, C.M., Hutchins, A.S., Zediak, V.P., Banica, M., DiCioccio, C.B., Gross, D.A., Mao, C.-A., et al. (2003). Control of Effector CD8⁺ T Cell Function by the Transcription Factor Eomesodermin. *Science* (80-.). *302*, 1041–1043.

Peijnenburg, A., Van Eggermond, M.C., Van den Berg, R., Sanal, O., Vossen, J.M., and Van den Elsen, P.J. (1999). Molecular analysis of an MHC class II deficiency patient reveals a novel mutation in the RFX5 gene. *Immunogenetics* *49*, 338–345.

Ramírez, F., Ryan, D.P., Grüning, B., Bhardwaj, V., Kilpert, F., Richter, A.S., Heyne, S., Dündar, F., and Manke, T. (2016). deepTools2: a next generation web server for deep-sequencing data analysis. *Nucleic Acids Res.* *44*, W160–W165.

Rankin, L.C., Groom, J.R., Chopin, M., Herold, M.J., Walker, J.A., Mielke, L.A., McKenzie, A.N., Carotta, S., Nutt, S.L., and Belz, G.T. (2013). The transcription factor T-bet is essential for the development of NKp46⁺ innate lymphocytes via the Notch pathway. *Nat Immunol* *14*, 389–395.

Ravindran, R., Foley, J., Stoklasek, T., Glimcher, L.H., and McSorley, S.J. (2005). Expression of T-bet by CD4 T cells is essential for resistance to *Salmonella* infection. *J Immunol* *175*, 4603–4610.

Robinson, J.T., Thorvaldsdóttir, H., Winckler, W., Guttman, M., Lander, E.S., Getz, G., and Mesirov, J.P. (2011). Integrative genomics viewer. *Nat. Biotechnol.*

Robinson, M.D., McCarthy, D.J., and Smyth, G.K. (2010). edgeR: a Bioconductor package for differential expression analysis of digital gene expression data. *Bioinformatics* *26*, 139–140.

Rosas, L.E., Snider, H.M., Barbi, J., Satoskar, A.A., Lugo-Villarino, G., Keiser, T., Papenfuss, T., Durbin, J.E., Radzioch, D., Glimcher, L.H., et al. (2006). Cutting edge: STAT1 and T-bet play distinct roles in determining outcome of visceral leishmaniasis caused by *Leishmania*

donovani. *J Immunol* 177, 22–25.

Ross-Innes, C.S., Stark, R., Teschendorff, A.E., Holmes, K.A., Ali, H.R., Dunning, M.J., Brown, G.D., Gojis, O., Ellis, I.O., Green, A.R., et al. Differential oestrogen receptor binding is associated with clinical outcome in breast cancer. *Nature* 481, 389.

Salem, S., Langlais, D., Lefebvre, F., Bourque, G., Bigley, V., Haniffa, M., Casanova, J.-L., Burk, D., Berghuis, A., Butler, K.M., et al. (2014). Functional characterization of the human dendritic cell immunodeficiency associated with the IRF8(K108E) mutation. *Blood* 124, 1894–1904.

Sanjana, N.E., Shalem, O., and Zhang, F. (2014). Improved vectors and genome-wide libraries for CRISPR screening. *Nat Methods* 11, 783–784.

de Santiago, I., and Carroll, T. (2018). Analysis of ChIP-seq Data in R/Bioconductor. pp. 195–226.

Sophie, V., D., G.J., Frank, B., P., M.P., Ahmet, D., Brigitte, N., Mathieu, B., Guy, T., Jean-Michel, G., Corinne, L., et al. (2012). Hereditary Systemic Amyloidosis Due to Asp76Asn Variant β 2-Microglobulin. *N. Engl. J. Med.*

Steimle, V., Otten, L.A., Zufferey, M., and Mach, B. (1993). Complementation cloning of an MHC class II transactivator mutated in hereditary MHC class II deficiency (or bare lymphocyte syndrome). *Cell* 75, 135–146.

Steimle, V., Durand, B., Barras, E., Zufferey, M., Hadam, M.R., Mach, B., and Reith, W. (1995). A novel DNA-binding regulatory factor is mutated in primary MHC class II deficiency (bare lymphocyte syndrome). *Genes Dev.* 9, 1021–1032.

Stuart, T., Butler, A., Hoffman, P., Hafemeister, C., Papalexi, E., Mauck, W.M., Hao, Y.,

Stoeckius, M., Smibert, P., and Satija, R. (2019). Comprehensive Integration of Single-Cell Data.

Cell 177, 1888-1902.e21.

Sullivan, B.M., Juedes, A., Szabo, S.J., von Herrath, M., and Glimcher, L.H. (2003). Antigen-driven effector CD8 T cell function regulated by T-bet. *Proc. Natl. Acad. Sci.*

Sullivan, B.M., Jobe, O., Lazarevic, V., Vasquez, K., Bronson, R., Glimcher, L.H., and Kramnik, I. (2005). Increased susceptibility of mice lacking T-bet to infection with *Mycobacterium tuberculosis* correlates with increased IL-10 and decreased IFN-gamma production. *J Immunol* 175, 4593–4602.

Svensson, A., Nordstrom, I., Sun, J.B., and Eriksson, K. (2005). Protective immunity to genital herpes simplex [correction of simpex] virus type 2 infection is mediated by T-bet. *J Immunol* 174, 6266–6273.

Swanberg, M., Lidman, O., Padyukov, L., Eriksson, P., Akesson, E., Jagodic, M., Lobell, A., Khademi, M., Börjesson, O., Lindgren, C.M., et al. (2005). MHC2TA is associated with differential MHC molecule expression and susceptibility to rheumatoid arthritis, multiple sclerosis and myocardial infarction. *Nat. Genet.* 37, 486–494.

Szabo, S.J., Sullivan, B.M., Stemmann, C., Satoskar, A.R., Sleckman, B.P., and Glimcher, L.H. (2002). Distinct effects of T-bet in TH1 lineage commitment and IFN-gamma production in CD4 and CD8 T cells. *Science* (80-.). 295, 338–342.

Tang, Y., Desierto, M.J., Chen, J., and Young, N.S. The role of the Th1 transcription factor T-bet in a mouse model of immune-mediated bone-marrow failure.

Tangye, S.G., Palendira, U., and Edwards, E.S.J. (2017). Human immunity against EBV—lessons from the clinic. *J. Exp. Med.* 214, 269–283.

Townsend, M.J., Weinmann, A.S., Matsuda, J.L., Salomon, R., Farnham, P.J., Biron, C.A., Gapin, L., and Glimcher, L.H. (2004). T-bet regulates the terminal maturation and homeostasis

of NK and Valpha14i NKT cells. *Immunity* 20, 477–494.

Villard, J., Reith, W., Barras, E., Gos, A., Morris, M.A., Antonarakis, S.E., Van den Elsen, P.J., and Mach, B. (1997a). Analysis of mutations and chromosomal localisation of the gene encoding RFX5, a novel transcription factor affected in major histocompatibility complex class II deficiency. *Hum. Mutat.* 10, 430–435.

Villard, J., Lisowska-Grospierre, B., van den Elsen, P., Fischer, A., Reith, W., and Mach, B. (1997b). Mutation of RFXAP, a regulator of MHC class II genes, in primary MHC class II deficiency. *N. Engl. J. Med.* 337, 748–753.

Villard, J., Masternak, K., Lisowska-Grospierre, B., Fischer, A., and Reith, W. (2001). MHC class II deficiency: a disease of gene regulation. *Medicine (Baltimore)*. 80, 405–418.

Villard, J., Lisowska-Grospierre, B., van den Elsen, P., Fischer, A., Reith, W., and Mach, B. (2002). Mutation of RFXAP, a Regulator of MHC Class II Genes, in Primary MHC Class II Deficiency. *N. Engl. J. Med.*

Wang, L., Wang, S., and Li, W. (2012). RSeQC: quality control of RNA-seq experiments. *Bioinformatics* 28, 2184–2185.

Wang, Y., Ma, C.S., Ling, Y., Bousfiha, A., Camcioglu, Y., Jacquot, S., Payne, K., Crestani, E., Roncagalli, R., Belkadi, A., et al. (2016). Dual T cell- and B cell-intrinsic deficiency in humans with biallelic RLTPR mutations. *J. Exp. Med.* 213, 2413–2435.

Wani, M.A., Haynes, L.D., Kim, J., Bronson, C.L., Chaudhury, C., Mohanty, S., Waldmann, T.A., Robinson, J.M., and Anderson, C.L. (2006). Familial hypercatabolic hypoproteinemia caused by deficiency of the neonatal Fc receptor, FcRn, due to a mutant beta2-microglobulin gene. *Proc. Natl. Acad. Sci. U. S. A.* 103, 5084–5089.

Wiszniewski, W., Fondaneche, M.C., Lambert, N., Masternak, K., Picard, C., Notarangelo, L.,

Schwartz, K., Bal, J., Reith, W., Alcaide, C., et al. (2000). Founder effect for a 26-bp deletion in the RFXANK gene in North African major histocompatibility complex class II-deficient patients belonging to complementation group B. *Immunogenetics* 51, 261–267.

Wiszniewski, W., Fondaneche, M.C., Louise-Plence, P., Prochnicka-Chalufour, A., Selz, F., Picard, C., Deist, F., Eliaou, J.F., Fischer, A., and Lisowska-Grospierre, B. (2003). Novel mutations in the RFXANK gene: RFX complex containing in-vitro-generated RFXANK mutant binds the promoter without transactivating MHC II. *Immunogenetics*.

Xu, G.J., Kula, T., Xu, Q., Li, M.Z., Vernon, S.D., Ndung'u, T., Ruxrungtham, K., Sanchez, J., Brander, C., Chung, R.T., et al. (2015). Comprehensive serological profiling of human populations using a synthetic human virome. *Science* (80-.). 348, aaa0698–aaa0698.

Yabe, T., Kawamura, S., Sato, M., Kashiwase, K., Tanaka, H., Ishikawa, Y., Asao, Y., Oyama, J., Tsuruta, K., Tokunaga, K., et al. (2002). A subject with a novel type I bare lymphocyte syndrome has tapasin deficiency due to deletion of 4 exons by Alu-mediated recombination. *Blood* 100, 1496–1498.

Yasutomi, M., Yoshioka, K., Mibayashi, A., Tanizawa, A., Imai, K., Ohara, O., and Ohshima, Y. (2015). Successful Myeloablative Bone Marrow Transplantation in an Infant With Wiskott-Aldrich Syndrome and Bacillus Calmette-Guerin Infection. *Pediatr. Blood Cancer* 62, 2052–2053.

Zhang, Y., Liu, T., Meyer, C.A., Eeckhoute, J., Johnson, D.S., Bernstein, B.E., Nussbaum, C., Myers, R.M., Brown, M., Li, W., et al. (2008). Model-based Analysis of ChIP-Seq (MACS). *Genome Biol.* 9, R137.